FLOOD HAZARD AND VULNERABILITY ASSESSMENT IN UPPER GIN RIVER BASIN IN SRI LANKA UNDER CLIMATE CHANGE

VIRENDRA KUMAR

(208354E)

Degree of Master of Science

Department of Civil Engineering

University of Moratuwa
Sri Lanka

February 2022

FLOOD HAZARD AND VULNERABILITY ASSESSMENT IN UPPER GIN RIVER BASIN IN SRI LANKA UNDER CLIMATE CHANGE

VIRENDRA KUMAR

(208354E)

Supervised by

Dr T. M. N. Wijayaratna

Thesis submitted in partial fulfillment of the requirements for the degree Master of Science in Civil Engineering

UNESCO Madanjeet Singh Centre for

South Asia Water Management (UMCSAWM)

Department of Civil Engineering

University of Moratuwa

Sri Lanka

February 2022

DECLARATION OF THE CANDIDATE AND SUPERVISOR

"I declare that this is my own work and this thesis does not incorporate without acknowledgement any material previously submitted for a Degree or Diploma in any other University or institute of higher learning and to the best of my knowledge and belief it does not contain any material previously published or written by another person except where the acknowledgement is made in the text".

Also, I hereby grant to University of Moratuwa the non-exclusive right to reproduce and distribute my thesis/dissertation, in whole or in part in print, electronic or other medium. I retain the right to use this content in whole or part in future works (such as articles or books).

UOM Verified Signature

28/01/2022

VIRENDRA KUMAR

Date

The above candidate has carried out research for the Masters thesis under my supervision

UOM Verified Signature

28/01/2022

Dr T. M. N. Wijayaratna

Date

ABSTRACT

Flood Hazard and Vulnerability Assessment in Upper Gin River Basin in Sri Lanka under Climate Change

Floods are a frequent major disaster throughout the world, usually resulting in fatalities and massive economic and environmental damage. Seasonal and localized flooding is one of the extremely common natural disasters in Sri Lanka. There are two monsoon seasons (Southwest and Northwest monsoon) and two inter- monsoons (First Inter and Second Inter monsoon) in Sri Lanka, each of these monsoon seasons are followed by floods induced by heavy rainfall. The Southwest monsoon, which comes between May and September, has the greatest impact on the southern region of Sri Lanka. This research is developed to assess the flood hazard, vulnerability, and risk of the Thawalama watershed for climate change in future representative concentration pathways (RCP) 8.5. The Research methodology begins with selecting Events, which was determined by different statistical approaches. The Gumbel method was the best fit for determining the event's return periods. A 12-year return period (2003) was selected for calibration, and a 5-year return period (1999) was selected for validation. Further, the future climate rainfall data was bias-corrected using the linear scaling method. The future climate rainfall data was divided into two centuries: mid-century (2040-2070) and end-century (2070-2099). Thereafter, the 5-year Return period and 12-year Return period were estimated through the Gumbel method for both mid and end centuries. The Hydrologic Engineering Centre's Hydrologic Modeling System (HEC-HMS) was calibrated for 2003 and validated for 1999 at the gauging station of the Thawalama catchment to obtain lateral flows and inflow inside the catchment. Thereafter, Hydrological Engineering Centre's River Analysis System (HEC-RAS) was calibrated and validated for the lateral flows and inflows obtained from HEC-HMS for 2003 and 1999 respectively. Similarly, the future lateral flows and inflow were derived using HEC-HMS by importing climatic rainfall data for selected events of 5-year and 12-year return periods in both mid and end centuries. Thereafter, HEC-RAS was used to get flood inundation, flood depth, and flood velocity maps. Finally, to achieve objectives, flood depth and flood velocity were imported to the Arc-GIS interface to develop flood hazards, and population density was used to develop flood vulnerability. Hence, a flood risk map was prepared by multiplying flood hazards and flood vulnerability. The HEC-HMS was calibrated with Nash Sutcliffe (NSE)=0.80, Root mean square error standard deviation (RMSE st dev.) =0.40, and Percent Bias (P-bias) =17.65% and Validated with NSE=0.67, RMSE st dev.=0.60 and P-bias=15%. Thereafter, HEC-RAS was calibrated with NSE=0.66, Coefficient of determination (R^2) =0.83 and P-bias=3.98% and Validated with NSE=0.62, Coefficient of determination (R^2) =0.79 and P-bias=3.28%. The results show an increasing trend of flood inundation area for both the 5-year return period (17.36 km^2,17.40 km^2,19.77 km^2 for years 1999,2052,2091, respectively) and 12-year return period (19.55 km^2, 20.06 km^2, 21.18 km^2 for years 2003, 2058, 2098, respectively). Thereafter, sudden increment of flood hazard, flood vulnerability, and flood risk was obtained after mid-century in both 5-year and 12- year return periods. Almost 22 Grama Niladhari Division (GND) were found to be a very high-risk category and 21 GND were found to be at a high-risk category at the end century of the 12-year Return period in the year 2098 whereas 19 GND were found to be a very high-risk category and 23 GND were found to be at a high-risk category at the end century of 5-year Return period in the year 2091. Flood hazard, flood vulnerability, and flood risk is increasing suddenly after mid-century in both 5-year and 12- year return periods. Hence, from the viewpoint of disaster reduction, the information derived from this study can help to estimate the probability of flood damage for the local population.

Keywords: Bias-correction, Flood-inundation, HEC-HMS, HEC-RAS, Return period, Risk

DEDICATION

“I would like to dedicate my work to my family”.

ACKNOWLEDGEMENT

I would like to express my sincere gratitude to my research supervisor, Dr. Nimal Wijayaratna, for his constant supervision, patient hearing of ideas, critical analysis of observation, and detecting flaws & amending thereby leading the thesis to success. This thesis would not have been completed on time if not for his committed supervision and ongoing mentoring. Throughout my period, he continuously let this study be my work but led me in the right direction whenever he believed I needed it. He's an excellent teacher.

I would like to extend my gratefulness to the Centre's Chairman, Prof. R.L.H. Lalith Rajapakse, and the Research Coordinator, Dr. Janaka Bamunawala, for providing me with all the essential help as well as continual encouragement and direction when needed.

I will never hesitate to convey my thanks to Professor N. T. S. Wijesekera for conveying a deeper sense of knowledge through his teaching which was valuable in this Research Study.

I also wish to express my gratitude to support staff Mr. Wajira Kumarasinghe, Mrs. Vinu Kalanika, Miss Janani for their assistance given during the master’s program

I would also like to thank Late. Shri Madanjeet Singh, the Fund's Management, and the University of Moratuwa for providing me with the opportunity to study for a master’s degree in Water Resource Engineering and Management at the UNESCO Madanjeet Singh Centre for South Asia Water Management, Department of Civil Engineering, University of Moratuwa, Sri Lanka.

I also like to thank the Department of Irrigation for permitting me to collect the essential data. I would like to convey my heartfelt thanks to my family for their unwavering support and encouragement during my thesis research. Finally, I would like to express my heartfelt gratitude to Mr. Utsab Phyual, Miss Farhana Azmi, and Sainee Thirukumar for their essential help in providing.

TABLE OF CONTENTS

Declaration of the candidate and supervisor V

ABSTRACT VII

Dedication IX

Acknowledgement XI

Table of contents XIII

List of figures XVII

List of tables XXI

List of abbreviations XXV

Chapter 1 1

1 Introduction 1

1.1 Problem Identification 3

1.2 Problem Statement 3

1.3 Objectives 3

1.3.1 Main Objective 3

1.3.2 Specific Objective 3

1.4 Significance 4

Chapter 2 5

2 Literature Review 5

2.1 Introduction 5

2.1.1 The weather pattern over Sri Lanka 5

2.1.2 Past Significant floods in the study area 9

2.2 Data and Data Checking 9

2.3 Climate Change 11

2.4 Bias Correction 12

2.5 Flood Frequency Analysis 13

2.6 Hydrological Model and Flood inundation model 14
2.6.1 HEC- HMS model parameters 15
2.6.2 HEC- RAS model development 21
2.6.3 Objective function 24
2.7 Flood Hazard Assessment 24
2.7.1 General Concept Flood Hazard 24
2.7.2 Past literature on Flood Hazard, Vulnerability and Risk Assessment 25
2.7.3 IPCC conceptualization of Vulnerability, Exposure, and Risk 28

Chapter 3 29

3 Materials and Methods 29

3.1 Study Area 29
3.2 Justification of Study Area 31
3.3 Methodology 34
3.4 Data Collection 35

Chapter 4 37

4 Data Checking and analysis 37

4.1 Observed period data checking 38
4.1.1 Pallegama Rainfall Station 38
4.1.2 Thawalama Rainfall Station 40
4.1.3 Anninkanda Rainfall Station 42
4.1.4 Kuduwa Rainfall Station 44
4.1.5 Single mass curve and Double mass curve analysis 46
4.2 Bias correction of Climate data 47
4.3 Future Projection of Rainfall 50
4.4 The Frequency Analysis for flood 52
4.4.1 Gumbel's Method- 52
4.4.2 Log-Pearson Type III distribution 53
4.4.3 Log-Normal distribution 54
4.4.4 Flood Frequency analysis for Mid-Century and End-Century 55
4.5 Population Demography 57

Chapter 5 59

5 Model development and applications 59

5.1 HEC- HMS Model Development 59

5.1.1 Thiessen polygon 59

5.1.2 Catchment Delineate 60

5.1.3 SCS CN (Soil Conservation Service Curve Number) 61

5.1.4 Reach routing-Muskingum 62

5.2 HEC- RAS Model Development 63

5.2.1 The terrain Layers 63

5.2.2 The 2D Computational Mesh development 64

5.2.3 Associating Land use and Manning's Layer with a Geometry 65

Chapter 6 67

6 Results and Analysis 67

6.1 Event selection 67

6.2 Model Calibration, Validation, and Future Simulation 68

6.2.1 HEC-HMS Calibration-Event 2003 68

6.2.2 HEC-HMS Validation -Event 1999 71

6.2.3 HEC-RAS Calibration -Event 2003 72

6.2.4 HEC-RAS Validation-Event April 1999 74

6.2.5 Future Simulation 75

6.3 Flood Inundation Maps 77

6.3.1 Flood Inundation Map verification of Event 2003 77

6.3.2 12-Year Return Period 80

6.3.3 5-Year Return Period 82

6.4 Flood Hazard and Vulnerability Map 84

6.4.1 Flood hazard maps 85

6.4.2 Flood Vulnerability Map 104

6.5 Flood Risk Map 112

6.5.1 12-Year Return Period 112

6.5.2 5-Year Return Period 115

Chapter 7 119

7 Discussion 119

7.1 Data Period for Bias correction 119

7.2 HEC-RAS Model Parameter Selection 119

7.3 Flood Hazard and vulnerability 120

7.4 12-Year Return Period 121

7.5 5-Year Return Period 126

Chapter 8 131

8 Conclusions 131

Chapter 9 133

9 Recommendations 133

Bibliography 135

Annexure 1 143

Rainfall seasonal graphs 143

Annexure 2 147

Single mass curve and Double mass curve 147

LIST OF FIGURES

Figure 2-1: Monsoon season in Sri Lanka ---- 6
Figure 2-2: Climatic zones in Sri Lanka ---- 7
Figure 2-3 Annual average rainfall distribution in wet, dry, intermediate, semi-arid zones, and Sri Lanka Source ---- 8
Figure 2-4: Frequency analysis of the flood at Thawalama station ---- 9
Figure 2-5: Projected atmospheric greenhouse gas emissions for the four RCP Scenarios ---- 12
Figure 3-1: Study Area ---- 30
Figure 3-2 Population density in the year 2022 at Lower and Upper Gin Ganga ---- 31
Figure 3-3 Population density in the year 2060 at Lower and Upper Gin Ganga ---- 32
Figure 3-4 Population density in the year 2100 at Lower and Upper Gin Ganga ---- 33
Figure 3-5: Methodology flow chart ---- 34
Figure 4-1 Rainfall seasonal variation of Pallegama rainfall station including four monsoon seasons in Sri Lanka ---- 38
Figure 4-2 Rainfall variation of Pallegama rainfall station according to hydrological year (1989/90 – 2017/18) ---- 39
Figure 4-3 Yearly streamflow vs yearly rainfall of Pallegama rainfall station in the Thawalama catchment ---- 39
Figure 4-4 Rainfall Seasonal Variation of Thawalama Rainfall Station including four monsoon seasons in Sri Lanka ---- 40
Figure 4-5 Rainfall Variation of Thawalama rainfall station according to hydrological year (1989/90 – 2017/18) ---- 41
Figure 4-6 Yearly Streamflow vs yearly rainfall of Thawalama rainfall station in the Thawalama catchment ---- 41
Figure 4-7 Rainfall seasonal variation of Anninkanda rainfall station including four monsoon seasons in Sri Lanka ---- 42
Figure 4-8 Rainfall variation of Anninkanda rainfall station according to hydrological year (1989/90 – 2017/18) ---- 43
Figure 4-9 Yearly streamflow vs yearly rainfall of Anninkanda rainfall station in the Thawalama catchment ---- 43
Figure 4-10 Rainfall seasonal variation of Kuduwa Rainfall station including four monsoon seasons in Sri Lanka ---- 44
Figure 4-11 Rainfall variation of Kuduwa rainfall station according to hydrological year (1989/90 – 2017/18) ---- 45
Figure 4-12 Yearly Streamflow vs yearly rainfall of Kuduwa rainfall station in the Thawalama catchment ---- 45
Figure 4-13: Single mass curve for all four-rainfall stations in the Thawalama catchment ---- 46

Figure 4-14 Double mass curve for all four-rainfall stations in the Thawalama catchment ---- 47
Figure 4-15 Bias corrected rainfall (mm) for MIROC-MIROC5 ---- 48
Figure 4-16 Bias corrected rainfall (mm) for NCC-NorESM1-M ---- 48
Figure 4-17 Bias corrected rainfall (mm) for MPI-M-MPI-ESM-MR ---- 49
Figure 4-18 Bias corrected rainfall (mm) for ICHEC-EC-EARTH ---- 49
Figure 4-19 Average annual rainfall of Historical, mid-century, and end a century of RCM data ---- 50
Figure 4-20 Monthly average RCM rainfall for historical, mid-century and end century ---- 51
Figure 4-21: Flood frequency of Gumbel's method on a semi-log scale ---- 52
Figure 4-22: Flood frequency of reduced variate vs Return period ---- 53
Figure 4-23: Flood frequency of thiessen rainfall plot using Log-Normal distribution ---- 54
Figure 4-24 Flood frequency of Gumbel's method on a semi-log scale (Mid-Century) ---- 55
Figure 4-25 Flood frequency of Gumbel's method on a semi-log scale (End-Century) ---- 56
Figure 4-26 Population for Districts in 2-D area ---- 57
Figure 5-1: Thiessen polygons and rainfall stations at Thawalama watershed ---- 60
Figure 5-2: HEC-HMS model Development ---- 61
Figure 5-3 Two-Dimensional Area ---- 64
Figure 5-4 Land use in the Two-Dimensional Area ---- 65
Figure 6-1 HEC-HMS model calibration ---- 68
Figure 6-2 HEC- HMS model validation ---- 71
Figure 6-3 HEC-RAS model calibration ---- 72
Figure 6-4 HEC-RAS model validation ---- 74
Figure 6-5 HEC-HMS simulation for future events ---- 75
Figure 6-6 HEC-RAS simulation for future events ---- 76
Figure 6-7 Flood Inundation map of the year 2003 event ---- 77
Figure 6-8 Flood Inundation map for event 2003 (Source: JICA, 2009) ---- 78
Figure 6-9 Flood Inundation Map for Event 2003 (Source: UNDP, 2010) ---- 79
Figure 6-10 Flood Inundation map of mid-century for the 12-year return period ---- 80
Figure 6-11 Flood Inundation map of end century for the 12-year return period ---- 81
Figure 6-12 Flood Inundation map of the year 1999 event ---- 82
Figure 6-13 Flood Inundation map of mid-century for the 5-year return period ---- 83
Figure 6-14 Flood Inundation map of End century for the 5-year Return period ---- 84
Figure 6-15 Matrix for hazard and risk mapping ---- 85
Figure 6-16 Flood depth map of the 2003-year flood event for the 12-year return period ---- 86
Figure 6-17 Flood velocity map of the 2003 flood event for the 12-year Return period ---- 87
Figure 6-18 Flood hazard map of the 2003 flood event for the 12-year return period ---- 88
Figure 6-19 Flood depth map of the mid-century flood event for the 12-year return period ---- 89
Figure 6-20 Flood velocity map of the mid-century flood event for the 12-year return period ---- 90
Figure 6-21 Flood hazard map of the mid-century flood event for the 12-year Return period ---- 91

Figure 6-22 Flood depth map of end-century flood event for the 12-year return period ---------- 92
Figure 6-23 Flood velocity map of end-century flood event for the 12-year Return period ---------- 93
Figure 6-24 Flood hazard map of end-century flood event for the 12-year return period ---------- 94
Figure 6-25 Flood depth map of 1999 flood event for the 5-year return period ---------- 95
Figure 6-26 Flood velocity map of 1999 flood event for the 5-year return period ---------- 96
Figure 6-27 Flood hazard map of the 1999-year flood event for the 5-year return period ---------- 97
Figure 6-28 Flood depth map of the mid-century flood event for the 5-year return period ---------- 98
Figure 6-29 Flood velocity map of the mid-century flood event for the 5-year return period ---------- 99
Figure 6-30 Flood hazard map of the mid-century flood event for the 5-year return period ---------- 100
Figure 6-31 Flood depth map of end-century flood event for the 5-year return period ---------- 101
Figure 6-32 Flood velocity map of end-century flood event for the 5-year return period ---------- 102
Figure 6-33 Flood hazard map of end-century flood event for the 5-year return period ---------- 103
Figure 6-34 Matrix for vulnerability mapping ---------- 105
Figure 6-35 Flood vulnerability map of the 2003-year flood event for the 12-year return period ---- 106
Figure 6-36 Flood vulnerability map of mid-century flood event for the 12-year return period ------ 107
Figure 6-37 Flood vulnerability map of end-century flood event for the 12-year return period ------ 108
Figure 6-38 Flood vulnerability map of 1999 flood event for the 5-year return period ---------- 109
Figure 6-39 Flood vulnerability map of mid-century flood event for the 5-year return period ------- 110
Figure 6-40 Flood vulnerability map of end-century flood event for the 5-year return period -------- 111
Figure 6-41 Flood risk map of 2003-year flood event for the 12-year return period ---------- 112
Figure 6-42 Flood risk map of mid-century flood event for the 12-year return period ---------- 113
Figure 6-43 Flood risk map of end-century flood event for the 12-year return period ---------- 114
Figure 6-44 Flood risk map of 1999-year flood event for the 5-year return period ---------- 115
Figure 6-45 Flood risk map of mid-century flood event for the 5-year return period ---------- 116
Figure 6-46 Flood risk map of end-century flood event for the 5-year return period ---------- 117
Figure 7-1 Hazardous area at various periods due to flood depth for 12 years return period --------- 121
Figure 7-2 Hazardous area at various periods due to flood velocity for 12 years return period ------- 121
Figure 7-3 Hazardous area at various periods due to flood hazard for 12 years return period -------- 122
Figure 7-4 Vulnerable area at various periods due to flood for 12 years return period ---------- 123
Figure 7-5 Risk area at various periods due to flood for 12 years return period ---------- 124
Figure 7-6 Area facing flood risk at a 12-year Return period ---------- 125
Figure 7-7 Hazardous area at various periods due to flood depth for a 5-year return period ---------- 126
Figure 7-8 Hazardous area at various periods due to flood velocity for a 5-year return period ------- 126
Figure 7-9 Hazardous area at various periods due to flood hazard for a 5-year return period --------- 127
Figure 7-10 Vulnerable area at various periods due to flooding for a 5-year return period ---------- 128
Figure 7-11 Risk area at various periods due to flood for a 5-year return period ---------- 128
Figure 7-12 Area facing flood risk in 5-year Rteun period ---------- 129

Figure A1- 1: Rainfall Seasonal Variation of Pallegama Rainfall Station ---------- 143
Figure A1- 2: Rainfall Seasonal Variation of Thawalama Rainfall Station ---------- 144
Figure A1- 3: Rainfall Seasonal Variation of Anninkanda Rainfall Station---------- 145
Figure A1- 4: Rainfall Seasonal Variation of Kududwa Rainfall Station---------- 146

Figure A2- 1: Single Mass Curve for Pallegama Station ---------- 147
Figure A2- 2: Single Mass Curve for Thawalama Station ---------- 148
Figure A2- 3: Single Mass Curve for Anninkanda Station ---------- 148
Figure A2- 4: Single Mass Curve for Kuduwa Station---------- 149
Figure A2- 5: Double Mass Curve of Pallegama rainfall station in the Thawalama Catchment------ 149
Figure A2- 6: Double Mass Curve of Thawalama rainfall station in the Thawalama Catchment ---- 150
Figure A2- 7: Double Mass Curve of Anninkanda rainfall station in the Thawalama Catchment --- 150
Figure A2- 8: Double Mass Curve of Kuduwa rainfall station in the Thawalama Catchment -------- 151

LIST OF TABLES

Table 2-1: Observed changes in Temperature 8
Table 2-2 HEC- HMS parameters (US Army Corps of Engineers, 2018) 15
Table 2-3 Max Canopy Storage (Ahbari et al., 2018) 16
Table 2-4 Surface Canopy (Ahbari et al., 2018) 17
Table 2-5 Flood Vulnerability classification (Hoque et al., 2019) 26
Table 2-6 Flood Hazard classification (Ongdas et al., 2020) 27
Table 3-1 Data Requirements 35
Table 3-2 Locations of gauging stations 36
Table 4-1 Return period for different reduced variate 53
Table 4-2 Return period for different reduced variate of mid-century and end-century 56
Table 5-1: Thiessen weights for the Gin River basin at Thawalama catchment 59
Table 5-2: HEC-HMS Model Parameters 60
Table 5-3: Sample calculation of Curve number 61
Table 5-4 Curve Number for various sub-catchment 62
Table 5-5: Time of concentration 62
Table 5-6 Muskingum K calculation 63
Table 5-7 Manning's n value for Land use classification 66
Table 6-1 Selected centuries of future climate rainfall data 67
Table 6-2 HEC-HMS model calibration performance 69
Table 6-3 Initial parameters and optimized parameters for base flow method in HEC-HMS model in the Thawalama catchment 69
Table 6-4 Initial parameters and optimized parameters for routing (Muskingum) method in HEC-HMS model in the Thawalama catchment 70
Table 6-5 HEC-HMS model validation performance 71
Table 6-6 HEC-RAS model calibration performance 73
Table 6-7 Initial parameters and optimized parameters for manning's value in the HEC-RAS model in the Thawalama catchment 73
Table 6-8 HEC-RAS model validation performance 74
Table 6-9 Area affected by flood depth according to hazard level in the 2003-year flood event for the 12-year Return period 87
Table 6-10 Area affected by flood velocity according to hazard level of the 2003 flood event for the 12-year Return period 88
Table 6-11 Area affected by flood hazard according to hazard level in the 2003 flood event for the 12-year return period 89
Table 6-12 Area affected by flood depth according to hazard level in the mid-century flood event for the 12-year return period 90

Table 6-13 Area affected by flood velocity according to hazard level in the mid-century flood event for the 12-year return period....91
Table 6-14 Area affected by flood hazard according to hazard level in the mid-century flood event for the 12-Year Return period....92
Table 6-15 Area affected by flood depth according to hazard level in end-century flood event for the 12-year return period....93
Table 6-16 Area affected by flood velocity according to hazard level in end-century flood event for the 12-year return period....94
Table 6-17 Area affected by flood hazard according to hazard level in end-century flood event for the 12-year return period....95
Table 6-18 Area affected by flood depth according to hazard level in the 1999 year flood event for the 5-year return period....96
Table 6-19 Area affected by flood velocity according to hazard level in the 1999 year flood event for the 5-year return period....97
Table 6-20 Area affected by flood hazard according to hazard level in 1999 flood event for the 5-year return period....98
Table 6-21 Area affected by flood depth according to hazard level in mid-century flood event for the 5-year return period....99
Table 6-22 Area affected by flood velocity according to hazard level in mid-century flood event for the 5-year return period....100
Table 6-23 Area affected by flood hazard according to hazard level in mid-century flood event for the 5-year return period....101
Table 6-24 Area affected by flood depth of end-century flood event for the 5-year return period....102
Table 6-25 Area affected by flood velocity according to hazard level of end-century flood event for the 5-year return period....103
Table 6-26 Area affected by flood hazard according to hazard level of end-century flood event for the 5-year return period....104
Table 6-27 Area affected by flood vulnerability according to the vulnerable level of the 2003-year flood event for the 12-year return period....106
Table 6-28 Area affected by flood vulnerability according to the vulnerable level of mid-century flood event for the 12-year return period....107
Table 6-29 Area affected by flood vulnerability according to the vulnerable level of end-century flood event for the 12-year return period....108
Table 6-30 Area affected by flood vulnerability according to the vulnerable level of 1999 flood event for the 5-year return period....109
Table 6-31 Area affected by flood vulnerability according to the vulnerable level of mid-century flood event for the 5-year return period....110

Table 6-32 Area affected by flood vulnerability according to the vulnerable level of end-century flood event for the 5-year return period 111
Table 6-33 Area affected by flood risk according to the risk level of 2003-year flood event for the 12-year return period..... 113
Table 6-34 Area affected by flood risk according to the risk level of mid-century flood event for the 12-year return period 114
Table 6-35 Area affected by flood risk according to the risk level of end-century flood event for the 12-year return period 115
Table 6-36 Area affected by flood risk according to the risk level of 1999-year flood event for the 5-year return period..... 116
Table 6-37 Area affected by flood risk according to the risk level of mid-century flood event for the 5-year return period..... 117
Table 6-38 Area affected by flood risk according to the risk level of end-century flood event for the 5-year return period..... 118
Table 7-1 Number of GND affected by various Risk level in 12-year return period 124
Table 7-2 Number of GND affected at various Risk levels in 5-year return period..... 129

LIST OF ABBREVIATIONS

CE	-	Coefficient of efficiency
DEM	-	Digital Elevation Model
GND	-	Grama Niladhari Division
HEC	-	Hydrologic Engineering Center
HMS	-	Hydrologic Modeling System
IPCC	-	Intergovernmental Panel on Climate Change
LULC	-	Land-use Landcover
MAE	-	Mean absolute error
NSE	-	Nash Sutcliffe Efficiency
P-Bias	-	Percentage bias
RAS	-	River Analysis System
RCP	-	Representative concentration pathway
RCM	-	Regional Climate Models
RMSE	-	Root Mean Square Error
SCS-CN	-	Soil Conservation Service Curve Number
SS	-	Skill Score

CHAPTER 1

1 INTRODUCTION

Flooding is defined as a broad historical condition characterized by the partial or total inundation of normally dry areas produced by inshore or tidal water overflow or unusually excessive deposition of runoff. (Birmah et al., 2021). Flooding occurs when the river water spills over the Riverbanks, floodplains, and nearby highlands are inundated to some extent, or the water level in the River exceeds a specific stage.

Since Sri Lanka is located between the Bay of Bengal and the Gulf of Mannar in the Indian Ocean, pressure shifts in the Bay of Bengal mixed with strong winds generate surprise torrential rainfall. Furthermore, Sri Lanka has two monsoonal rains and two inter-monsoonal rains every year. Because of these circumstances, the lower banks of the Rivers Kalu-Ganga, Gin-Ganga, and Kelani-Ganga are regularly inundated (Samarasinghea, 2010).

Seasonal and localized flooding and landslides are the most prevalent hazards in Sri Lanka, followed by cyclones, droughts, storm surges, and high winds. Sri Lanka has two monsoon seasons, each of which is followed by floods produced by heavy rains. They also exhibit a high degree of geographic diversity. The Southwest monsoon, which occurs between May and September, has the most influence on the southern and Sabaragamuwa provinces. (UNDRR, 2019).

Floods in Sri Lanka are mostly caused by excessive monsoon rainfall season, as well as severe rains generated by depressions over the Bay of Bengal (UNDRR, 2019). Flood damages are becoming more severe in property damage and human casualties. Therefore, the government has to spend a large amount of national funding for relief works during floods.

Flood effects may occur in the future as a result of the watershed's ever-growing population, as well as climate change driven by natural and man-made factors, posing

risks to people living in floodplains. (Nur & Shrestha, 2017). This finding lends support to a substantial number of research on the influence of change in climate on floods, with an emphasis on altering flood amplitude and frequency. (Booij, 2005). Flood risk assessment for future climate change scenarios serves as a foundation for flood management decision-making at the global, national, regional, and local levels. (International Sava River Basin Commission, 2014).

Flood hazard assessment is the assessment of the unfavorable impacts of floods based on hazard factors such as flood depth, flood duration, flood wave velocity, and percentage increase of water level (Samarasinghe A, 2010). The vulnerability defines the state of susceptibility to damage and marginalization in both physical and social systems, as well as for guiding the evaluative analysis of actions to improve well-being through risk reduction (Nandalal & Ratnayake, 2010).

As a result, flood hazard mapping and vulnerability assessment serve as a basis for risk assessment and management by offering information such as readily available graphs and maps necessary to explain the nature and extent of the vulnerability and risk to flooding, enabling administrators and decision-makers toward emphasizing mitigation measures.

In this context, bias-corrected Regional Climate models (RCM) results have to be performed in this study for selected RCP's covering the Upper Gin Ganga River basin to produce flood hazard and vulnerability maps which will facilitate for making adaptation and mitigation strategies for the future development of Sri Lanka.

1.1 Problem Identification

- In May 2003, the Gin Ganga River of Sri Lanka experienced devastating floods, which caused nearly 17 deaths and damaged 32000 housing units (Yoshitani et al., 2007).
- Flood levels in the lower reaches of the Gin Ganga (at Baddegama) in 2017 were greater than previously reported readings of events. (Disaster management center, 2018)

1.2 Problem Statement

Flooding is quite frequent in the Gin River basin. However, the extents of flood hazards and vulnerabilities are still not properly documented and therefore, the flood risk is not adequately known. In addition, how the change in climate will affect the flood hazards and vulnerabilities in the future is also poorly known.

1.3 Objectives

1.3.1 Main Objective

To assess flood hazards, vulnerability, and risk for the Upper Gin River basin under the impact of future climate change.

1.3.2 Specific Objective

- To select a suitable regional climate model for the Upper Gin River basin.
- To select the flood events using a statistical approach.
- To develop, calibrate and validate a hydrologic and hydraulic model for the Upper Gin Ganga River basin and to estimate future flood hazards.
- To generate flood vulnerability and flood risk maps.

1.4 Significance

- A validated hydrodynamic model of the Thawalama catchment which can be used in planning the flood mitigation measures.
- The conclusions of this research are suitable for recognizing the hazardous areas due to floods and can be beneficial to develop the areas more vulnerable to floods to reduce the risk of damages to the general public.
- Thereafter, flood alert systems may be established, and evacuation centers in low-risk regions can be built to avoid future losses.
- The findings also could be used as a guideline for other areas throughout Sri Lanka.
- Areas that are categorized as low or no flood risk areas could be earmarked for future development projects such as township expansions, new settlements, and new infrastructure facilities.

CHAPTER 2

2 LITERATURE REVIEW

2.1 Introduction

The publications related to climate change, rainfall, and floods in the Gin River basin, hazard, vulnerability, and risk mapping were reviewed. Further, floodplain inundation mapping, flood hazard, and risk assessment are also studied. This section aims at a study of significant studies on flood hazard, vulnerability, and risk globally, as well as the IPCC concepts of Vulnerability, Exposure, and Risk.

2.1.1 The weather pattern over Sri Lanka

Sri Lanka is vulnerable to a variety of hazards, including weather-related phenomena such as cyclones and monsoonal rain, which cause flooding and landslides. Droughts are also widespread as a result of monsoon changes, which are followed by lightning strikes, coastal erosion, diseases, and pollution. Localized and seasonal floods represent the largest threat to communities, and the flood risk profile is growing as the effect and frequency of hydro-meteorological hazards are predicted to increase (UNDRR, 2019).

The island enjoys mainly two monsoons and two inter-monsoons seasons governed by the change of winds as shown in Figure 2-1 (Samarasinghe, 2009)-

- First Inter-Monsoon season (March and April)
- Southwest Monsoon season (May to September)
- Second Inter-Monsoon season (October and November)
- Northeast Monsoon season (December to February)

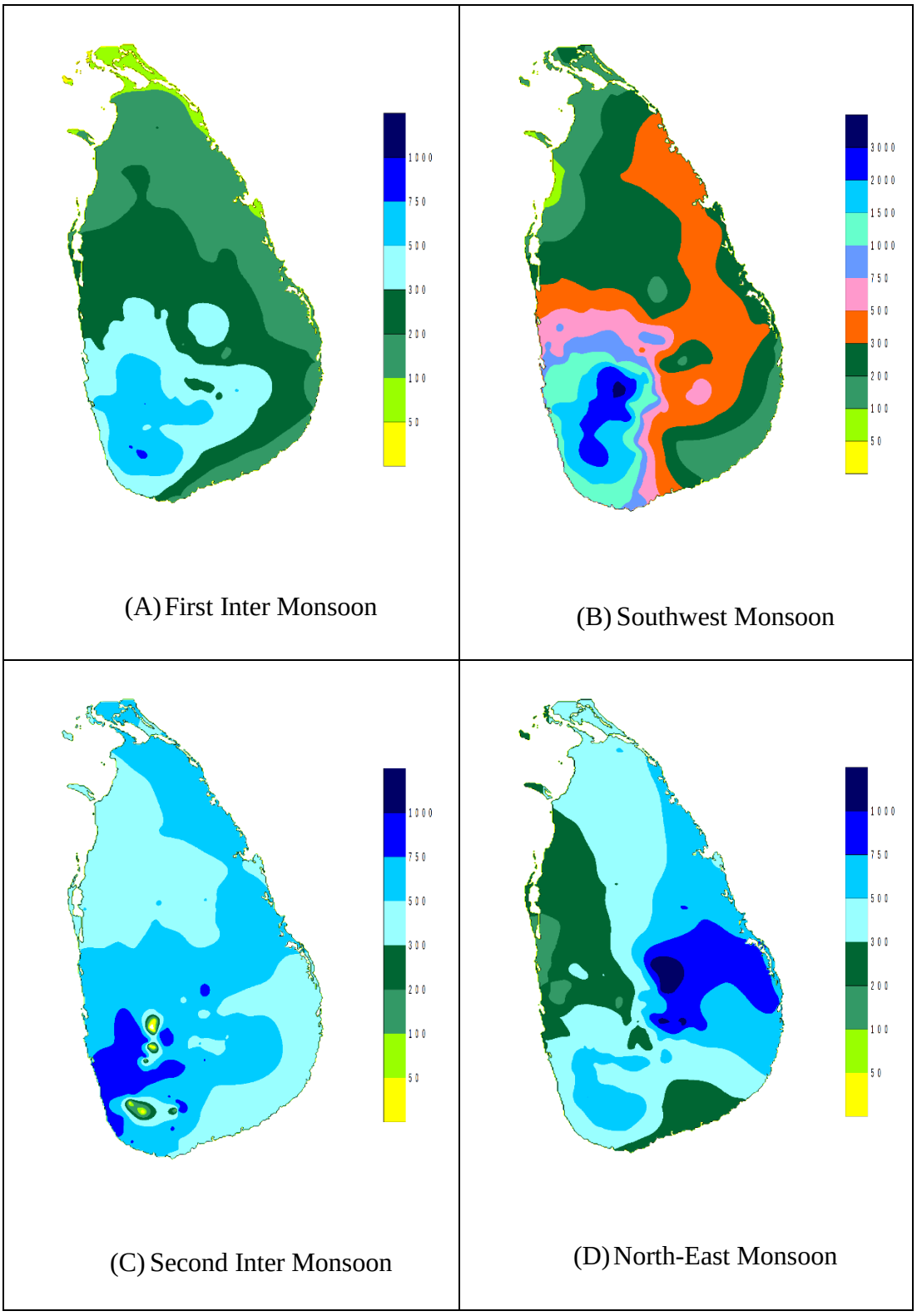

Figure 2-1: Monsoon season in Sri Lanka

(Source: Samarasinghe, 2009)

Sri Lanka exhibits a wide range of weather conditions based on the geographical settings of the various places (Samarasinghe, 2009).

- The total annual rainfall in the wet zone is greater than 2500 mm (Figure 2-2).
- The total annual rainfall in the Intermediate zone is between 1750 mm to 2500 mm.
- The total annual rainfall in the Dry zone is less than 1250 mm.

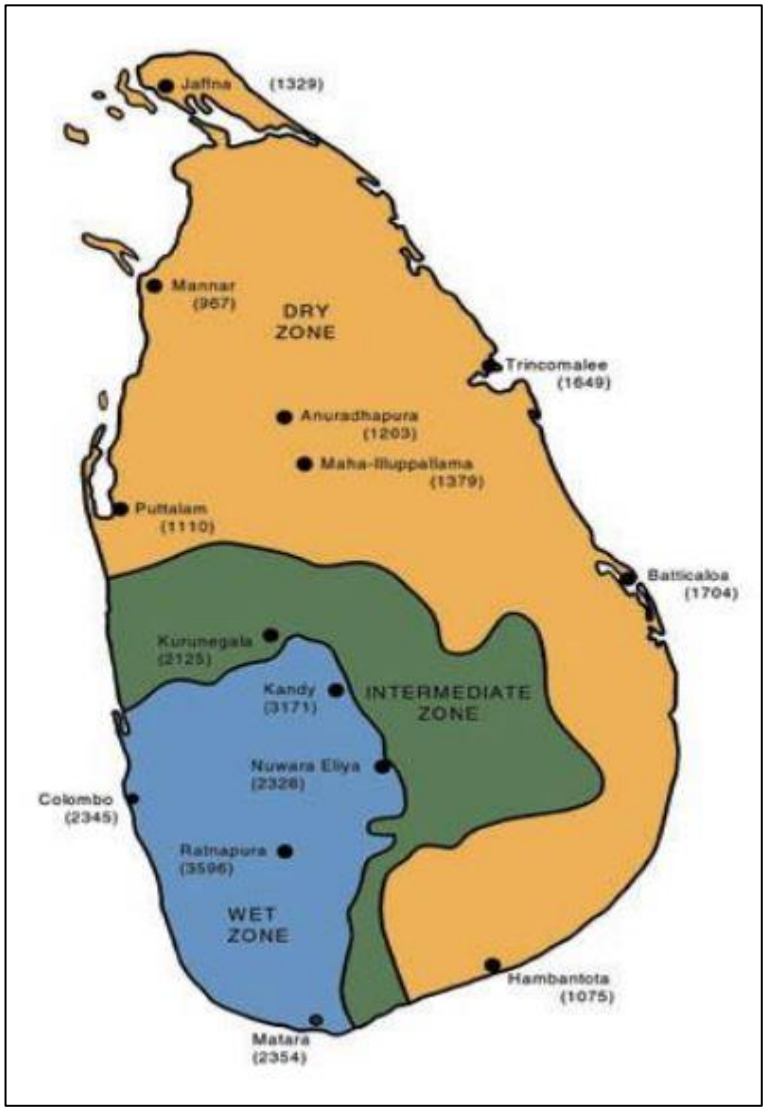

Figure 2-2: Climatic zones in Sri Lanka

(Source: Samarasinghe, 2009)

Table 2-1 shows the rate of temperature increases from 1961 to 1990 was 0.016° C annually, which is greater than the world average rate of 0.013° C annually from 1956 to 2005, according to the IPCC report of 2007 (Eriyagama & Smakhtin, 2009).

Table 2-1: Observed changes in Temperature

(*Source:* Samarasinghe, 2009)

	1901-2000			1961-2000		
Station	**Minimum**	**Maximum**	**Mean**	**Minimum**	**Maximum**	**Mean**
Nuwara Eliya	2.00	-0.04	0.98	1.80	-1.12	0.34
Anuradhapura	1.35	0.73	1.04	1.64	2.53	2.09
Ratnapura	0.69	0.31	0.50	1.60	0.28	0.94
Kurunegala	1.26	1.00	1.13	0.40	1.48	0.94
Colombo	0.50	0.34	0.42	1.36	0.92	1.14
Puttalam	0.63	2.09	1.36	-0.16	1.40	0.62

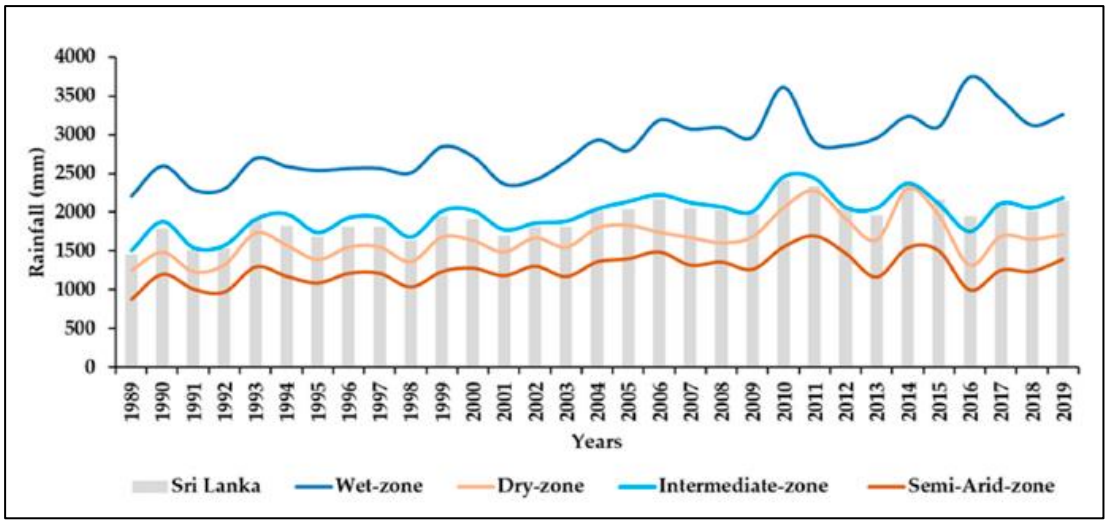

Figure 2-3 Annual average rainfall distribution in wet, dry, intermediate, semi-arid zones, and Sri Lanka Source

Source: (Alahacoon & Edirisinghe, 2021)

From 2015 to 2019, the wet zone and the dry zone received relatively low rainfall. The wet zone received relatively higher rainfall as a comparison to other zones. The intermediate-zone annual average rainfall was observed to be almost the annual average rainfall of Sri Lanka.

2.1.2 Past Significant floods in the study area

According to the annual maximum water levels in Thawalama since 1979, the May 2003 flood was the worst as shown in Figure 2-4. Major floods have occurred in the basin in 1979, 1993, 1999, and 2003 (Ministry of Disaster Management and Human Rights, 2009).

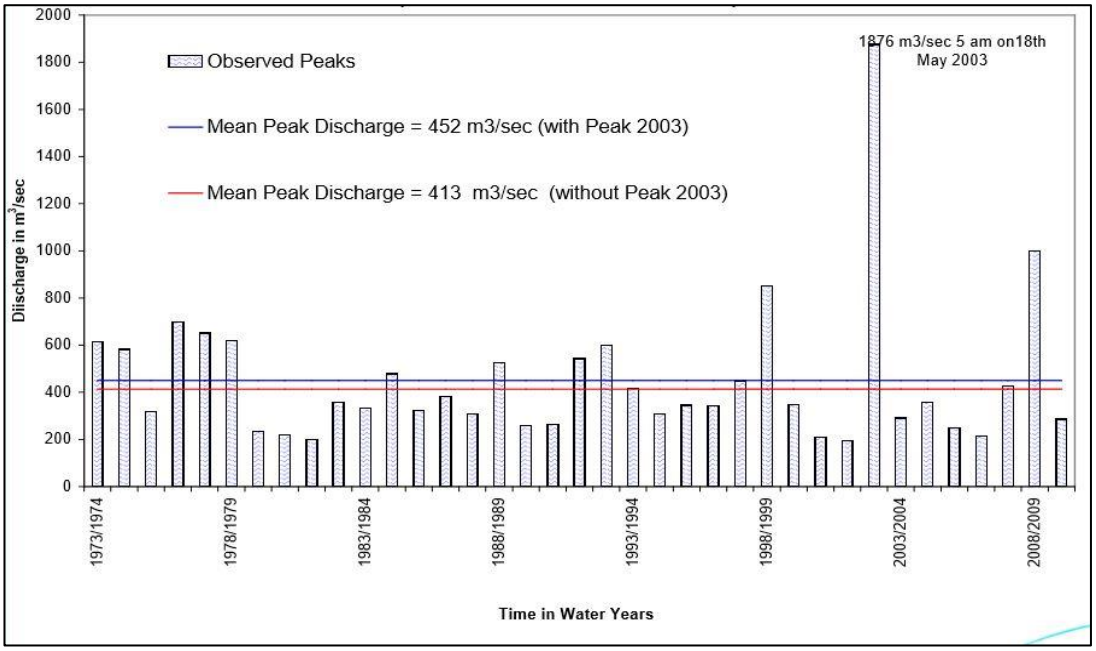

Figure 2-4: Frequency analysis of the flood at Thawalama station

(*Source*: Irrigation Department & Survey Department, 2011)

2.2 Data and Data Checking

A visual data check was performed for all stations by producing hydrographs and double mass curve plots to ensure the correctness of the acquired data. Visual and statistical checks were used to identify missing data periods and inconsistencies.

Missing Data

To obtain more realistic conclusions from hydrologic results, the confidence level for the given data must be determined by data validation. (Wijesekera & Perera, 2012). When dealing with complicated water resource systems, streamflow data from several locations is essential for watershed management planning and design. Although a few series may be sufficient, it is typically discovered that many are insufficient. In addition, an inadequate

dataset complicates and reduces the model's reliability. As a result, before the series can be used in practice, missing data must be filled up (Campozano et al., 2014).

Spatial interpolation procedures are frequently used methods for gap filling in daily rainfall series by predicting the unidentified rainfall quantity using known data from neighbouring stations to some extent (Hasan & Croke, 2013). In the literature, there are three primary types of infill approaches. They are deterministic techniques, (ii) stochastic methods, and (iii) artificial intelligence techniques (Jara Torres et al., 2016). The closest station strategy for filling in daily missing data performs admirably (B. I. L. Garcia, Sentelhas, 18 Tapia, & Sparovek, 2006). Spatial interpolation techniques like inverse distance, normal ratio, arithmetic average, correlation coefficient, and so on relate to the process of predicting unidentified data values for a point utilizing well-known data values from adjacent stations (Ismail & Ibrahim, 2017). Another research evaluates four data filling methods: "simple substitution," "classical least squares univariate parametric regression," "ranked regression," and the "Theil approach." Furthermore, a distance of 10 km between meteorological stations is sufficient to account for spatial fluctuation of the station. As a consequence of the studies, the simple replacement has adequate reliability for filling missing data. Empirical approaches, statistical methods, and function fitting can all be used to estimate missing data. Among the traditional approaches, multiple regression analysis is the most suited. Thiessen polygon spatial interpolation was used as a result because station sites are stable and do not fluctuate spatially (Hasanpour & Dinpashoh, 2012).

The quality and consistency of data decide the effectiveness of data analysis. This research is aimed at several methods for filling in missing rainfall data. Monthly rainfall data gathered at six distinct locations was used to evaluate the appropriateness of the various strategies for filling in missing data. Monthly rainfall is estimated using complete sets (no missing variables). The arithmetic averaging approach, multiple linear regression, and the non-linear iterative partial least squares algorithm outperform the others. The multiple regression techniques successfully estimated the missing precipitation data, as evidenced by the findings reported in the literature (Sattari et al., 2017).

To establish the best approach for filling in the missing precipitation data in Ethiopia, 21 traditional methods were investigated. The monthly data obtained from fifteen

distinct stations from 1980 to 2013 were taken into account. The data was checked using homogeneity and trend tests. With Pearson correlation coefficient (Pearson's r) of 0.94, mean absolute error of 22.90 mm, Root mean square error (RMSE) of 33.69 mm, similarity index of 0.99, Coefficient of efficiency (CE) index of 0.99, and skill score of 0.99, the Normal ratio technique delivers the most accurate estimations. When the observed and estimated findings from the Multiple Linear Regression, Normal Ratio, Correlation Coefficient Weighted, Inverse Distance Weighting, and Simple Arithmetic Average methods, the Mean absolute error (MAE) and Root mean square error (RMSE) were found to be low, and high values of Coefficient of efficiency (CE), Skill score (SS), Similarity index (S-index), and Pearson correlation coefficient (Pearson's r) were achieved (Armanuos et al., 2020).

2.3 Climate Change

A Representative Concentration Pathway (RCP) scenario

A Representative Concentration Pathway (RCP) is a greenhouse gas concentration trajectory proposed by the IPCC in its 5th Assessment Report (AR5) in 2014, which recommended 4 pathways for climate modeling and research representing diverse climatic situations. RCP 2.6, RCP 4.5, RCP 6, and RCP 8.5 are the names of the four RCPs.

Emissions continue rising in RCP 8.5 throughout the twenty-first century (Meinshausen, et al., 2011) as demonstrated in Figure 2-5.

Figure 2-5 shows that the RCP 8.5 was adopted as the worst high emission scenario in this study, out of the four scenarios accepted by the IPCC's 5th assessment report (IPCC, 2014).

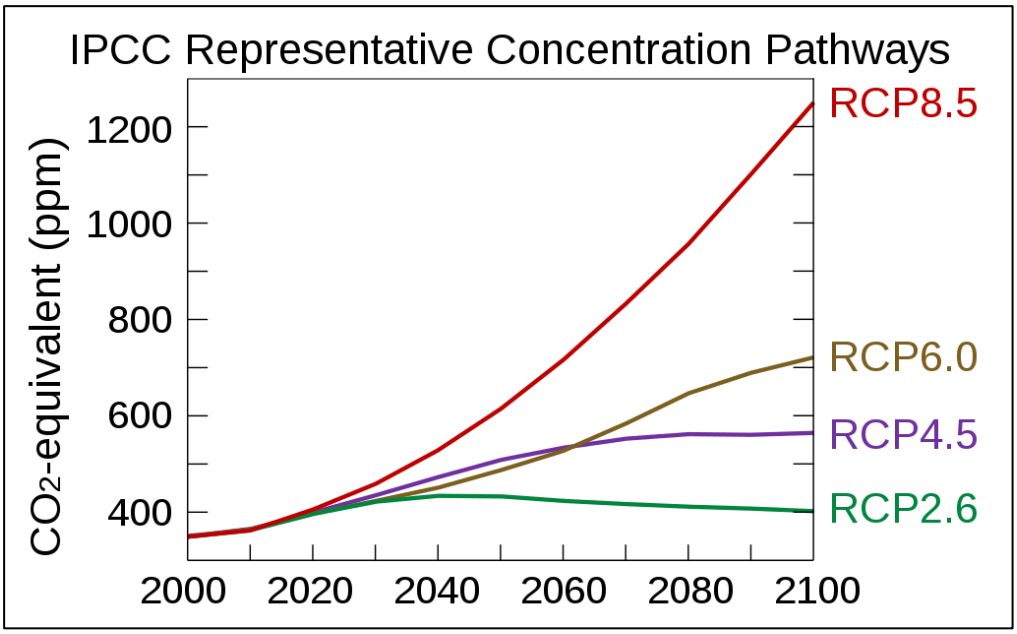

Figure 2-5: Projected atmospheric greenhouse gas emissions for the four RCP Scenarios

(*Source: IPCC,2014*)

2.4 Bias Correction

1) Linear scaling (LS)

The LS approach attempts to match the monthly average of revised values to that of observed data perfectly. It employs monthly adjustment values depending on observed and raw data differences. Monthly, rainfall is frequently compensated with a multiplier and temperature with an additional term (Fang et al., 2015).

$$P_{hst,m,d}^{cor} = P_{hst,m,d} * [\frac{\mu(P_{obs,m})}{\mu(P_{hst,m})}] \quad [2\text{-}1]$$

where 'P_{cor}, m, d' is modified precipitation on the d^{th} day of m^{th} month, 'P_{raw}, m, d' is the raw precipitation on the d^{th} day of m^{th} month and, '$\mu(P_{obs}, m)$' represents the mean value of observed precipitation at a given month m whereas '$\mu(P_{hst}, m)$ represents the mean value of historical precipitation at a given month m.

2) Power transformation (PT) of precipitation

To further alter the standard deviation of a precipitation series, the Power transformation approach employs an exponential form. Because the Power transformation is limited in its capacity to fix the wet-day probability (Fang et al., 2015).

For the implementation of the PT method, firstly, estimate b_m, which minimizes

$$f(bm) = \left[\frac{\sigma(Pobs, m)}{(\mu(Pobs, m)}\right] - \left[\frac{\sigma(Pbm\ LOCI, m)}{(\mu(Pbm\ LOCI, m)}\right] \quad [2\text{-}2]$$

Where 'σ'represents the standard deviation, 'b_m' is the exponent for the m^{th} month, and 'P_{bm} LOCI, m' is the LOCI corrected precipitation in the m^{th} month.

If 'b_m' is greater than one, the LOCI-corrected precipitation has a smaller coefficient of variation in month 'm'.

2.5 Flood Frequency Analysis

The statistical technique has the considerable benefit of estimating floods at any place in a homogeneous region with very little or no data. Annual peak discharge data of the Kosi River at the Kosi barrage Ramnagar were collected for the study from measurements recorded by the Irrigation Department Ramnagar from 1985 to 2014 (30 years of flood data). The Gumbel, and Log Gumbel distributions, the Normal, the Pearson type III, Log-Normal, the Log Pearson type III, were used in the on-site analysis of yearly flood series using the technique of moments. The value (R^2) indicates a dispersed and thin pattern. The highest (R^2) value of the Log Gumbel distribution has been determined to be 0.96. As a result, the best-fit distribution for projecting predicted flow in the Kosi Rivers using the method of a moment as parameters estimate was the Log Gumbel distribution for the Kosi River and other locations in the region (Sah, 2015).

Peak discharge (Q_p) and Corresponding Return Period (T) may be linked mathematically and graphically. Simple statistical equations, such as the Weibull

formula, California formula, Hazen formula, etc., which are commonly employed in the practical field, were used in this work. The model was chosen based on the extremely satisfying values of Average percent Deviation, Standard Deviation of percent Deviation, and Correlation co-efficient between the parameters studied (Mukherjee, 2012).

2.6 Hydrological Model and Flood inundation model

The US Army Corps of Engineers developed the HEC-HMS hydrological model in 1998. The HEC-HMS is predominantly an event-based model (Feldman, 2010), It is currently commonly utilized for continuous rainfall and runoff simulation. It can replicate both short-term and long-term runoff occurrences (Gebre, 2015). It is useful not just for modeling runoff from rural watersheds, but also for estimating discharge from urban watersheds (Gholami & Mohseni Saravi, 2010; Goff & Gentry, 2006). Feldman (2010) stated that most of the processes in HEC-HMS are empirical.

As floods and their severe consequences are frequent in many regions of the world, there is a growing public, governmental, and scientific awareness of the importance of appropriate flood control and management (Becker & Grünewald, 2003).

The US Army Corps of Engineers Hydrologic Engineering Center developed the Hydrologic Engineering Center-River Analysis System (HEC-RAS) and is available for free download, along with additional supporting documentation on how to utilize the model for mapping for the flood. The HEC-GeoRAS is a GIS extension that contains a collection of methodologies, tools, and utilities for preparing River geometry data for input into HEC-RAS and producing the final inundation map (Gebre SL, 2015).

2.6.1 HEC- HMS model parameters

Table 2-2 HEC- HMS parameters (US Army Corps of Engineers, 2018)

Hydrologic Element	Calculation Type	Method
Sub-basin	Canopy	Dynamic, Simple (also grided)
	Surface	Simple (also grided)
	Loss Rate	Deficit and constant (also gridded), Exponential Green and Ampt (also gridded), Initial and constant SCS curve number (also gridded), Smith Parlange, Soil moisture accounting (also gridded),
	Transform	Clark unit hydrograph, Kinematic wave, Mod Clark, SCS unit hydrograph, Snyder unit hydrograph, User-specified s-graph, User specified unit hydrograph
	Baseflow	Bounded recession, Constant monthly, Linear reservoir, Nonlinear Boussinesq, Recession
Sub-basin Reach	Routing	Kinematic wave, Lag, Lag and K, Modified Puls, Muskingum, Muskingum-Cunge, Normal Depth, Straddle stagger
	Gain/Loss	Constant, Percolation

Table 2-2 shows the types of methods available for HEC-HMS modeling under two hydrological elements Sub-basin and Sub-basin reach.

SCS Curve Number (CN) method to estimate the loss, SCS Unit Hydrograph method as a transform method, Muskingum method routing method was used for Event modeling on Ravi River catchment area in the Pathankot district of Punjab, India (Singh et al., 2019).

A) *Subbasin Element calculation*

- ***Simple canopy method-***

  Initial canopy storage (%): It is an initial condition input that reflects the percentage of the maximum canopy storage that has been filled at the start of the simulation. They advocated starting the simulation after a time of no rainfall, which makes a value of 0% reasonable as an initial value. This assumption must be observed when selecting simulation periods later in the hydrologic modeling process (Ahbari et al., 2018).

  Max canopy storage (mm): A formalism parameter reflecting the maximal depth of water that vegetation may intercept. The original value is estimated using the basin's SCS land use map, and the suggested values are mentioned in Table 2-3 (Ahbari et al., 2018).

Table 2-3 Max Canopy Storage (Ahbari et al., 2018)

Types of vegetation	Max canopy Storage (mm)
Species of vegetation is not directly known	1.27
Grasses and deciduous trees	2.03
Coniferous trees	2.54

- ***Surface Storage***

  Initial surface storage (%): It is an initial condition input that reflects the percentage of the maximum surface storage that has been filled at the start of the simulation. As a beginning value, they advise starting the simulation after a time of no rainfall, which causes all of the water held in the basin depression to either

evaporate or infiltrate. A value of 0% is reasonable in this situation (Ahbari et al., 2018).

Max surface storage (mm): It is calculated in proportion to the catchment surface's slope (%) and the suggested values are mentioned in Table 2-4.

Table 2-4 Surface Canopy (Ahbari et al., 2018)

Surface Description	Slope (%)	Max surface storage(mm)
Paved impervious area	NA	3.2-6.4
Steep, smooth slopes	>30	1
Moderate to gentle slope	5-30	12.7-6.4
Flat, Furrowed land	0-5	50.8

- ***Loss Rate***

  SCS CN loss method parameters' estimation-

  The water balance equation serves as the foundation for the SCS curve number approach (Handbook of Hydrology, 1972).

  a) **Percent of impervious (%):** An non calibrated input parameter representing the percentage of the basin surface that is impervious to and directly related to the streamflow (Ahbari et al., 2018).

  b) **Curve Number (CN):** An input parameter that is mostly determined by the SCS soil and land use maps. The SCS method was initially created for use in 15 km^2 watersheds, but it has been adapted for use in larger watersheds by weighting curve numbers according to watershed/land cover area. The Weighted CN equation is given below (Tailor & Shrimali, 2016).

$$CN_w = \frac{\sum(CN_i * A_i)}{A} \quad [2\text{-}3]$$

  Where, CN_w = weighted curve number, CN_i = curve number from 1 to any number, Ai = area with curve number CNi

c) **Initial abstraction I_a (mm):** It denotes the existence of vegetation that prevents permanent or intermittent precipitation from reaching the soil's surface (Ahbari et al., 2018).

$$I_a = 0.2S \quad [2\text{-}4]$$

$$S = \frac{25400}{CN} - 254 \quad [2\text{-}5]$$

Where, I_a = initial abstraction, S = the potential infiltration, CN= Curve number

- ***Transform***

  Mockus invented the SCS method for the watershed lag in 1961. It encompasses a wide range of circumstances, from severely forested watersheds with sharp channel slope and a high percentage of runoff occurring from subsurface flow through grazing land with strong surface runoff retardance, to smooth land surfaces and huge paved areas (USDA-NRCS, 2010).

- **Time of Concentration-** Time of concentration (Tc) is the time amount of time it takes for runoff to flow from the furthest distance point in the watershed to the outlet (USDA-NRCS, 2010).

- **The Kirpich Equation-** According to Subramanya (2013), formula relating the time of concentration to the length of transit and catchment slope as

$$t_c = 0.01947 L^{0.7} S^{-0.385} \quad [2\text{-}6]$$

t_c= time of concentration (minutes)

L = maximum length of travel of water (m), and

S = catchment's slope = $\Delta H \,/\, L$ in which

ΔH = difference in altitude between the catchment's most distant point and the outflow.

- **Relation between lag and time of concentration-**

According to USDA-NRCS (2010), For average natural watershed conditions and approximately uniform distribution of runoff:

$$L = 0.6T_c \quad [2\text{-}7]$$

Where, L= lag, h, and T_c = Time of concentration, h.

- **Baseflow**

According to Hall (1968), baseflow is the percentage of the flow that originates from groundwater or other delayed sources. Appleby (1970) expanded on the recession and baseflow problem, citing Hall's work in particular.

Ahbari et al (2018), explained method for calculating baseflow recession as-

- Using the daily discharge, identify all hydrograph occurrences (instant discharge is better),
- For each event do the following: enlarge the portion of the decreasing discharge with the slowest slope,
- Calculate Kr (Constant recession) using the equation,

$$k_r = t\sqrt{\frac{Q_t}{Q_0}} \quad [2\text{-}8]$$

Where, Q_t is discharge at time t after the peak; Q_0 is the initial discharge at the beginning of the event, t is the time step.

B) *Sub-basin Reach Element calculation*

Routing

Muskingum Routing Method-

According to the US Army Corps of Engineers (2018), The Muskingum *K* parameter is comparable to the travel time of reach. A variety of methods are available to calculate this parameter, including:

- **Using known hydrograph data-** The variation between "similar locations" on known inflow and outflow hydrographs can be used to estimate the travel duration of a flood wave flowing through a reach. Similar locations may be the peaks of either hydrograph, the centroid of the region beneath each hydrograph, or the intersection of any reference flow on either hydrograph's ascending limb.
- **Comparison of the flow length to a flood flow velocity-** The travel time, T, of a flood flow moving through a reach may be calculated by dividing the reach length, L, by the flood flow velocity, v_w:

$$T = \frac{L}{v_w} \qquad [2\text{-}9]$$

Several methodologies may be used to determine flood wave velocity:

a) Manning's Equation (Manning, 1891)
b) Kleitz-Seddon Law (Seddon, 1900)

Kleitz-Seddon Law:

$$v_w = \frac{1}{B}\frac{dQ}{dy} \qquad [2\text{-}10]$$

Where, B = the water surface top width and $\frac{dQ}{dy}$ = slope of the flow-stage rating curve

- Using regression equations derived from observed data in a similar region.

According to the US Army Corps of Engineers (2018), The Muskingum *X* parameter is a dimensionless coefficient with no physical significance. This value must be between 0.0 and 0.5. When this parameter is set to zero, the storage area inside the reach is calculated entirely based on outflow. If the parameter is set to 0.5, the inflow and outflow are given equal weight when evaluating the storage area within the reach. In conclusion, there is no attenuation of the input hydrograph as it travels along the reach. In most cases, for model calibration, '*X*' is initially taken as 0.25.

2.6.2 HEC- RAS model development

Within the software's unsteady flow analysis, HEC-RAS can perform two-dimensional (2D) hydrodynamic routing. 2D flow modeling is performed by introducing 2D flow area components into the model in a similar manner that a storage area is added. A 2D flow area is created by illustrating a 2D flow area polygon, creating a 2D computational mesh, and then linking the 2D flow areas to 1D model components and directly attaching boundary conditions to the 2D areas (Brunner, 2021).

- ***Developing a Terrain Model and Geospatial Layers***

A precise and detailed terrain model is required to produce an accurate and detailed hydraulics model. The user's ability to develop a high-quality hydraulics model may be limited by the quality of the topographical data. Terrain data is derived from a variety of formats, sources, and levels of information. HEC-RAS presently models topography using gridded data.

Terrain data should be exported into a gridded data format that HEC-RAS can read (Brunner, 2021).

- ***Spatial Reference Projection***

Firstly, Terrain data should be projected to the required coordinate for the catchment area. Establishing a spatial coordinate system is not mandatory (for example, in the case of evaluating imaginary data), although it has several benefits in HEC-RAS Mapper. Choose the set projection menu item from the RAS Mapper menu bar and enter the project's spatial reference system. (Brunner, 2021).

Using Manning's n values creating Land cover

Land use Land cover (LULC) is used to allocate Manning's n value, with reference to Manning's n values applied for the NLCD map. (Tenzin & Bhaskar, 2017).

In RAS Mapper, a spatially variable land cover layer may be produced and subsequently correlated along with a certain geometry data set. Manning's n values for every land cover type can be defined after creating Land cover type data collection. Furthermore, the land cover category polygons (user-defined polygons) can be created if required and override the base land cover layers inside those polygons to create a new land cover type. After creating a Landcover layer, a calibration region may be created and can be associated with a chosen Geometry data collection. To override all Manning's n values related to land cover inside the polygon, a Calibration Region polygon is employed. Calibration Regions are created for a certain Geometry and do not affect the basic land cover/n Manning's value layer (Brunner, 2021).

1. The 2D Model development

According to Brunner (2021), HEC-RAS can be used to develop a 2D Model or a combined 1D/2D model by-

- Construction of a 2D computational mesh
- Constructing hydraulic property tables for 2D Flow Areas
- Linking 2D Flow Areas with 1D hydraulic elements
- Hydraulic structures within the 2D Flow Areas
- Geospatial coordinates for hydraulic outlets linked to 2D Flow Areas
- Modeling bridges within 2D Flow Areas
- Modeling Pump Stations within 2D Flow Areas

a. The 2D Computational Mesh development

The Finite-Volume solution approach is used by the HEC-RAS 2D modeling capabilities. This approach was designed to work with either a structured or unstructured computational mesh. Hence, the computational mesh can be a combination of 3-edge, 4-edge, 5-edge, and so on (HEC-RAS has a maximum of 8 edges in a computational cell). A nominal grid resolution adopted by most of the

operators is ‘200 ft x 200 ft, and the automatic tools in HEC-RAS will generate the computational mesh (Brunner, 2021).

b. Boundary and Initial Conditions

According to Brunner (2021), external boundary conditions of four types may be directly linked to the boundary of 2D Flow Areas: -

- Flow Hydrograph
- Stage Hydrograph
- Normal Depth
- Rating Curve

The rating curve and the normal depth criteria may only be used when the flow is about to escape a 2D flow zone. The boundary conditions for flow and stage hydrographs can be used to insert or remove flow from a 2D flow area. Positive flow values direct flow into a 2D flow zone, whereas negative flow values direct flow away from a 2D area. The flow will be delivered in by stages greater than the water surface in a 2D flow zone, while flow will be delivered out by stages smaller than the water surface in the same 2D flow region.

$$v_w = \frac{1}{B}\frac{dQ}{dy} \qquad [2\text{-}11]$$

c. Variable Time Step Capabilities

The unsteady flow engine now has variable time step capabilities for both 1-D and 2-D unsteady flow modeling (Brunner, 2021).

When choosing the computing time step, aim to meet the Courant Condition to gain stability and accuracy. In general, a lower time step results in a less incremental change inside the calculation and a more stable model (Mountz & Crowley, 2009).

Mihu-pintilie et al (2019), To assure the model's stability, the time steps were approximated using the Courant–Friedrichs–Lewy condition c,

$$C = \frac{V\Delta T}{\Delta x} \leq 1.0 \text{ (With } C_{max} = 3.0) \qquad [2\text{-}12]$$

where C = Courant number, V = flood wave velocity (m/s), ΔT = computational time step (s), and Δx = average cell size (m).

2.6.3 Objective function

The objective function is utilized to assess the outcome of the hydrological model simulation. Unlike manual calibration, automated calibration employs a visual evaluation of similarities and contrasts between model simulations and data. As a result, The goodness-of-fit among the estimated outflow and observed streamflow at the specified element is measured by the objective function (US Army Corps of Engineers, 2018).

Three prominent measures, namely the coefficient of determination (R^2), percent deviation (P-bias), and Nash–Sutcliffe efficiency (NSE), were derived from actual and simulated flows to assess model performance. The R^2 values show how closely the simulated flow follows the fluctuations of the measured flow, P-bias indicates the mean percent divergence between the simulated and measured flows, and P-bias shows how well the simulated plot corresponds with the observed figure (Mahmood & Jia, 2016).

2.7 Flood Hazard Assessment

2.7.1 General Concept Flood Hazard

The Riverine flood "magnitude" is often assessed as stream discharge, which may subsequently be used to determine water surface elevation (WSE), and consequently flood depth, at several sites along a stream. For example, in particular stream cross-sections and appropriate topography, a stream discharge with a 0.01 likelihood of exceedance per annum may be utilized to compute the elevation with a 0.01 probability of being surpassed by floodwater. Flood hazard is defined by the depth of flooding and the yearly likelihood of inundation higher than that depth, which is illustrated in a depth-frequency curve (Scawthorn et al., 2006).

Flood hazards are classified as major primary hazards, secondary hazards, tertiary hazards. The primary hazards are flood-related consequences caused by direct contact with floodwaters. Streams with high velocities can convey bigger particles as suspended load. These huge particles may contain not just boulders and dirt, but also major things such as automobiles, homes, and bridges during the flood. Secondary hazards are those that arise because of the primary hazards (flooding), for example, service interruption and health damage (food crisis and infection). Long-term changes, such as alterations in the environment, are examples of tertiary hazards (Buslima et al., 2018).

2.7.2 Past literature on Flood Hazard, Vulnerability and Risk Assessment

The flood hazard assessment is the calculation of the total unfavorable impacts on flooding in a certain location. It is determined by several factors, including the flood depth, the flood duration, the velocity of the flood waves, and the rate at which the water level rises. Depending on the features of the research region and floods, one or more parameters may be incorporated in the hazard assessment. For the evaluation of the hazard of land areas investigated, two primary elements, namely depth of flooding and percentage area of flooding, were taken into account based on the features of the research region (Nandalal & Ratnayake, 2010).

Vulnerability is a measure of an element's inherent susceptibility to potentially harmful natural events. The vulnerability is measured on a level of 0 (no loss) to 1 (complete loss). The vulnerability factor (VF) for every land unit was calculated utilizing data such as the type of material used for the floor and walls, as well as the density of structures per land unit (Nandalal & Ratnayake, 2010).

Many elements must be considered when calculating flood risk in a given location. Population, irrigation infrastructure, soil erosion potential, soil utility for agriculture, shopping market locations, transportation network, and overall infrastructure in the Kelantan River basin was used to produce a flood vulnerability index (Ibrahim et al., 2017).

Table 2-5 shows the flood vulnerability for the different categories which was classified at Kalapara Upazila in Bangladesh (Hoque et al., 2019).

Table 2-5 Flood Vulnerability classification (Hoque et al., 2019)

Flood Vulnerability classes	Population density (km²)	Literacy rate (%)	Elevation (m)
Very Low	<360	>55	>10
Low	360-400	50-55	7-10
Moderate	400-450	45-50	5-7
High	450-500	40-45	2-5
Very High	>500	<40	<2

In the lower reach of the Kelani River basin, flood inundation mapping examines anticipated high precipitations and resultant flood inundation along the lower Kelani River. The granular grid atmospheric characteristics are given by Global Climate Model (GCM) models for the Intergovernmental Panel on Climate Change (IPCC, 2007) scenarios A2 (high emission scenario) and B2 (low emission scenario) were downscaled to the local level utilizing the Statistical Downscaling Model (De Silva et al., 2012).

Flood hazard assessment in the Upper Ping River basin, Thailand was carried out, as well as performance assessment of local adaptation strategies. 1D and 2D hydrodynamic models were created and calibrated using observed discharge and water level (1D) and flood extent (2D). Flood inundation and hazard maps were recreated and classified into several groups based on determining critical depths for return periods of 2, 5, 10, 25, 32, 50, and 100 years (Tansar et al., 2021).

A GIS-based method was used to identify Kelantan's (of Malaysia) most susceptible sub-basins and develop flood risk maps that show the geographical distribution of risk as well as the locations and frequency of events that are likely to occur. Using the GIS, each parameter was converted into a grid spatial database. The technique relies on

indices designed to quantify several forms of flood risk to determine the relative susceptibility of the Kelantan River basin and sub-basins (Ibrahim et al., 2017).

The evaluation and mapping of social flood risk in West Africa's Lower Mono River Basin used GIS, Remote Sensing, and indicator-based flood risk assessment approaches to map flood disaster risk (Ntajal et al., 2017).

"Flood Hazard, Vulnerability, and Risk Assessment for Different Land Use Classes Using a Flow Model" is focused on assessing flood risk by combining GIS, hydraulic modeling, and relevant field information. A significant aspect of flood risk assessment is that, while the flood hazard in a particular location is the same in terms of severity, the risk might vary based on a combination of variables (flood vulnerability). Risk is determined by hazard and vulnerability (Baky et al., 2020).

"Large-scale flood hazard assessment under climate change: A case study" focused on the Flood Hazard Index (FHI) map, which was created using a multi-criteria index approach based on defining the greater influence of seven flood-related factors: distance from the drainage network, runoff coefficient, elevation, slope, land use, and rainfall intensity (Shadmehri Toosi et al., 2020).

Ongdas et al (2020), At Yesil (Ishim) River in Kazakhstan, the flood inundation areas were classified according to flood hazard classes as shown in Table 2-6.

Table 2-6 Flood Hazard classification (Ongdas et al., 2020)

Flood Hazard Classes	Flood depth (m)	Velocity
Very low	<0.5	<0.01
Low	0.5-1.0	0.01-0.05
Medium	1.0-2.0	0.05-0.1
High	2.0-5.0	0.1-1.0
Extreme	>5.0	>1.0

2.7.3 IPCC conceptualization of Vulnerability, Exposure, and Risk

The IPCC AR5 defines risk as "the possibility of consequences if something of value is at stake and the result is unpredictable, taking into account the range of values." The interplay of hazard, vulnerability, and exposure produces risk." (Pelling, 2006). Hazard is described by the IPCC as "the possible existence of a natural or human-induced physical event that may result in loss of life, injury, or other health consequences, as well as damage and loss to property, livelihoods, infrastructure, service provision, and environmental resources.". Vulnerability is defined as "the tendency or inclination to be negatively influenced." Vulnerability involves several theories, including sensitivity to damage and a lack of ability to cope and adapt.(Pelling, 2006). Exposure, on the other hand, is described as "the presence of people, livelihoods, environmental services, species or ecosystems, and resources, infrastructure, or economic, social, or cultural assets in potentially adversely affected areas" (Pelling, 2006). According to this concept, exposure is frequently measured by locating people and infrastructure items in a zone possibly affected by a natural disaster.

Since the risk is a function of hazard and vulnerability. To calculate risk assessment, the predicted loss of the risk element was calculated by first combining the alternative values assigned to the components and then using the stage-loss function (Baky et al., 2020).

Flood risk is defined as a composite of flood hazard, exposure, and vulnerability. Flood risk can be expressed as-

$$\text{Flood Risk} = (\text{Hazard}) \times (\text{Exposure}) \times (\text{Vulnerability}) \qquad [2\text{-}13]$$

CHAPTER 3

3 MATERIALS AND METHODS

3.1 Study Area

- Thawalama catchment is a sub-catchment of the Gin Ganga basin (Figure 3-1) that is approximately 355 km² in the area and is located in the Galle, Matara, and Kalutara districts, bordering the Kalu Ganga basin to the north and the Nilwala Ganga basin to the south. The selected catchment is in Sri Lanka's wet climatic zone.
- Thawalama River initiates in the Gonagala mountains in Deniyaya, in the Matara district of Sri Lanka's Southern Province, and runs approximately 75 kilometers through Tawalama, Neluwa, and Agaliya before entering the Indian Ocean in Gintota, Galle.
- The catchment's main soil type is Red Yellow Podzolic, with hilly, rolling topography.
- The catchment's average temperature is around 28 degrees Celsius.

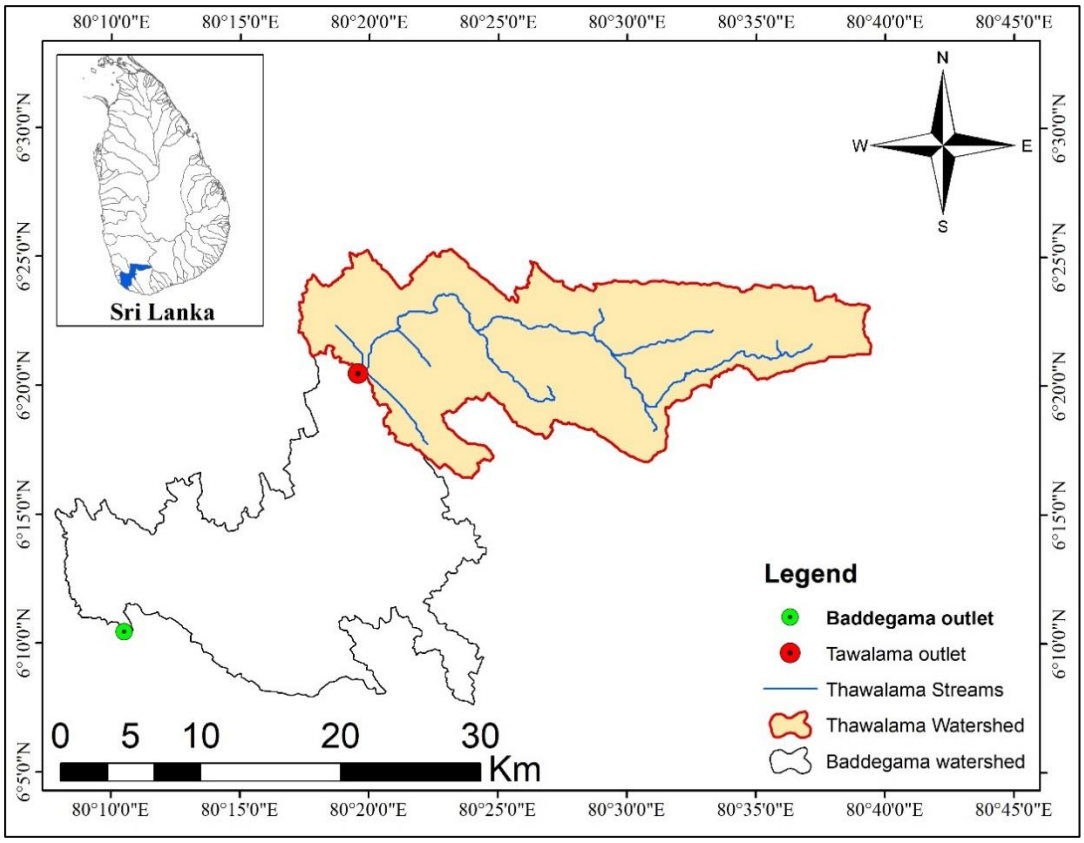

Figure 3-1: Study Area

- Geographical coordinates at the outlet of Thawalama catchment –06°03′47″N 80°10′27″E
- The Gin Ganga basin is mostly affected by southwest monsoon rainfall, and floods are common in May and June. Floods occur during the October-November inter-monsoon season, though to a smaller extent than during the May-June monsoons (Seneviratne, 2004).
- The mean annual flow into the sea is around 1,600 million cubic meters and the average annual rainfall is about 3048mm.

3.2 Justification of Study Area

The Gin Ganga is one of the most flooded Rivers in Sri Lanka. Hence, flood hazards and vulnerabilities should be properly documented for mitigation measures. To control flood damages many projects have been proposed and are ongoing along the lower reaches of Gin Ganga. Levees, spillway, pumping stations for drainage, water gates, bridges, diversion aqueducts of about 30 m in width around the downstream area are some of the existing flood control structures of the 182 km² area in the 22 km or so the interval between Agaliya and the mouth of the Gin Ganga River (Yoshitani et al., 2007).

Population density is one of the essential elements for flood vulnerability. Hence, it is essential to know the population density from present to future.

Population density for the present year 2022 and future years (2060 and 2100) has been documented below using various vulnerability categories (Hoque et al., 2019).

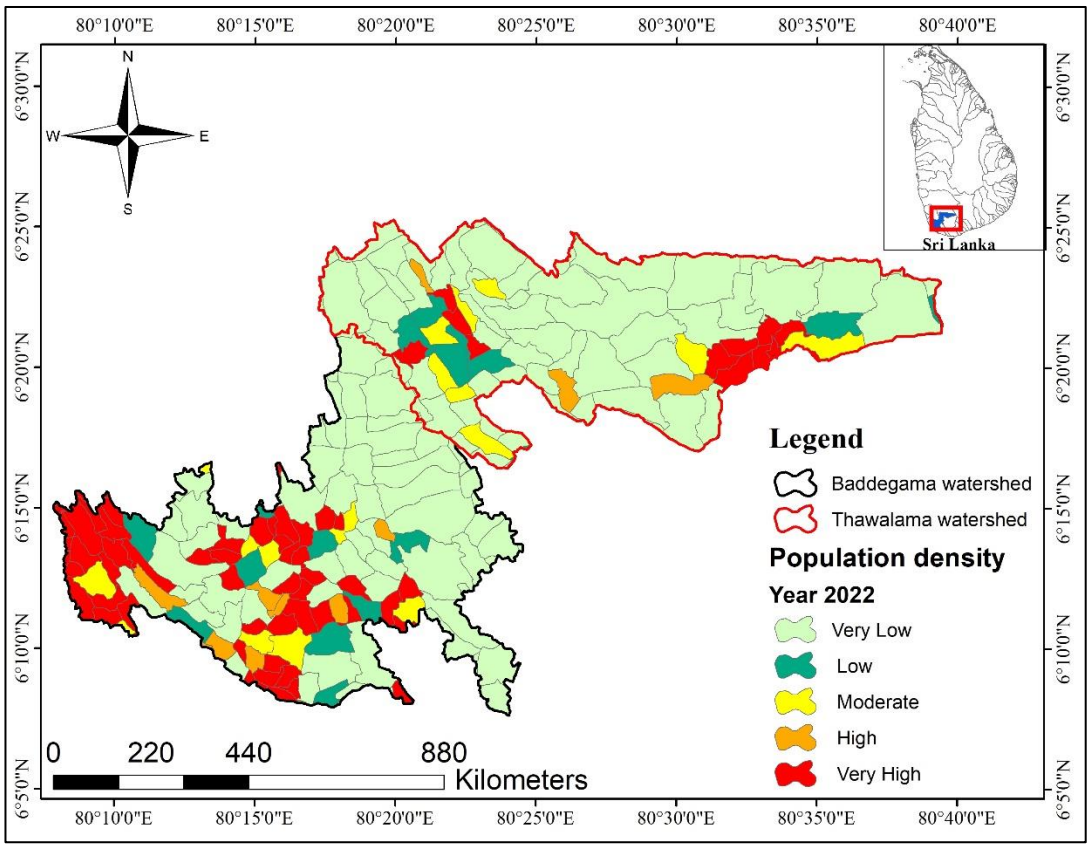

Figure 3-2 Population density in the year 2022 at Lower and Upper Gin Ganga

Figure 3-2 gives a clear view that Gin Ganga is most vulnerable to flooding at lower reaches in the present year of 2022.

The present year 2022 population and future population for the year 2060 and 2100 was forecasted from the present population census available in Sri Lanka (Department of Census and Statistics, 2012).To forecast population for the present year 2022, and future years (2060 and 2100), the geometric increase method was used from the previous literature study “Comparative Study of Population Forecasting Methods” (Gawatre et al., 2016).

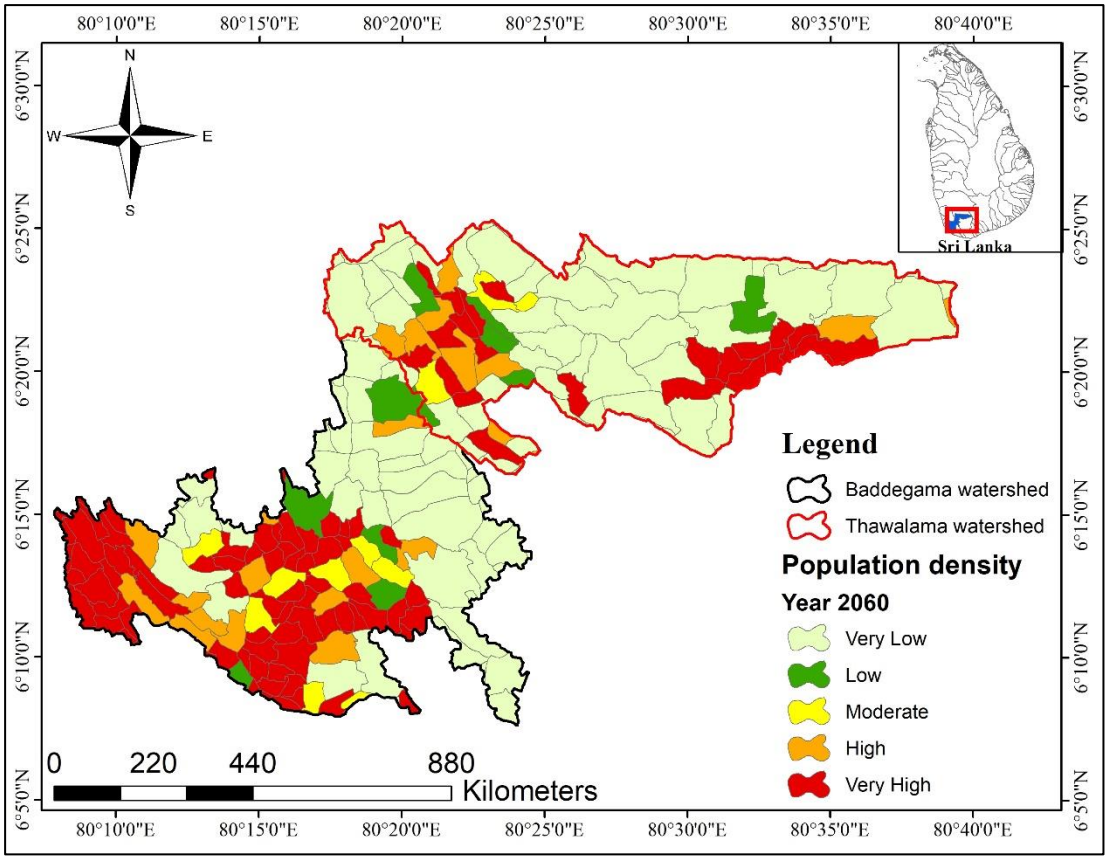

Figure 3-3 Population density in the year 2060 at Lower and Upper Gin Ganga

Figure 3-3 gives a clear view that in the year 2060 flood vulnerability at the lower reaches of Gin Ganga is high as compared to Upper Gin Ganga. Also, it can be seen from Figure 3-2 and Figure 3-3 that how vulnerabilities area of flood has been increased in the future year of 2060.

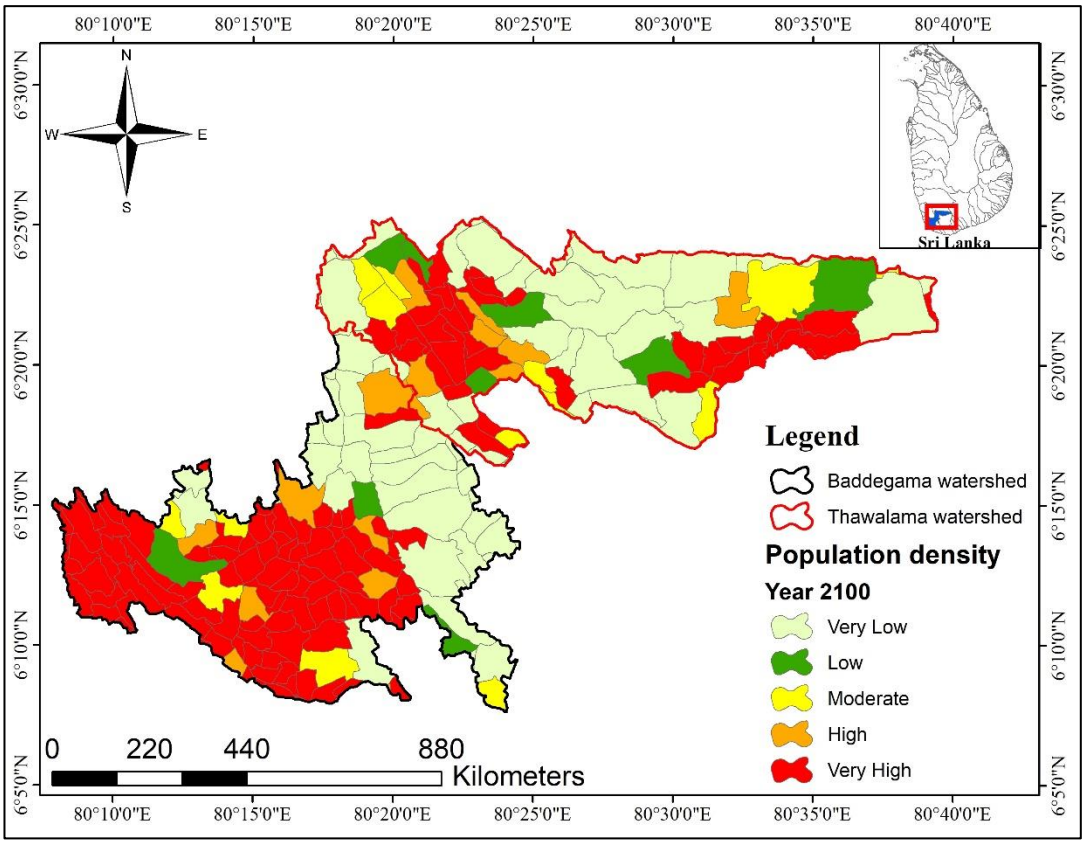

Figure 3-4 Population density in the year 2100 at Lower and Upper Gin Ganga

Figure 3-4 shows that at the end of the century flood vulnerabilities for the population will increase to a very high category in almost 50 % of Grama Niladhari division's (GND's) of the Gin Ganga River basin.

From figure Figure 3-2, Figure 3-3, and Figure 3-4 it can be concluded that flood vulnerabilities for the population in upper Ging Ganga (ie., Thawlama catchment) are increasing at a high rate from present to the end century. Since Flood control structures are mostly present in the lower Gin Ganga and also many projects have been proposed and are ongoing in the lower part of Gin Ganga. Therefore, it can be said that flood vulnerabilities will be reduced at the lower reach of Gin Ganga. It is well known that "Adaptation actions reduce vulnerability to climate change and manages risk to life, property, well-being and key economic sectors" (Ministry of Mahaweli Development and Environment, 2016).

In the future, Thawalama catchment may be more vulnerable as insufficient adaptative measures are present currently and may increase the risk to human beings, structure, economy, etc. So, Thawlama catchment is essential to study flood Risk in the future.

3.3 Methodology

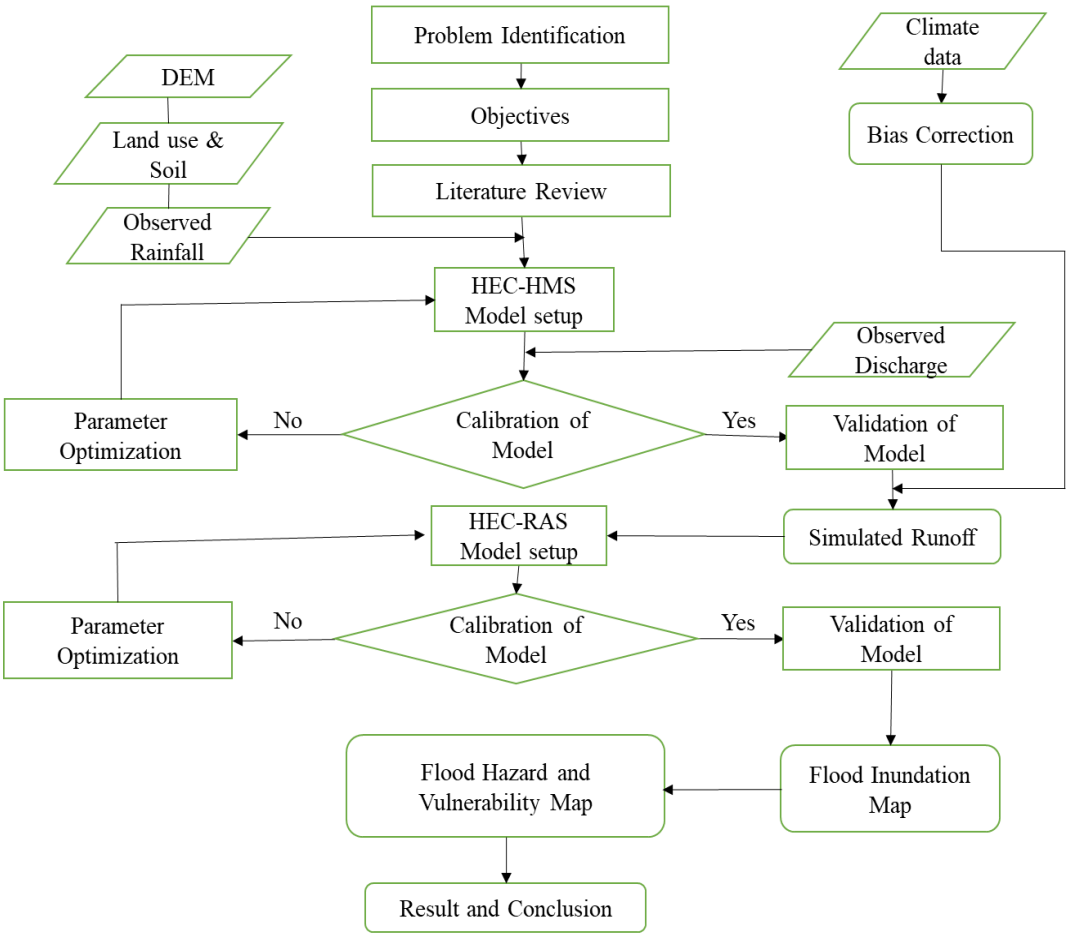

Figure 3-5: Methodology flow chart

The approach adopted for this research work is shown in Figure 3-5. Following the identification of the need for research and the establishment of the overall and specific objectives, a comprehensive literature review was completed to determine the numerous types of hydrological models available, their applications, and various objective functions to evaluate model performance during calibration and validation procedures. Data on rainfall and streamflow were obtained from the Meteorological Department and the Irrigation Department, respectively. Linear regression has been

used to fill in missing data periods using data from the nearest station. A statistical approach like the Gumbel method was used to find the return period.

For this study, only the SCS Curve number approach was used for event hydrological modeling, out of the loss methods available in HEC-HMS. Using streamflow data, the HEC-HMS was calibrated and validated for a specific event. Future lateral flows and inflow hydrographs were created by HEC-HMS using bias-adjusted precipitation data of the selected RCM model.

Sequentially, an HEC-RAS 2D model was developed and simulated for different flood events to generate flood inundation maps under Climate Change.

Flood hazard and vulnerability maps were generated from the results of the flood inundation map by using population density for vulnerability parameters and flood depth and velocity for flood hazard. Furthermore, the risk map was prepared by taking the union of hazard and vulnerability.

3.4 Data Collection

Table 3-1 Data Requirements

Data Type	Spatial/Temporal Resolution	Data Source
Digital Elevation Model	30 m	Survey Department, Sri Lanka
Rainfall Data	Daily	Meteorology Department, Sri Lanka
Discharge	Daily	Irrigation Department, Sri Lanka
Evaporation	Monthly	Meteorology Department (Agromet Division), Sri Lanka
Land use & Soil	1:50,000	Survey Department, Sri Lanka
Water Level	Daily	Irrigation Department, Sri Lanka
Population	2012	Department of Census and Statistics, Sri Lanka
Climate Scenario Data (CMIP5)-RCP 8.5	RCM (25 km)	https://esgf-data.dkrz.de/search/cordex-dkrz/

In the study area, there was one streamflow gauging station (at the catchment outlet), and one evaporation station (the closest one was selected). Four rain gauges were selected for the Thawalama catchment. Resolution and the data source are given in Table 3-1 and geographical coordinates in Table 3-2.

Table 3-2 Locations of gauging stations

Gauging station	**Data period**	**Station coordinates**	
Anningkanda rainfall	1989-2018	80.61°E	6.35°N
Thawalama rainfall	1989-2018	80.33°E	6.33°N
Pallegama rainfall	1989-2018	80.53°E	6.35°N
Kuduwa rainfall	1989-2018	80.42°E	6.43°N
Thawalama streamflow	1989-2018	80.33°E	6.34°N
Rathnapura evaporation	1989-2015	80.24°E	6.41°N

Furthermore, Regional Climate Models (RCM) data were obtained from the cordex website mentioned in Table 3-1, and then data checking for the observed station was carried out in chapter 4. Thereafter, climate RCM data were extracted through MATLAB for every observed rainfall station geographical coordinate, and then bias correction was performed to obtain future climate RCM data.

CHAPTER 4

4 DATA CHECKING AND ANALYSIS

This chapter proposes a basic statistical approach based on rainfall data. Rainfall data is generally far more abundant than runoff data, and it is not subject to unusual changes to account for shifting watersheds situations. A regional statistical analysis can be performed on the data. Local government rainfall and stream gauge data are frequently collected and synthesized by authorized data and by compiling regional rainfall data summaries that provide a range of estimations rainfall depth-duration values versus frequency of return.

Inconsistencies in the hydrological and meteorological data series might be recognized using statistical techniques that discover trends and change points.

Inconsistency, which reveals systemic faults while recording, and non-homogeneity, which originates from either natural or man-made alterations to the gauging environment, are both important for accurate time series analysis. It has also been established that statistical tests, as well as physical or historical proof and reasons based on metadata, must be included for a thorough investigation (Wijesekera & Perera, 2012).

Rainfall, evaporation, and streamflow data have been checked visually, with missing data identified and filled in, and consistency checked. Table 3-2 shows the locations of river gauging stations, rainfall and evaporation stations.

4.1 Observed period data checking

Visual data checking was done by plotting graphs for single data sets & observing inconsistencies. For the rainfall and streamflow data a single mass curve analysis was performed, taking into account the consistency in yearly cycles, which is the same perception as linear regression, which has been effectively utilized for evaluation of missing rainfall (Sharifi, 2015; Caldera, Piyathisse, & Nandalal, 2016).

4.1.1 Pallegama Rainfall Station

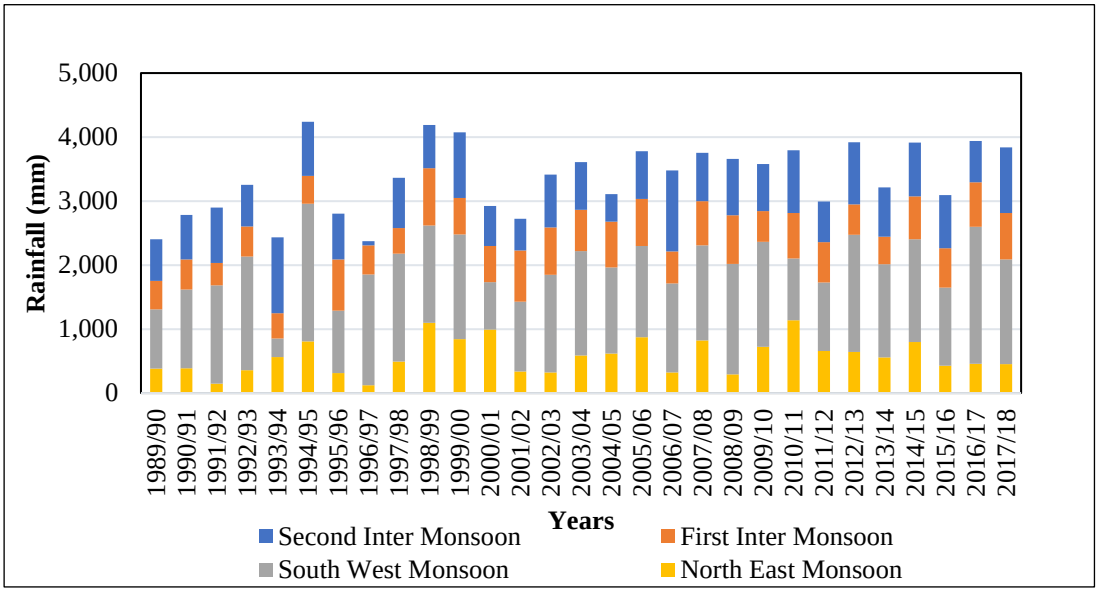

Figure 4-1 Rainfall seasonal variation of Pallegama rainfall station including four monsoon seasons in Sri Lanka

From data analysis of the Pallegama rainfall station, the monthly average precipitation for the 4 monsoon seasons as shown in Figure 4-1 is-

- First Inter-Monsoon season- 596 mm
- Southwest Monsoon season- 1426 mm
- Second-Inter Monsoon season- 770 mm
- Northeast Monsoon season- 569 mm

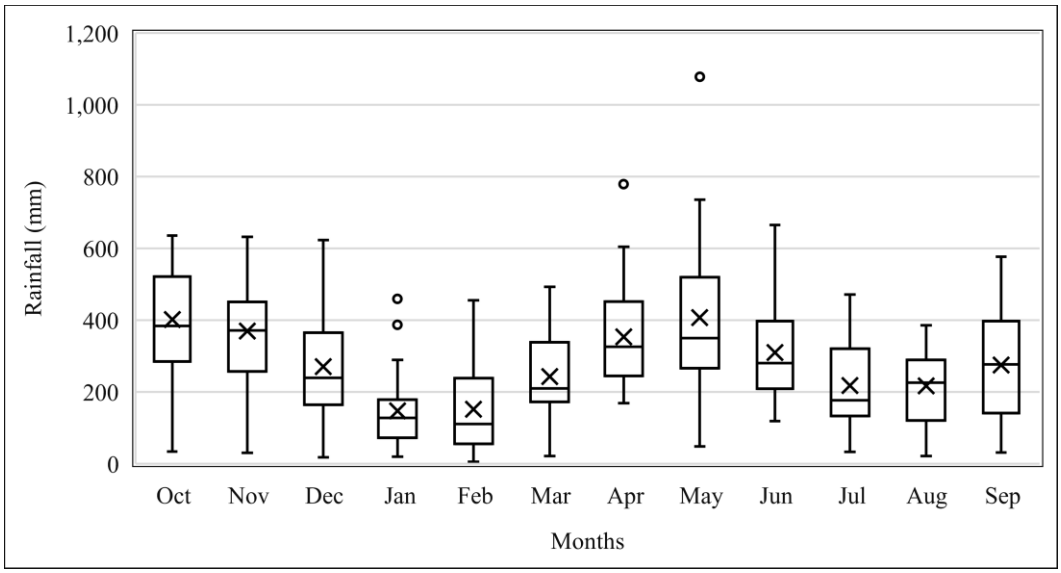

Figure 4-2 Rainfall variation of Pallegama rainfall station according to hydrological year (1989/90 – 2017/18)

From box and whisker plot analysis of Pallegama rainfall station as shown in Figure 4-2:

- The monthly mean average rainfall differs from 147 mm to 400 mm.
- The monthly minimum average rainfall differs from 5 mm to 168 mm.
- The monthly maximum average rainfall differs from 385 mm to 1078 mm.

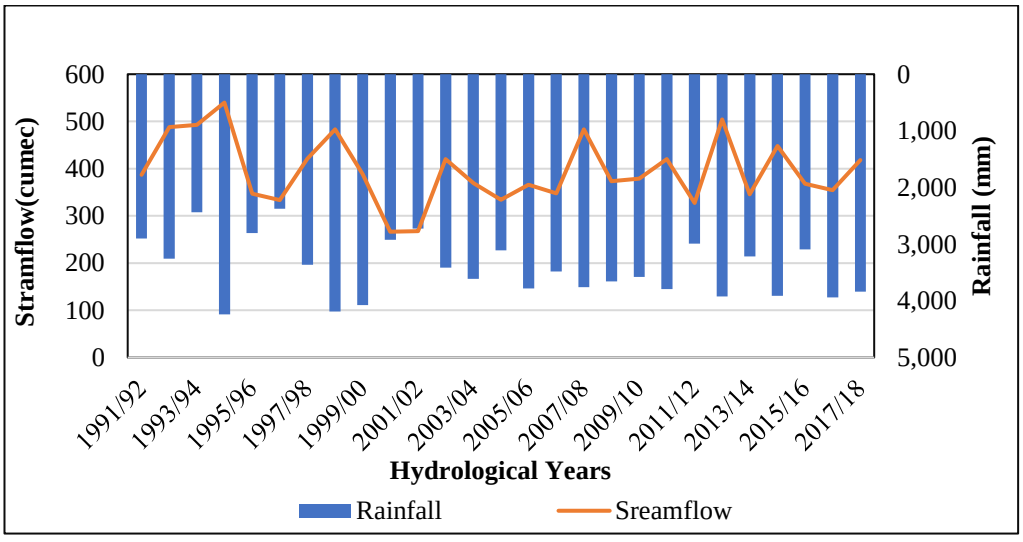

Figure 4-3 Yearly streamflow vs yearly rainfall of Pallegama rainfall station in the Thawalama catchment

From Figure 4-3, the annual streamflow vs annual rainfall of Pallegama rainfall station shows data is accurate enough at the annual scale as patterns of rainfall are similar to streamflow.

4.1.2 Thawalama Rainfall Station

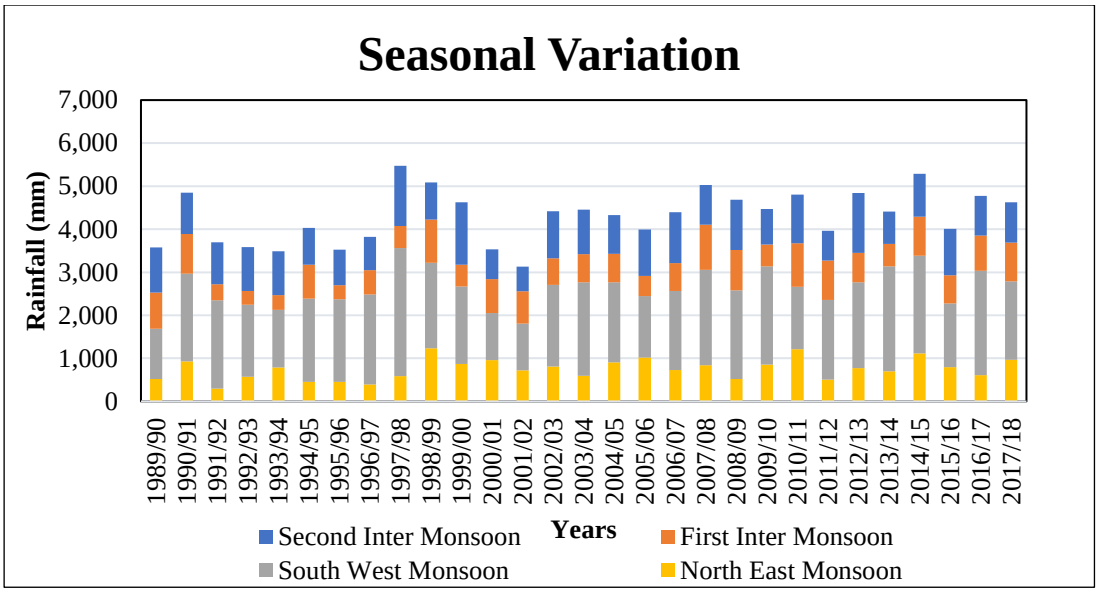

Figure 4-4 Rainfall Seasonal Variation of Thawalama Rainfall Station including four monsoon seasons in Sri Lanka

From data analysis of the Thawalama rainfall station, the monthly average precipitation for the 4 monsoon seasons as shown in Figure 4-4 are-

- First Inter-Monsoon season- 989 mm
- Southwest Monsoon season- 1882 mm
- Second-Inter Monsoon season- 985 mm
- Northeast Monsoon season- 749 mm

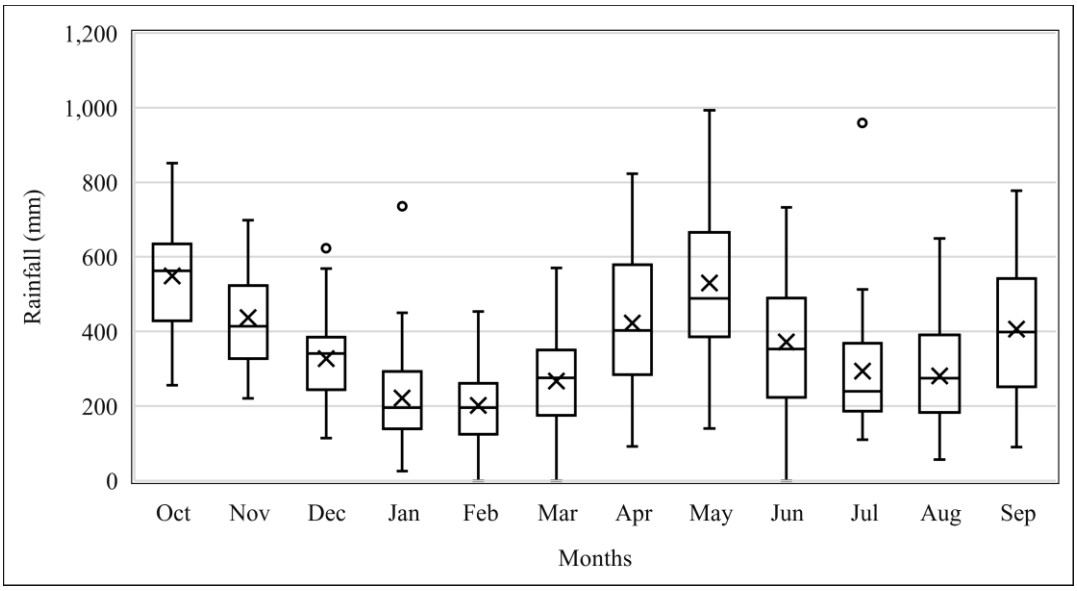

Figure 4-5 Rainfall Variation of Thawalama rainfall station according to hydrological year (1989/90 – 2017/18)

From box and whisker plot analysis of Thawalma rainfall station as shown in Figure 4-5:

- The monthly mean average rainfall differs from 220 mm to 611 mm.
- The monthly minimum average rainfall differs from 0 mm to 256 mm.
- The monthly maximum average rainfall differs from 450 mm to 990 mm.

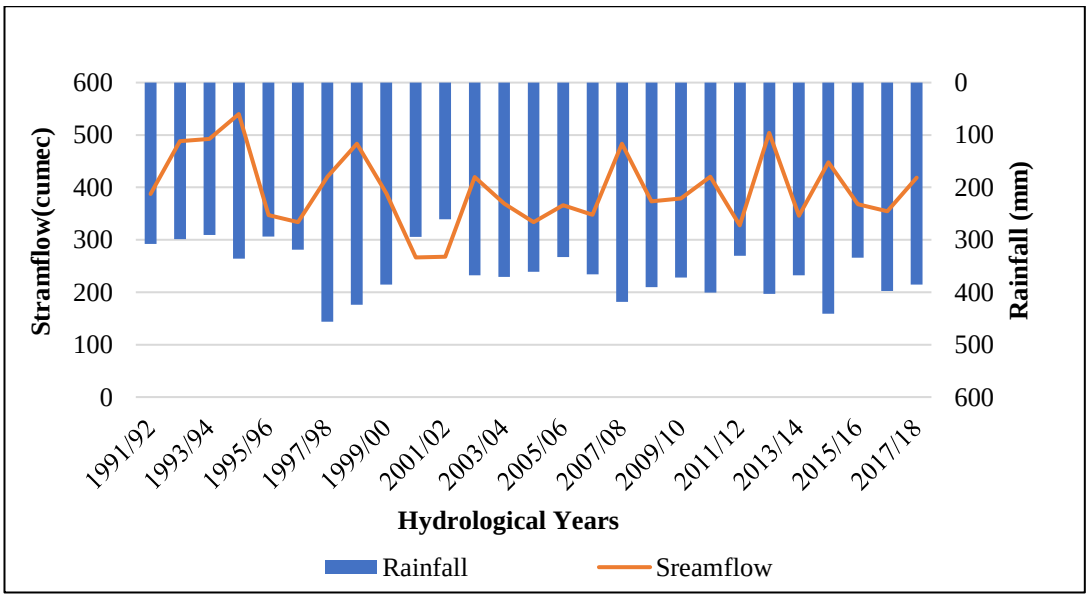

Figure 4-6 Yearly Streamflow vs yearly rainfall of Thawalama rainfall station in the Thawalama catchment

From Figure 4-6, the annual streamflow vs annual rainfall of the Thawalma rainfall station shows data is accurate enough at the annual scale as patterns of rainfall are similar to streamflow.

4.1.3 Anninkanda Rainfall Station

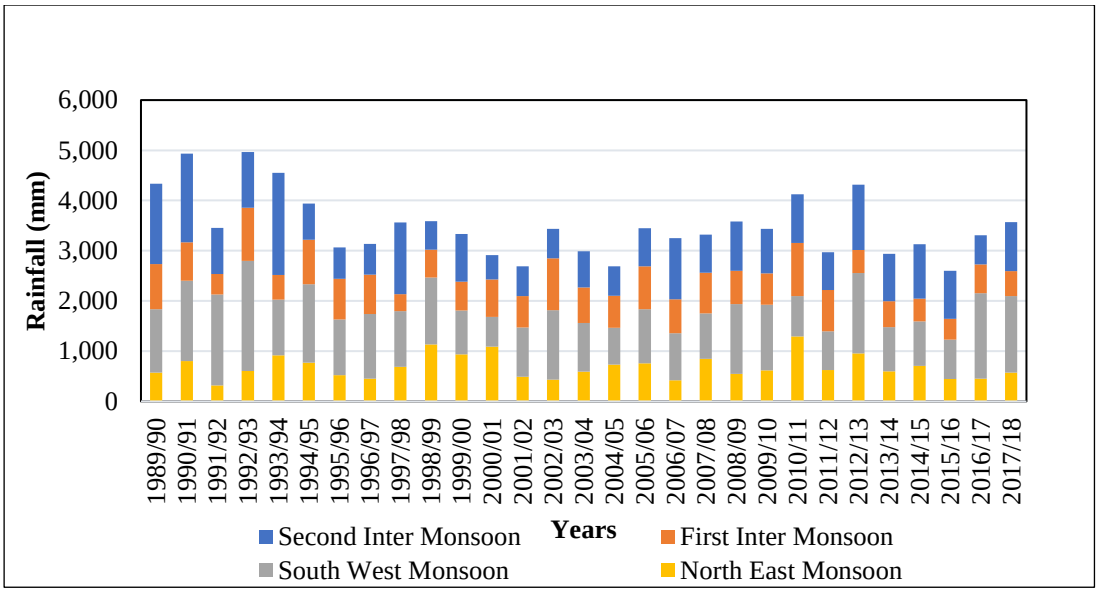

Figure 4-7 Rainfall seasonal variation of Anninkanda rainfall station including four monsoon seasons in Sri Lanka

From data analysis of the Anninkanda rainfall station, the monthly average precipitation for the 4 monsoon seasons as shown in Figure 4-7 are-

- First Inter-Monsoon season- 680 mm
- Southwest Monsoon season- 1189 mm
- Second-Inter Monsoon season- 947 mm
- Northeast Monsoon season- 686 mm

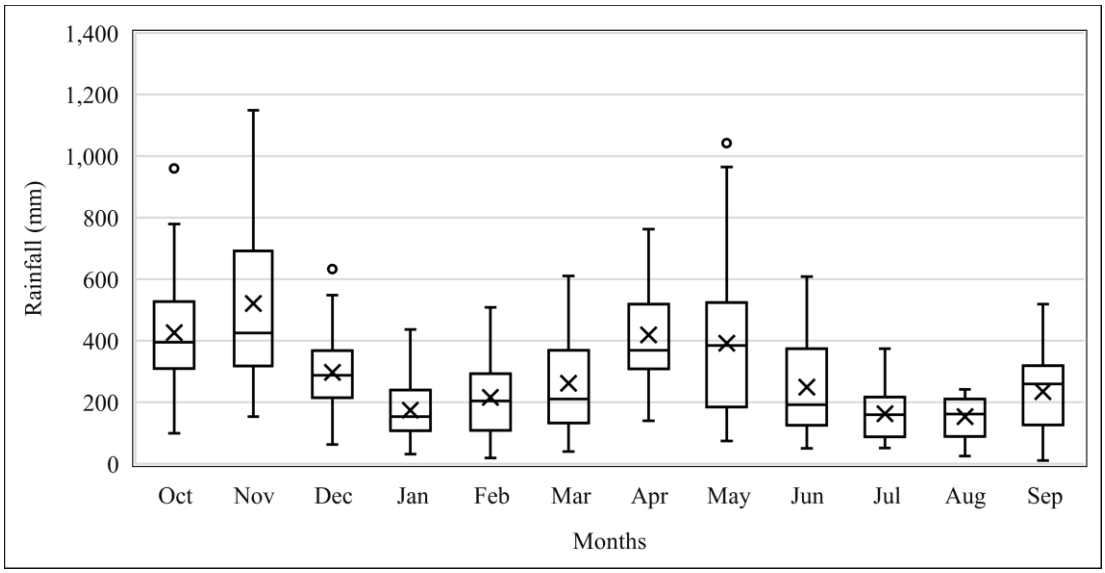

Figure 4-8 Rainfall variation of Anninkanda rainfall station according to hydrological year (1989/90 – 2017/18)

From box and whisker plot analysis of Anninkanda rainfall station as shown in Figure 4-8:

- The monthly mean average rainfall differs from 170 mm to 581 mm.
- The monthly minimum average rainfall differs from 10 mm to 153 mm.
- The monthly maximum average rainfall differs from 241 mm to 1148 mm.

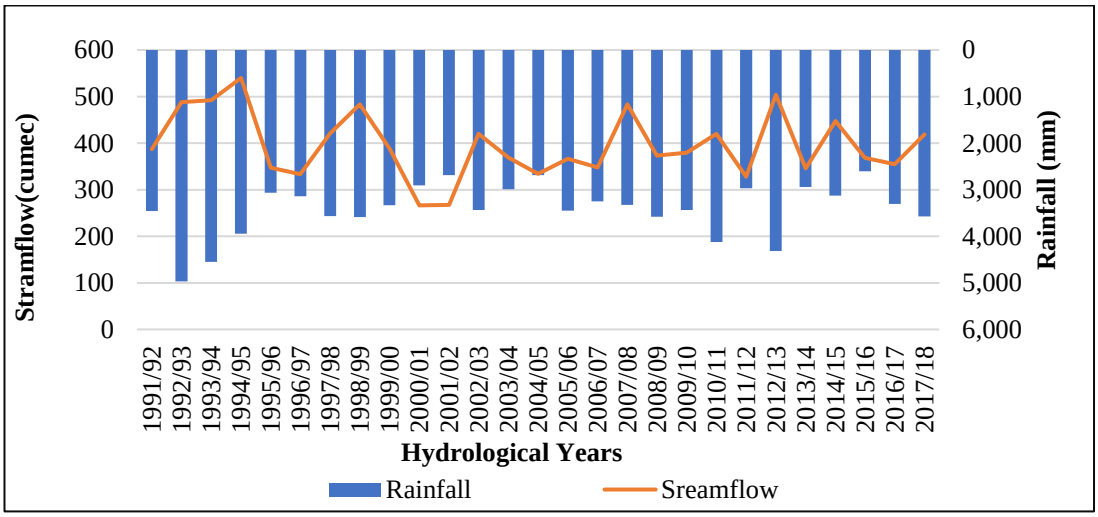

Figure 4-9 Yearly streamflow vs yearly rainfall of Anninkanda rainfall station in the Thawalama catchment

From Figure 4-9, the annual streamflow vs annual rainfall of Anninkanda rainfall station shows data is accurate enough at the annual scale as patterns of rainfall are similar to streamflow.

4.1.4 Kuduwa Rainfall Station

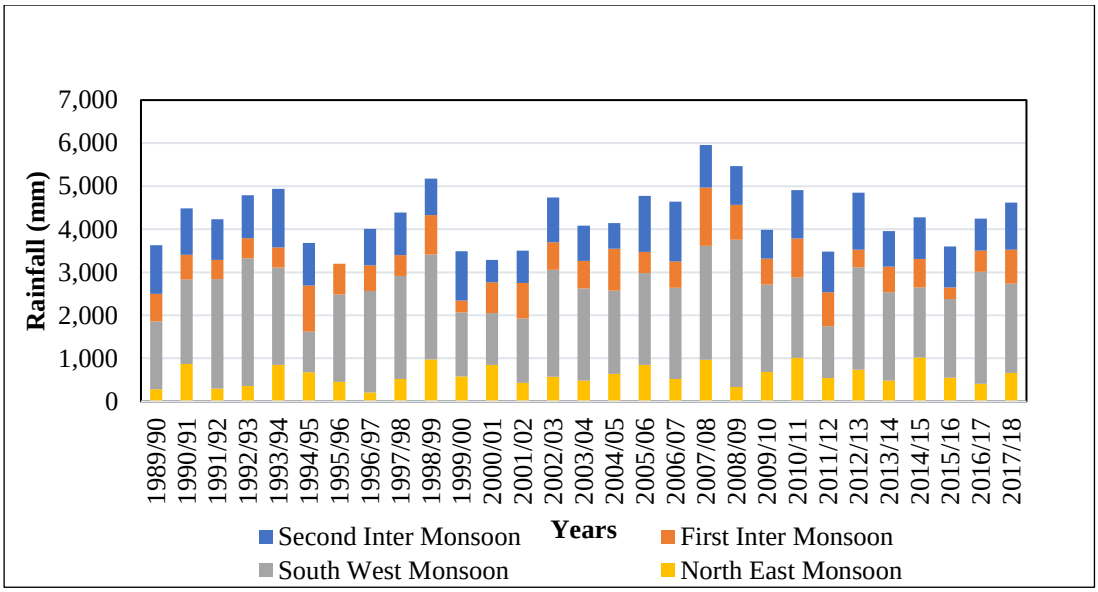

Figure 4-10 Rainfall seasonal variation of Kuduwa Rainfall station including four monsoon seasons in Sri Lanka

From data analysis of the Kuduwa rainfall station, the monthly average precipitation for the 4 monsoon seasons as shown in Figure 4-10 is-

- First Inter-Monsoon season- 664 mm
- Southwest Monsoon season- 2075 mm
- Second-Inter Monsoon season- 940 mm
- Northeast Monsoon season- 613 mm

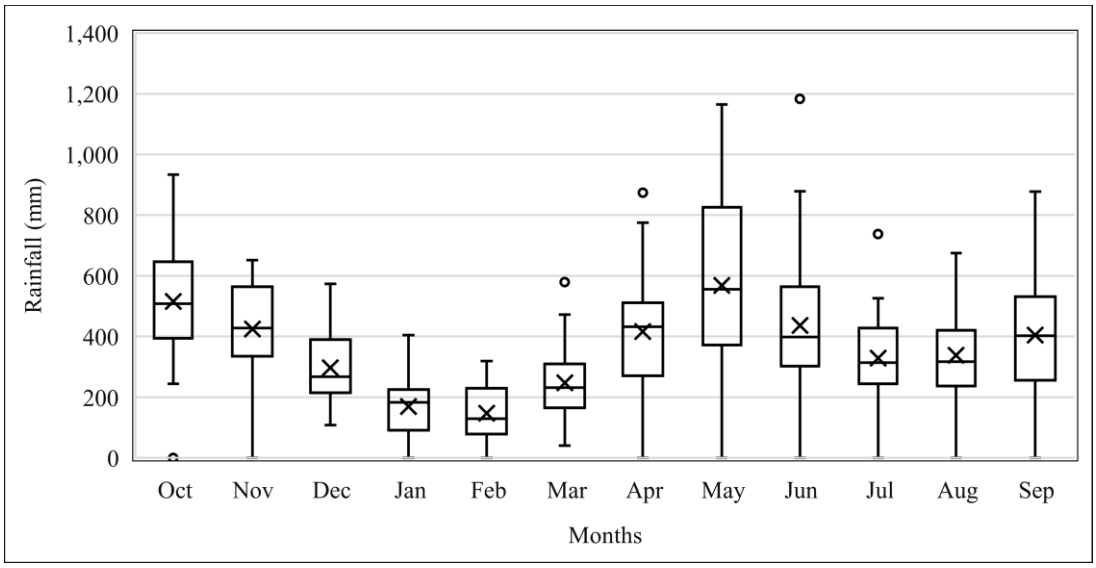

Figure 4-11 Rainfall variation of Kuduwa rainfall station according to hydrological year (1989/90 – 2017/18)

From box and whisker plot analysis of Kuduwa rainfall station as shown in Figure 4-11:

- The monthly mean average rainfall differs from 164 mm to 634 mm.
- The monthly minimum average rainfall differs from 0 mm to 107 mm.
- The monthly maximum average rainfall differs from 319 mm to 1183 mm.

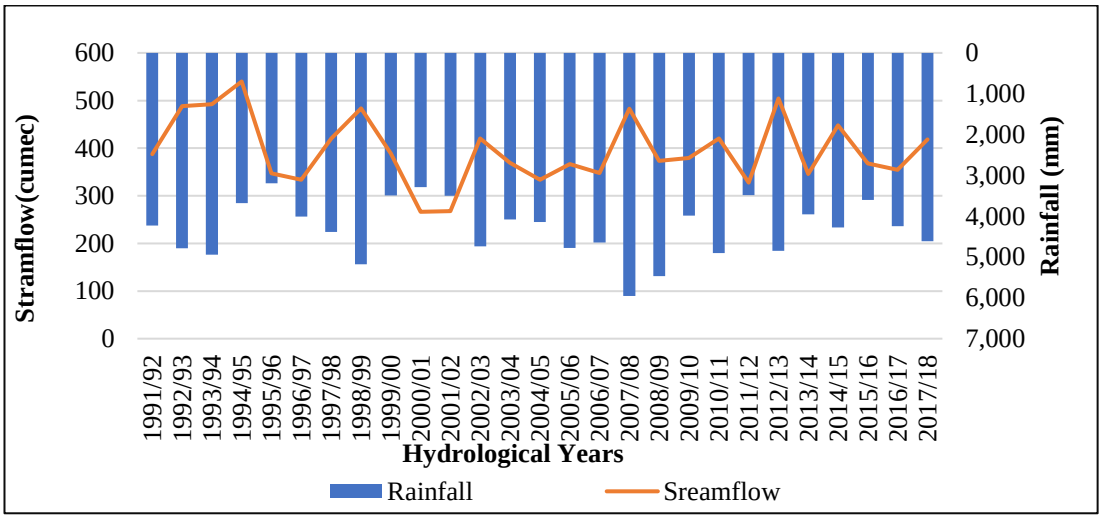

Figure 4-12 Yearly Streamflow vs yearly rainfall of Kuduwa rainfall station in the Thawalama catchment

From Figure 4-12, the annual streamflow vs annual rainfall of the Kuduwa rainfall station shows data is accurate enough at the annual scale as patterns of rainfall are similar to streamflow.

4.1.5 Single mass curve and Double mass curve analysis

4.1.5.1 *The Single mass curve for rainfall analysis*

A single mass curve evaluation was performed for all rainfall stations to check consistency for all rainfall stations, taking into account the consistency in yearly cycles, which is a similar approach as linear regression, which has been successfully used to calculate approximately missing rainfall. Rainfall data from selected stations showed a high degree of consistency in Figure 4-13.

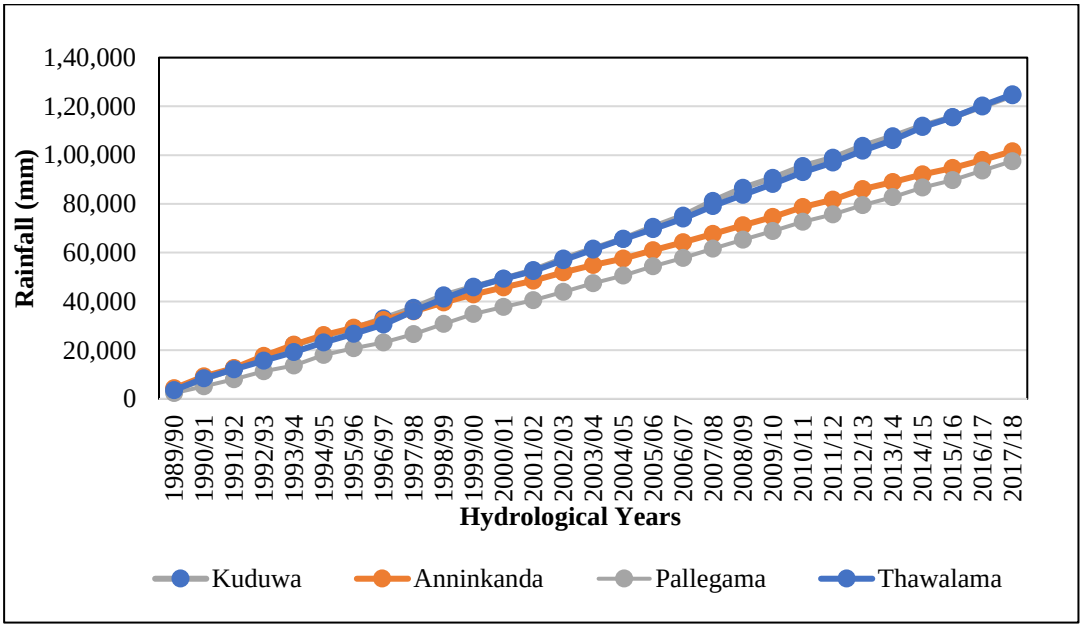

Figure 4-13: Single mass curve for all four-rainfall stations in the Thawalama catchment

All rainfall station shows consistency in the single mass curve. All individual station double mass curve is attached in Annexure-II.

4.1.5.2 *The double mass curve for rainfall analysis*

To verify the consistency of precipitation data for a Thawalama catchment a double mass curve was plotted. Figure 4-14 shows a straight line connecting all rainfall stations. As a result, it suggests that no data inconsistency will be utilized in this investigation.

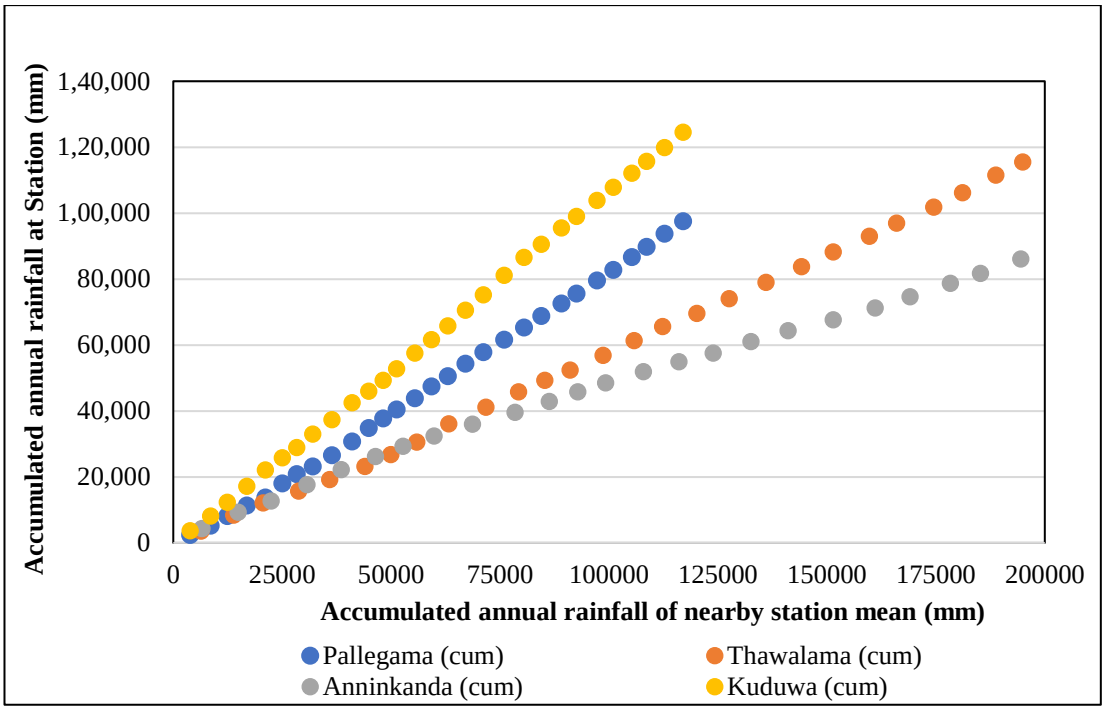

Figure 4-14 Double mass curve for all four-rainfall stations in the Thawalama catchment

All rainfall station shows consistency in the double mass curve. All individual station double mass curve is attached in Annexure-II.

4.2 Bias correction of Climate data

RCM data has been collected as climate data for this research work and four Regional Climate Model (RCM) data have been downloaded to choose the best model for bias correction and downloaded data has been extracted by MATLAB.

For bias correction, two methods have been used such as the linear scaling method and the Power transformation (PT) method. From these two methods, linear scaling has shown good '$R^{2'}$. Hence, the Linear Scaling method has been used for doing bias, and equations are mentioned in the section.

- Bias correction reference period -1990 to 2005
- Linear Scaling and Power Transformation bias correction methods were used to correct selected climate models.
- The coefficient of determination (R^2) was determined between the monthly average observed rainfall and the monthly average corrected bias model rainfall.

- MPI-M-MPI-ESM-MR was found to be the best-selected bias-corrected model using Linear scaling.

1. MIROC-MIROC5 Model

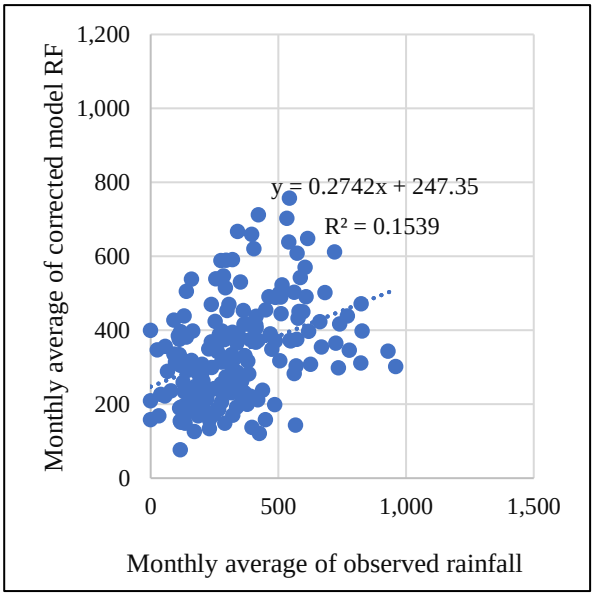

Figure 4-15 Bias corrected rainfall (mm) for MIROC-MIROC5

The Coefficient of determination (R^2) obtained is 0.15 for the 'MIROC-MIROC5' Regional Climate Model (RCM) in Figure 4-15.

2. NCC-NorESM1-M

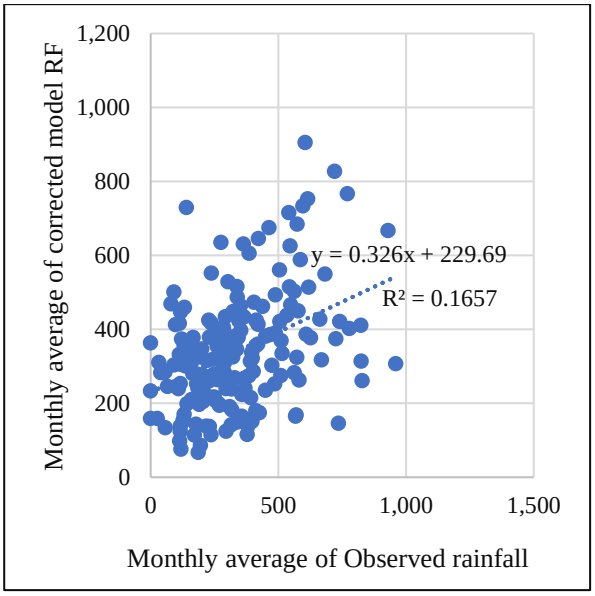

Figure 4-16 Bias corrected rainfall (mm) for NCC-NorESM1-M

The Coefficient of determination (R^2) obtained is 0.16 for the 'NCC-NorESM1-M' Regional climate model (RCM) in Figure 4-16.

3. MPI-M-MPI-ESM-MR

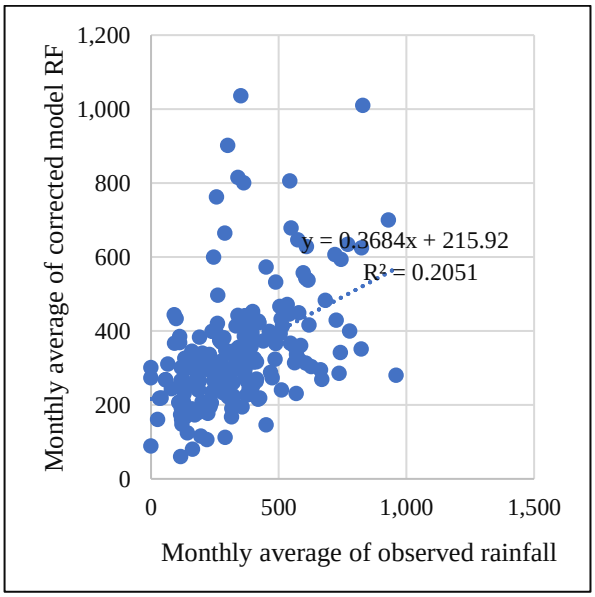

Figure 4-17 Bias corrected rainfall (mm) for MPI-M-MPI-ESM-MR

The Coefficient of determination (R^2) obtained is 0.20 for the 'MPI-M-MPI-ESM-MR' Regional climate model (RCM) in Figure 4-17.

4. ICHEC-EC-EARTH

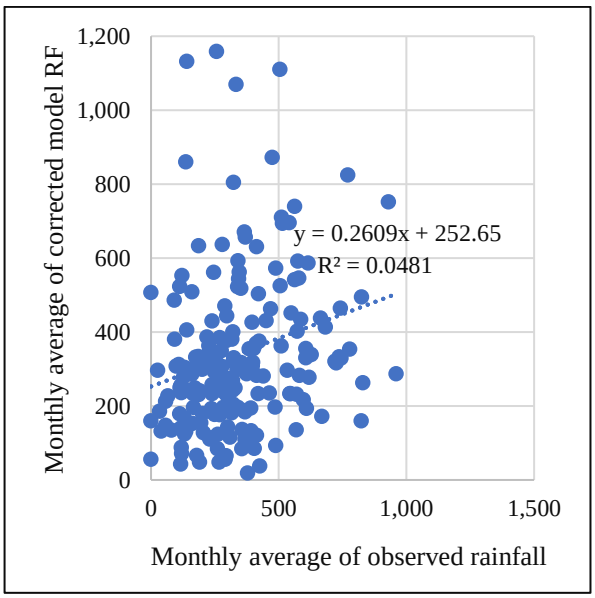

Figure 4-18 Bias corrected rainfall (mm) for ICHEC-EC-EARTH

The coefficient of determination (R^2) obtained is 0.04 for the 'ICHEC-EC-EARTH' Regional Climate Model (RCM) in Figure 4-18.

4.3 Future Projection of Rainfall

After bias correction of historical rainfall with ground station rainfall the future Regional Climate Model (RCM) was bias-corrected with the monthly factor obtained between historical and ground station data.

For bias correction, Linear scaling was used as per section 2.4.

1) **Average Annual Rainfall**

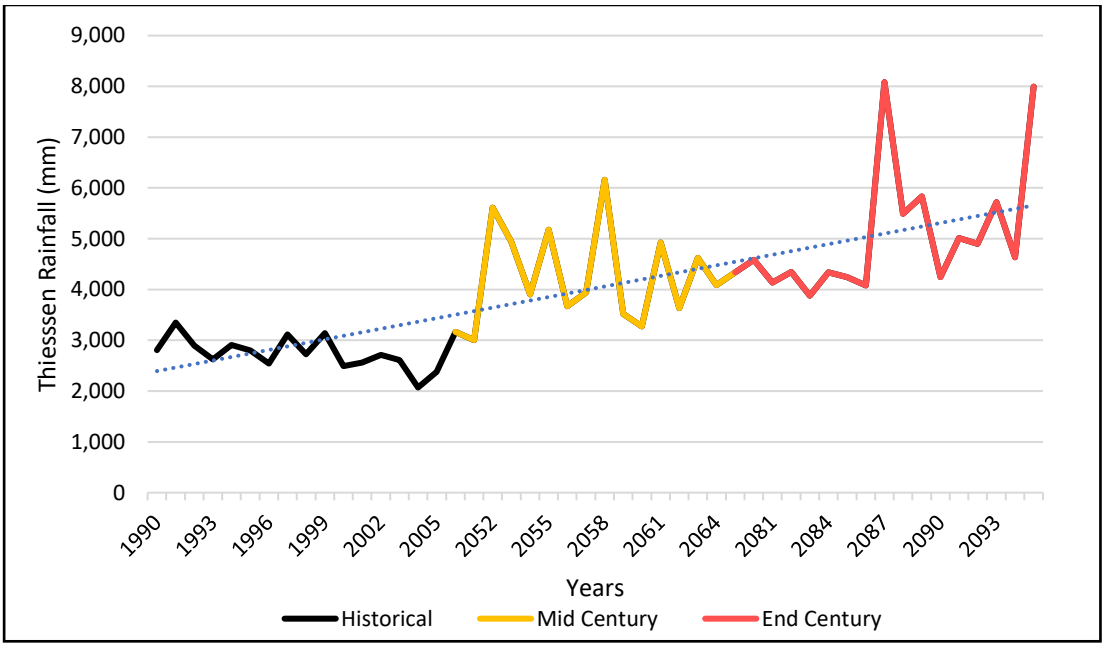

Figure 4-19 Average annual rainfall of Historical, mid-century, and end a century of RCM data

Projected Regional Climate Model (RCM) and historical Regional Climate Model (RCM) data were plotted to observe variation between the historical, mid-century, and end centuries.

Figure 4-19 clearly shows that rainfall is going to increase in the future by which the frequency of flood occurrence will increase.

Annual average rainfall for 15 years of Historical, Mid and End century was observed as-

- Historical - 2733 mm
- Mid-century - 4247 mm
- End-century -5045 mm

2) Average Monthly Rainfall

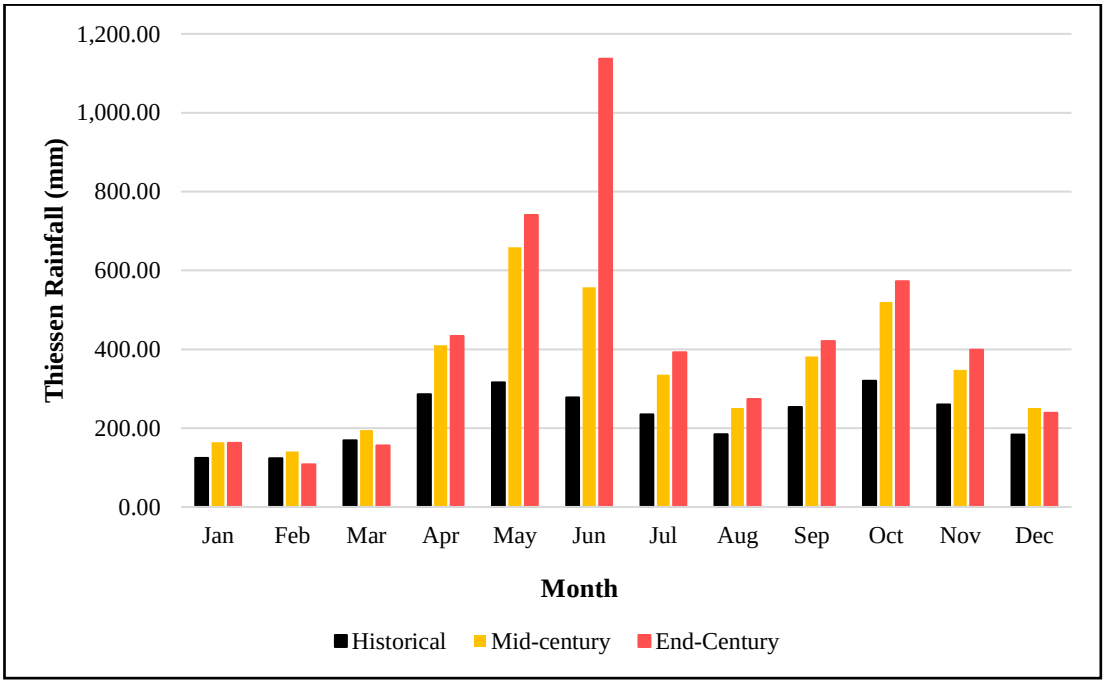

Figure 4-20 Monthly average RCM rainfall for historical, mid-century and end century

Figure 4-20 clearly shows that monthly average rainfall is going to increase in the future except in February and March which indicates that after mid-century rainfall will be decreased.

In June, there are large chances of flooding as there is a large variation from mid to end century.

Monthly average rainfall was observed as-

- Historical – 227 mm
- Mid-century - 351 mm
- End -century - 419 mm

4.4 The Frequency Analysis for flood

The annual thiessen rainfall series analysis was accomplished to estimate the flood peak at various return periods in the Thawalama catchment of the Gin Ganga River. Gumbel's Method, Log-Pearson Type III distribution and Log-normal distribution using the method of moments are the statistical methods presented.

4.4.1 Gumbel's Method-

Assumption-The annual maximum thiessen rainfall follows the Gumbel distribution.

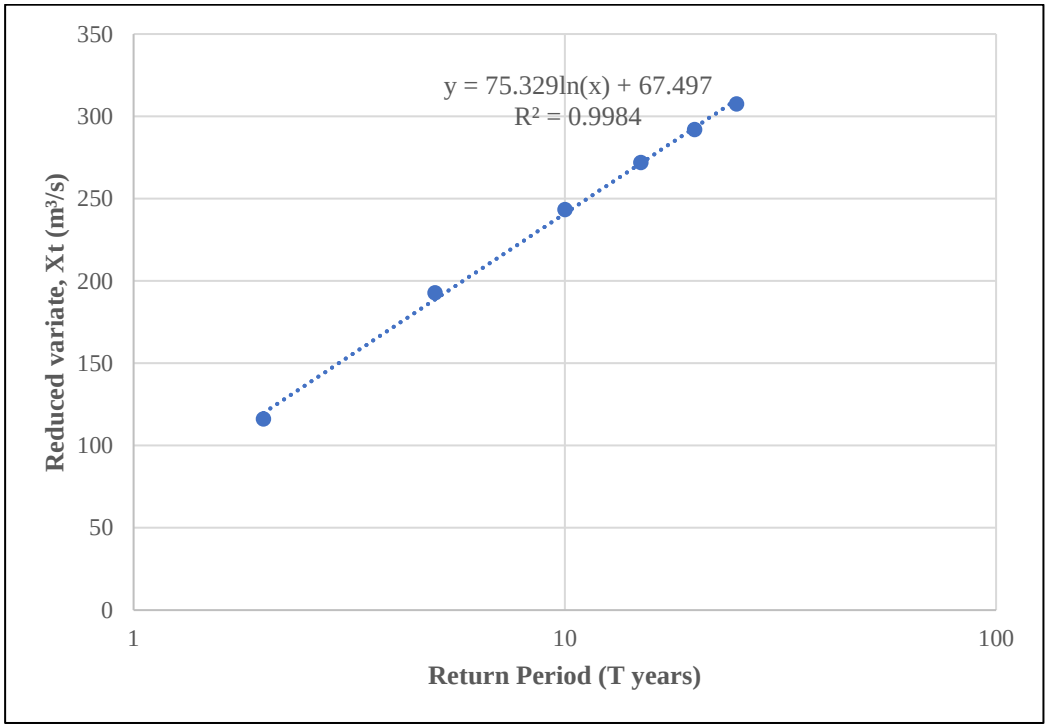

Figure 4-21: Flood frequency of Gumbel's method on a semi-log scale

The following approach was used to determine if the presented data follows the expected Gumbel distribution (Subramanya, 2013).

- For various return periods (T<N), the reduced variate 'Xt' is generated using the Gumbel formula and represented as X_t vs T on a semi-log scale as shown in Figure 4-21.
- If the plot yields a straight line for Xt vs T plot, then it follows Gumbel distribution

Table 4-1 Return period for different reduced variate

Return period (T years)	Reduced variate 'Xt'(m^3/s)
2	116.22
5	192.76
10	243.44
15	272.04
20	292.06
25	307.48

4.4.2 Log-Pearson Type III distribution

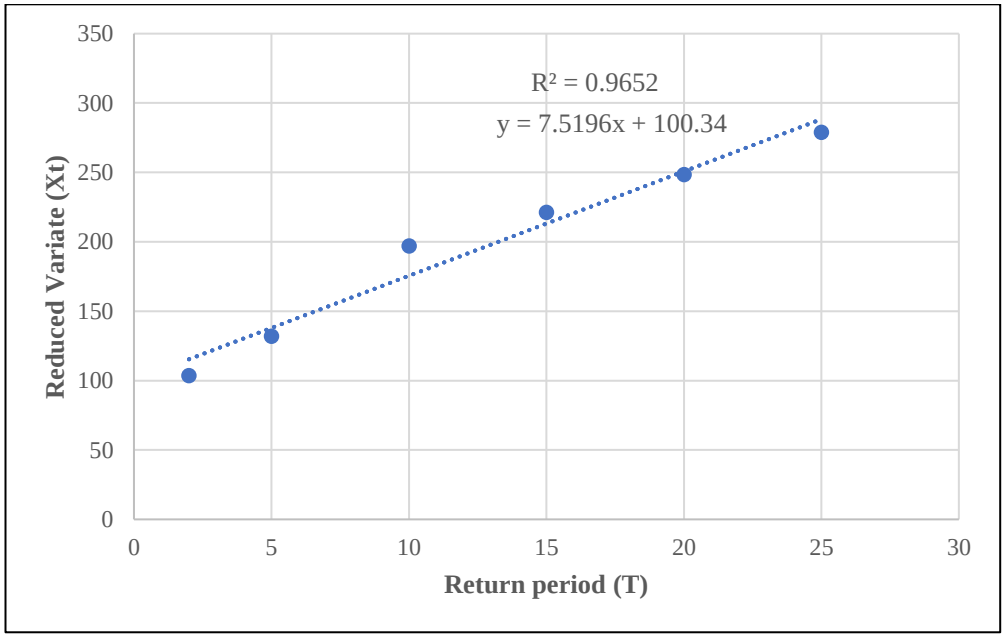

Figure 4-22: Flood frequency of reduced variate vs Return period

The coefficient of determination (R^2) obtained is 0.96 which is less than the Gumbel method as shown in Figure 4-22. Hence, it can be said that maximum annual thiessen

rainfall generally fits in the Gumbel distribution more accurately than Log Pearson Type III.

4.4.3 Log-Normal distribution

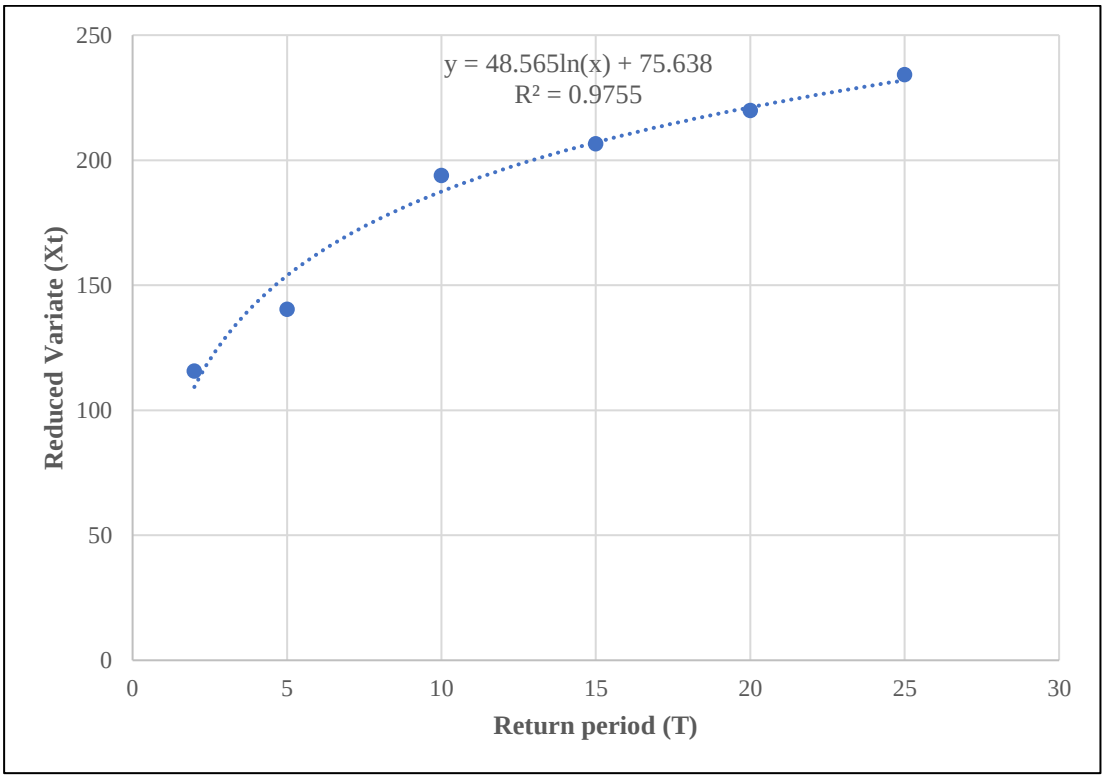

Figure 4-23: Flood frequency of thiessen rainfall plot using Log-Normal distribution

The coefficient of Determination (R^2) was obtained in the Log-Normal distribution as 0.97 in Figure 4-23.

When the coefficient of skew (Cs) is zero then the Log Pearson Type III distribution reduces to a log-normal distribution.

From the above three methods (Gumbel method, Log Pearson type III, and Log-normal distribution), it can be said that Gumbel distribution is the best fit for maximum annual thiessen rainfall for the Thawalama catchment due to the high coefficient of determination obtained as 0.99.

4.4.4 Flood Frequency analysis for Mid-Century and End-Century

The annual thiessen rainfall series of mid-century (2040-2070) and end-century (2071-2099) analysis was accomplished to estimate the flood peak at various return periods in the Thawalama catchment of the Gin Ganga River. Gumbel's method using the method of moments was used to perform frequency analysis.

The reduced variate for mid-century and end-century of different return periods are mentioned in Table 4-2.

4.4.4.1 *Flood Frequency Analysis for Mid-Century Using Gumbel's Method*

Assumption-The annual maximum thiessen rainfall follows the Gumbel distribution.

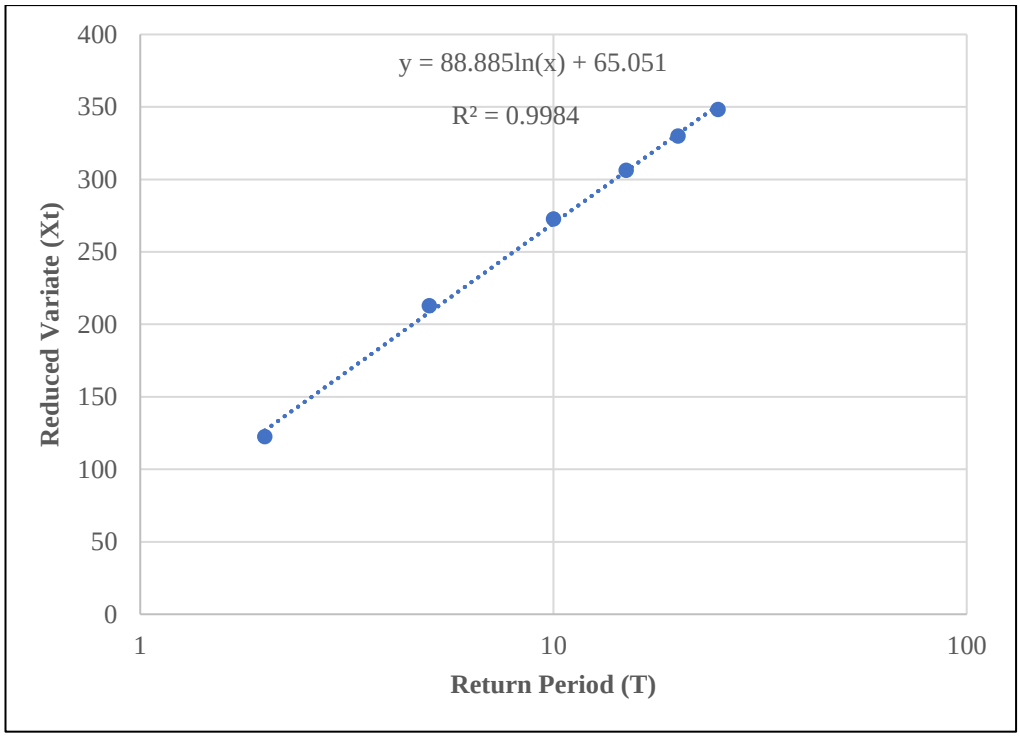

Figure 4-24 Flood frequency of Gumbel's method on a semi-log scale (Mid-Century)

The semi-log graph was plotted between reduced variate (Xt) and return period (T) to verify whether the assumed distribution follows the Gumbel distribution or not.

Figure 4-24 shows a straight line which justifies that Gumbel distribution is followed by assumed distribution.

4.4.4.2 *Flood Frequency Analysis for End-Century Using Gumbel's Method*

Assumption-The annual maximum thiessen rainfall follows the Gumbel distribution.

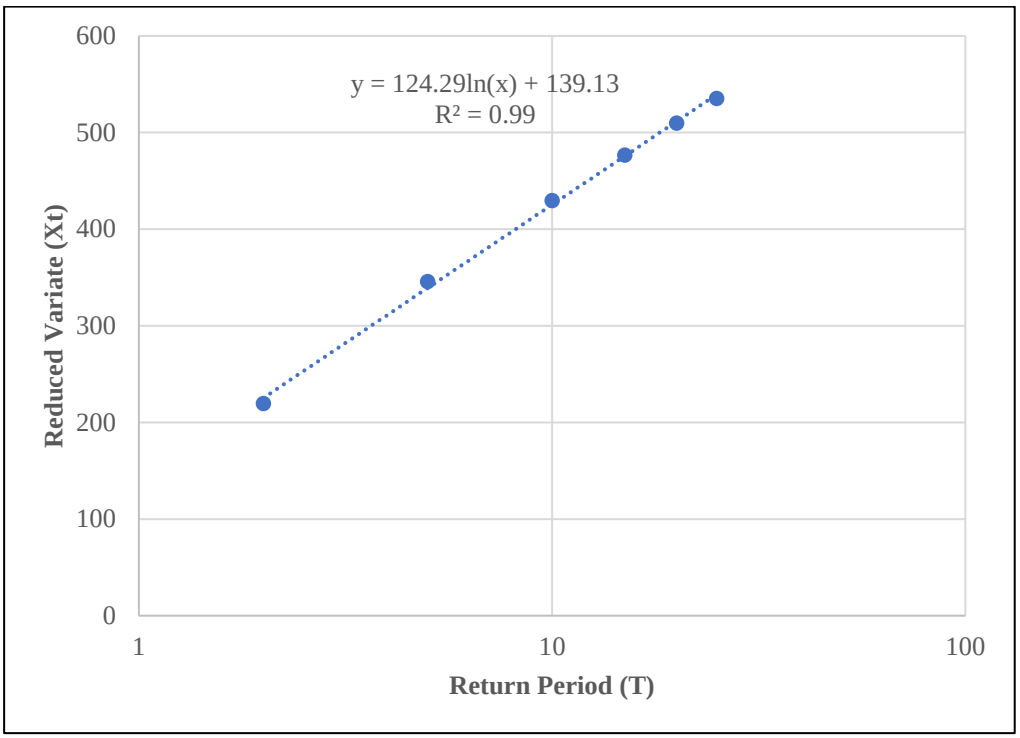

Figure 4-25 Flood frequency of Gumbel's method on a semi-log scale (End-Century)

The semi-log graph was plotted between reduced variate (Xt) and return period (T) to verify whether the assumed distribution follows the Gumbel distribution or not.

Figure 4-25 shows a straight line which justifies that Gumbel distribution is followed by assumed distribution.

Table 4-2 Return period for different reduced variate of mid-century and end-century

Return period (T years)	Reduced variate for mid-century 'Xt'(m^3/s)	Reduced variate for end-century 'Xt'(m^3/s)
2	122.54	219.52
5	212.86	345.81
10	272.66	429.43
15	306.40	476.61
20	330.02	509.64
25	348.22	535.09

4.5 Population Demography

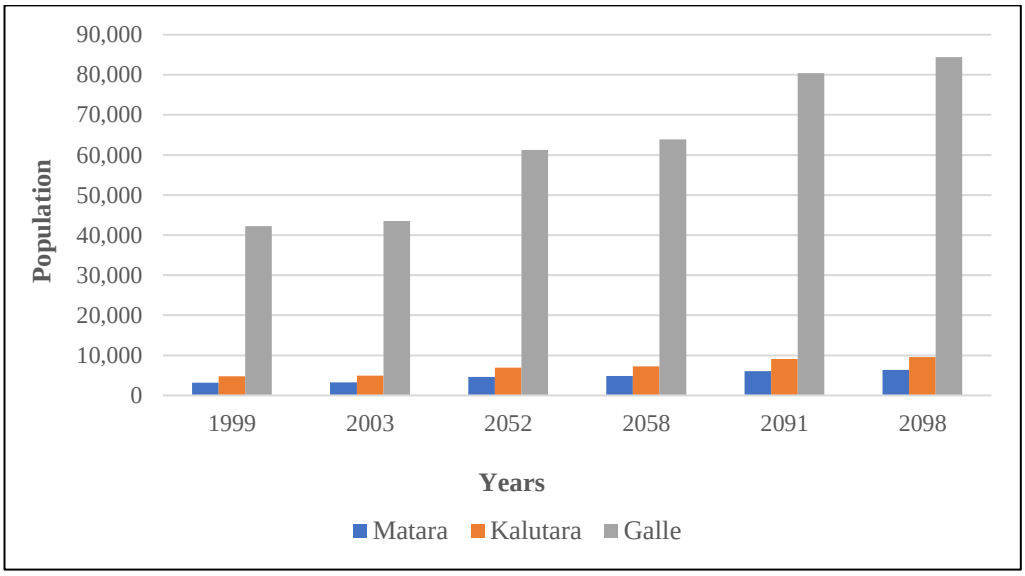

Figure 4-26 Population for Districts in 2-D area

The population data were obtained from the department of census and statistics, Sri Lanka for the year 2012. To estimate population only a 2-D area (Figure 5-3) within the Thawalama catchment was assessed for flood vulnerability assessment. Thereafter, the population was forecasted only for those particular years which was selected as a flood event. There was a total of three districts (Galle, Kalutara, and Matara) found under the 2-D area. The population was estimated Grama Niladari Division (GND) wise within the districts of 2-D area. The maximum population was estimated in Galle district and the minimum population was estimated in Matara district as shown in Figure 4-26. The rate of increase of population for the year 2001 to 2012 was estimated to be 0.70 % (Department of Census and Statistics, 2012).

The Geometric Increase method was selected for population growth forecasting (Gawatre et al., 2016).

$$P_n = P\left(1 + \frac{r}{100}\right)^n \qquad [4\text{-}1]$$

Where, P_n= future population after n decades; P = current population

n = number of decades; r = percentage increase per decade

CHAPTER 5

5 MODEL DEVELOPMENT AND APPLICATIONS

5.1 HEC- HMS Model Development

The Hydrologic Modeling System (HEC-HMS) simulates the whole hydrologic process of the watershed by using inbuilt parameters which need to be calculated. In this section HEC- HMS model parameters were estimated with context to literature review 2.6.1.

5.1.1 Thiessen polygon

The Thiessen method is a popular approach in the literature for calculating mean areal precipitation. For each measuring station, this approach assigns a Thiessen polygon. Every point within this polygon is expected to have the same amount of rainfall with a constant weight. Arc-GIS was used to generate Thiessen polygons for the Thawalama catchment using four rain gauge stations are represented in Table 5-1 with thiessen weight and thiessen polygon area. The coverage area of each gauging station is shown by a different colour in Figure 5-1.

Table 5-1: Thiessen weights for the Gin River basin at Thawalama catchment

Station name	Thiessen polygon area (km^2)	Thiessen weight
Anninkanda	45.65	0.13
Kudawa	62.64	0.18
Pallegama	134.15	0.38
Thawalama	112.68	0.32

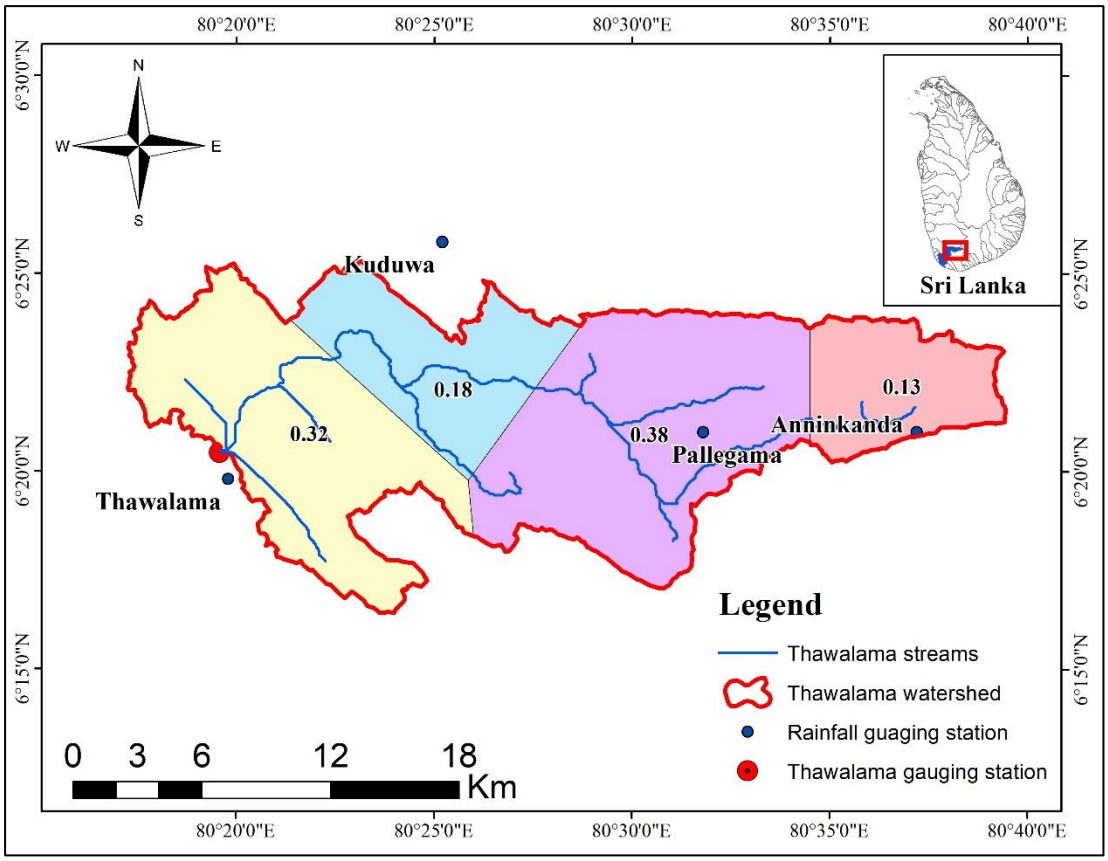

Figure 5-1: Thiessen polygons and rainfall stations at Thawalama watershed

5.1.2 Catchment Delineate

The HEC-HMS model parameters were selected as mentioned in Table 5-2. The method selected for these parameters is well used by different researchers for Event-based modeling as mentioned in section 2.6.1

Table 5-2: HEC-HMS Model Parameters

Sl. No.	Model parameters	Method
1	Subbasin loss	SCS Curve Number
2	Subbasin transform	SCS Curve Hydrograph
3	Subbasin baseflow	Recession
4	Reach routing	Muskingum

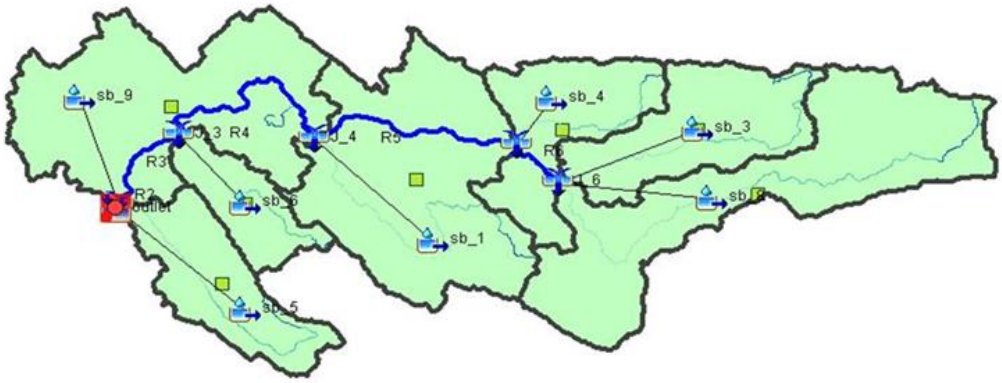

Figure 5-2: HEC-HMS model Development

The GIS interface in HEC-HMS was used to construct the sub-basin of the Thawalama catchment. A total of 8 sub-basin and 7 reaches were delineated as shown in Figure 5-2. Further, the HEC-HMS model parameters listed in Table 5-2 were calculated sub-basin-wise.

5.1.3 SCS CN (Soil Conservation Service Curve Number)

Table 5-3: Sample calculation of Curve number

Sub catchment	GFCODE	Area (sq. km)	Area in Percentage	Soil Group	Curve Number (CN)	CN x A
S_1	CHNAA	0.27	0.79	C	97	26.04
	FRSUA	2.59	7.59	C	58	149.95
	HOMSA	6.07	17.81	C	90	546.27
	OTHRA	0.77	2.26	C	81	62.39
	PDDYA	3.17	9.30	C	95	301.03
	RBBRA	0.21	0.61	C	67	13.98
	SCRBA	7.06	20.72	C	64	451.98
	STRMA	0.23	0.66	C	97	21.87
	TEAA	13.72	40.25	C	77	1056.19
	UNCLA	0.01	0.02	C	90	0.65
Total		**34.08**	**100.00**	**Weighted Average C**		**77.18**

The weighted average curve number was calculated using a land use map in the GIS interface. Table 5-3 shows a sample calculation of the SCS curve number using equation [2-3] and Table 5-4 shows the SCS curve number for every individual sub-catchment. The curve number for different land use classifications was adopted from the Engineering hydrology textbook (Subramanya, 2013).

Table 5-4 Curve Number for various sub-catchment

Sub catchment	Curve no.	Impervious %
S_1	77.18	6.00
S_2	71.31	1.39
S_3	73.50	10.32
S_4	58.59	8.04
S_5	66.15	2.69
S_6	57.10	4.16
S_7	79.71	2.42
S_8	72.64	2.47

Table 5-5: Time of concentration

Sub-basin	**Longest flow path Length (km)**	**Basin Slope**	**Maximum potential Retention (S), inch**	**Time lag (L) (hour)**	**Time of concentration (L/0.6) hour**	**Initial abstraction, (mm)**
S_1	16.17	0.23	2.96	39.59	65.99	15.02
S_2	10.44	0.21	4.02	31.60	52.66	20.44
S_3	11.83	0.25	3.61	35.66	59.43	18.32
S_4	19.61	0.30	7.07	87.90	146.49	35.91
S_5	16.87	0.29	5.12	62.66	104.43	25.99
S_6	17.52	0.30	7.51	82.69	137.82	38.17
S_7	14.85	0.25	2.54	35.56	59.27	12.93
S_8	9.27	0.29	3.77	32.40	54.00	19.13

5.1.4 Reach routing-Muskingum

For routing an inflow hydrograph, the Muskingum routing practice employs conservation of mass approach. The Muskingum approach can also take into consideration "looped" storage vs. outflow connections that are prevalent in most Rivers (US Army Corps of Engineers, 2018).

Estimate Initial Parameter Values

1) The Muskingum K

The travel time, T can be calculated by using the equation [2-9] as mentioned in the literature review and the lag time calculated for every reach is mentioned in Table 5-6.

To calculate flood wave velocity, the Kleitz-Seddon Law by following the equation [2-10] presented in the literature review.

The slope of the flow-stage rating curve was calculated by using water level and discharge data of 2010-2011.

The average top width was calculated by observing River width for every reach in Google Earth Pro.

Table 5-6 Muskingum K calculation

Reach	Lag (min)
R1	55.44
R2	137.52
R3	405.12
R4	306.92
R5	69.06
R6	41.43
R7	48.26

2) The Muskingum X

As per the literature review, Muskingum *X* value was taken as 0.25 initially and further was optimized.

5.2 HEC- RAS Model Development

5.2.1 The terrain Layers

The RAS Mapper supports the import of floating-point grid format (*.fit), GeoTIFF (*tif), and other formats. The terrain layers utilized to build the terrain model for this investigation were 30m Dem.

5.2.2 The 2D Computational Mesh development

HEC-RAS 2D modeling tools enable users to design a computational mesh. The modeler can define the borders of the computational mesh that surrounds the channel as well as any surrounding floodplain regions in the Geometric Data Editor.

Nominal grid resolution selected -60 m X 60 m

The 2D Flow Area Editor button may be used to create spatial information characterizing the polygon. The size of the particular 2D flow cells, as well as Manning's values for every cell, are included in the spatial information. Finally, utilizing a 2D Area, the boundary conditions at the upstream, lateral, and downstream ends were determined as shown in Figure 5-3.

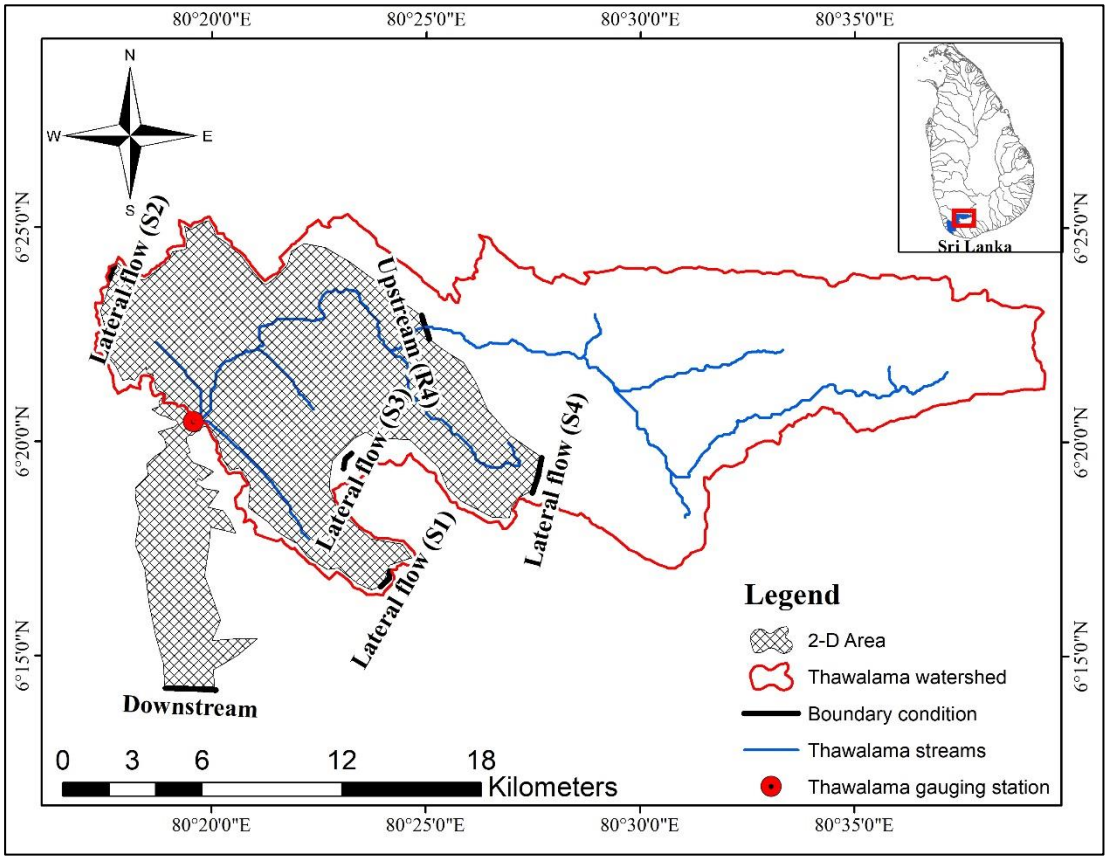

Figure 5-3 Two-Dimensional Area

The total two-dimensional area selected was 170 km² and for hazard, vulnerability, and risk mapping, a total area of approximately 136 km² was studied above the Thawalama gauging station.

5.2.3 Associating Land use and Manning's Layer with a Geometry

Manning's formula is used by HEC-RAS to calculate friction losses along the ground surface. The RAS Mapper opens a land-use shapefile prepared in ArcGIS with the related roughness values to the two-dimensional mesh. Polygons are constructed in the RAS mapper for every land use categorization based on a manning's n value.

The table menu in geometry data allows operators to display all land cover identifiers as well as an update for calibration and validation.

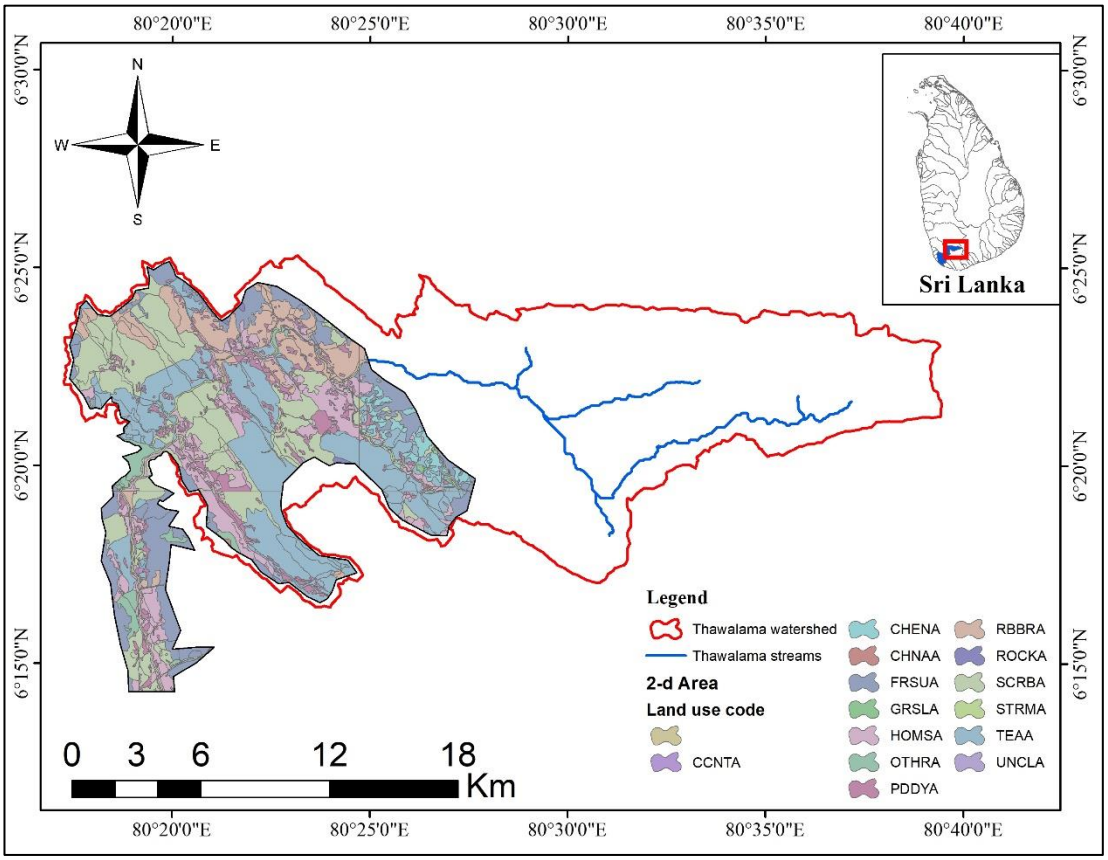

Figure 5-4 Land use in the Two-Dimensional Area

Figure 5-4 shows land use generated through Arc Map and imported in HEC-RAS. The land-use code and manning are n value are shown in Table 5-7. The manning's n value was taken from literature section 2.6.2.

Table 5-7 Manning's n value for Land use classification

(*Source*: Chow et al., 1998)

Land use code	Land use name	Manning's n value
CCNTA	Coconut	0.035
CHENA	Chena	0.035
CHNAA	Channel	0.030
FRSUA	Forest	0.150
GRSLA	Grassland	0.030
HOMSA	Homestead	0.030
OTHRA	Other Cultivation	0.035
PDDYA	Paddy field	0.035
RBBRA	Rubber	0.040
ROCKA	Rock	0.035
SCRBA	Scrub land	0.035
STRMA	Minor Streams	0.030
TEAA	Tea	0.035
UNCLA	Unclassified	0.035

CHAPTER 6

6 RESULTS AND ANALYSIS

6.1 Event selection

The event was selected by comparing the coefficient of determination (R^2) of the above three statistical methods mentioned in Section 4.2. according to the literature review section 2.5.

Since the R^2 value of Gumbel's method and Log Pearson are similar to 0.99. So, both methods were best among the three most commonly used methods worldwide. Since Gumbel's method is the more often utilized of the two, it has been given preference for the selection of events in this research work.

According to section 2.1.2, the catastrophic events occurred during 2003 and 1999. Therefore, events 2003 and 1999 were selected for calibration and validation period respectively. The return period for events 2003 and 1999 was found to be 12-year and 5-year respectively.

Further, future climate bias-corrected rainfall data was divided into two centuries (namely mid-century and end-century) mentioned in Table 6-1.

Table 6-1 Selected centuries of future climate rainfall data

Century	Years
Mid Century	2040-2070
End Century	2070-2099

The 5 year and 12-year return period events were selected between above mentioned two centuries using the Gumbel method.

6.2 Model Calibration, Validation, and Future Simulation

In this chapter, HEC-HMS and HEC-RAS results are presented for calibration and validation with their optimized parameters. Further, future simulation of the selected mid-century and end-century is also presented.

6.2.1 HEC-HMS Calibration-Event 2003

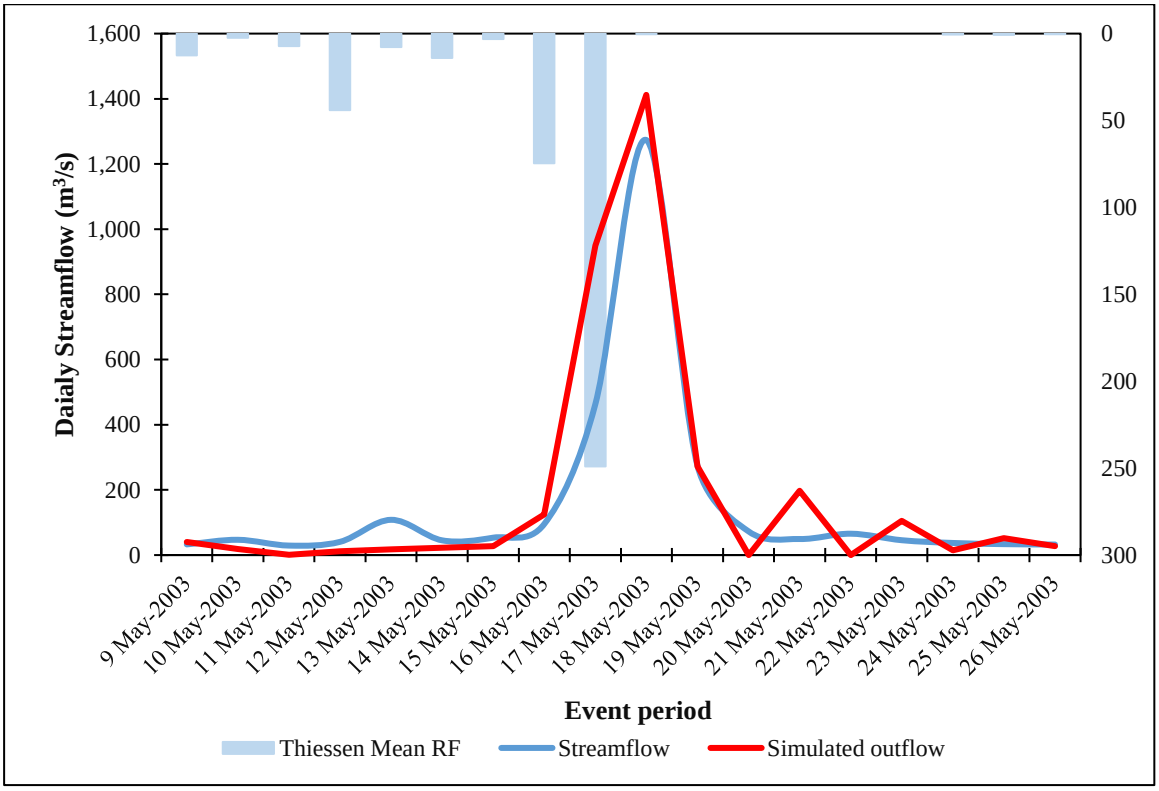

Figure 6-1 HEC-HMS model calibration

The HEC- HMS was calibrated as shown in Figure 6-1 with good objective function mentioned in Table 6-2, although percent bias was observed as 17.65 % with Satisfactory results. Model outflow peak was observed to be 1412 m^3/s whereas, the observed streamflow peak was 1273 m^3/s.

The Initial parameters and the optimized parameters for HEC-HMS are mentioned in Table 6-3.Table 6-3 Initial parameters and optimized parameters for base flow method in HEC-HMS model in the Thawalama catchment

Table 6-2 HEC-HMS model calibration performance

Calibration Goals	Model Performance	Performance Rating
Nash Sutcliffe	0.80	Very good
RMSE st dev.	0.40	Very good
Percent Bias	17.65 %	Satisfactory

Table 6-3 Initial parameters and optimized parameters for base flow method in HEC-HMS model in the Thawalama catchment

Sub-Catchment	Parameters	Initial Value	Optimized value
S_1	Initial storage	5.00	3.95
S_2	Initial storage	5.00	2.36
S_3	Initial storage	5.00	3.08
S_4	Initial storage	5.00	3.8
S_5	Initial storage	5.00	4.51
S_6	Initial storage	5.00	5.23
S_7	Initial storage	5.00	5.95
S_8	Initial storage	5.00	3.73
S_1	Recession Constant	0.30	0.10
S_2	Recession Constant	0.30	0.10
S_3	Recession Constant	0.30	0.10
S_4	Recession Constant	0.30	0.10
S_5	Recession Constant	0.30	0.10
S_6	Recession Constant	0.30	0.10
S_7	Recession Constant	0.30	0.10
S_8	Recession Constant	0.30	0.10
S_1	Ratio to peak	0.50	0.90
S_2	Ratio to peak	0.50	0.90
S_3	Ratio to peak	0.50	0.90
S_4	Ratio to peak	0.50	0.90
S_5	Ratio to peak	0.50	0.90
S_6	Ratio to peak	0.50	0.90
S_7	Ratio to peak	0.50	0.90
S_8	Ratio to peak	0.50	0.90

Initial storage was optimized using an automatic calibration tool in HEC-HMS whereas the recession constant and ratio to the peak were manually calibrated.

Table 6-4 Initial parameters and optimized parameters for routing (Muskingum) method in HEC-HMS model in the Thawalama catchment

Reaches	Parameters	Initial Value	Optimized Value
R1	Muskingum K	0.92	0.72
R2	Muskingum K	2.29	0.54
R3	Muskingum K	6.75	0.84
R4	Muskingum K	5.12	0.94
R5	Muskingum K	1.15	6.90
R6	Muskingum K	0.69	1.82
R7	Muskingum K	0.80	0.74
R1	Muskingum x	0.25	0.20
R2	Muskingum x	0.25	0.20
R3	Muskingum x	0.25	0.20
R4	Muskingum x	0.25	0.20
R5	Muskingum x	0.25	0.20
R6	Muskingum x	0.25	0.20
R7	Muskingum x	0.25	0.20

The Muskingum parameters ‘K’ and ‘X’ initial value and optimized value are mentioned in Table 6-4 for 7 different reaches.

The initial value of Muskingum ‘K’ was calculated in Table 5-6 and the Muskingum ‘X’ value was adopted from literature chapter 2.6.1.

The Muskingum K was optimized using an automatic calibration tool in HEC-HMS whereas Muskingum X was manually calibrated.

6.2.2 HEC-HMS Validation -Event 1999

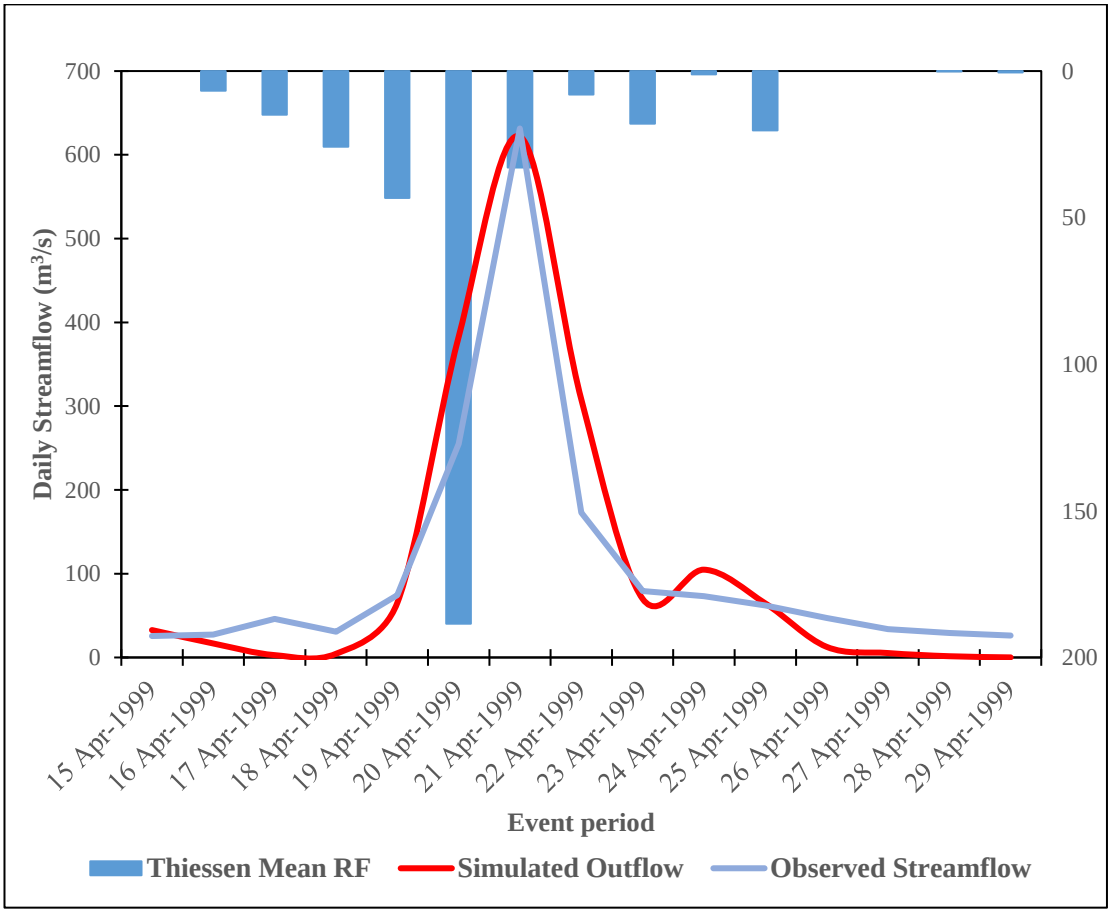

Figure 6-2 HEC- HMS model validation

The HEC-HMS was validated as shown in Figure 6-2 with a good objective function mentioned in Table 6-5 with the value of the same parameter which was used in the calibration event of 2003. Model outflow peak was observed to be 630 m³/s whereas, the observed streamflow peak was 631 m³/s.

Table 6-5 HEC-HMS model validation performance

Validation Goals	Model Performance	Performance Rating
Nash Sutcliffe	0.677	Good
RMSE st dev.	0.60	Good
Percent Bias	15 %	Good

6.2.3 HEC-RAS Calibration -Event 2003

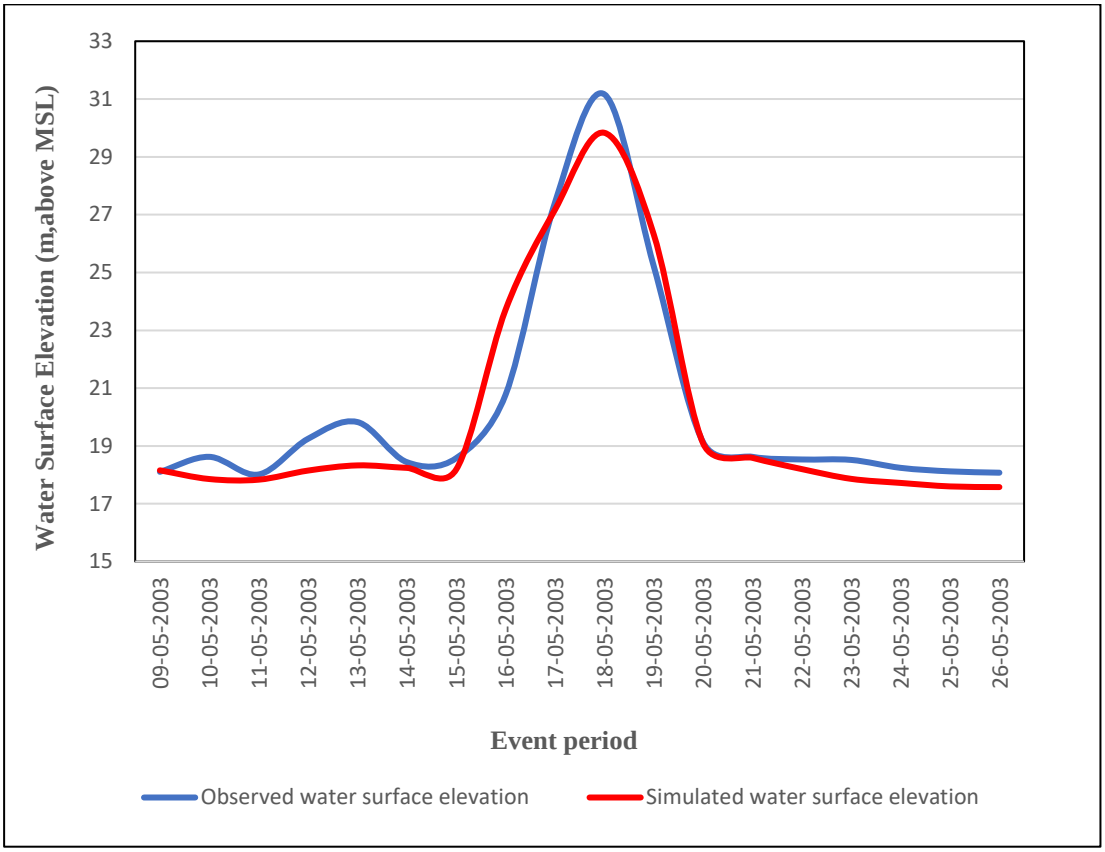

Figure 6-3 HEC-RAS model calibration

The HEC-RAS was calibrated for event 2003 as shown in Figure 6-3 and shows a very good performance rating mentioned in Table 6-6.

The calibration was done for maximum daily water surface elevation above mean sea level. The observed maximum daily water surface elevation was 31.16 m above mean sea level whereas the model maximum daily water surface elevation was estimated as 29.83 m above mean sea level.

Table 6-6 HEC-RAS model calibration performance

Calibration Goals	Model Performance	Performance Rating
Nash Sutcliffe	0.66	Very good
Coefficient of determination	0.83	Very good
Percent Bias	3.98%	Very good

Table 6-7 Initial parameters and optimized parameters for manning's value in the HEC-RAS model in the Thawalama catchment

GFCODE	Description	Initial Value	Optimized value
CCNTA	Coconut	0.035	0.0315
CHENA	Chena	0.035	0.0315
CNNAA	Channel	0.03	0.027
FRSUA	Forest	0.15	0.135
GRSLA	Grassland	0.03	0.027
HOMSA	Homestead/Garden	0.03	0.027
OTHRA	Other Cultivation	0.035	0.0385
PDDYA	Paddy field	0.035	0.0315
RBBRA	Rubber	0.04	0.036
ROCKA	Rock	0.035	0.0385
SCRBA	Scrub land	0.035	0.0315
STRMA	Minor Streams	0.03	0.027
TEAA	Tea	0.035	0.0315
UNCLA	Unclassified	0.035	0.0315

The HEC- RAS was calibrated by changing manning's n value. Trial and error were done to get good results. The initial value of manning's n value was calculated using Land use as shown in Table 6-7. The optimized manning's n value was achieved by increasing or decreasing initial manning's n value by 10%.

6.2.4 HEC-RAS Validation-Event April 1999

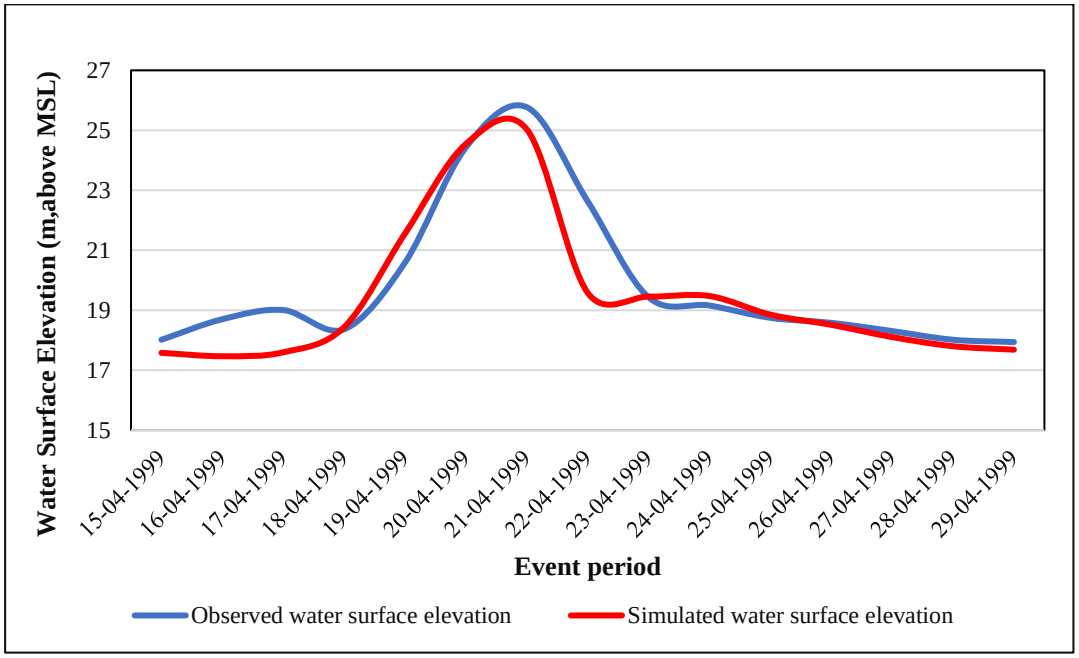

Figure 6-4 HEC-RAS model validation

The HEC-RAS was validated for event 1999 as shown in Figure 6-4 with a good performance rating as shown in Table 6-8. The validation was done for maximum daily water surface elevation above mean sea level. The observed maximum daily water surface elevation was 25.77 m above mean sea level, whereas the model maximum daily water surface elevation was estimated as 25.03 m above mean sea level.

Table 6-8 HEC-RAS model validation performance

Calibration Goals	Model Performance	Performance Rating
Nash Sutcliffe	0.62	Very good
Coefficient of determination	0.79	Very good
Percent Bias	3.28 %	Very good

6.2.5 Future Simulation

1. HEC-HMS mid-century and end- century simulation results

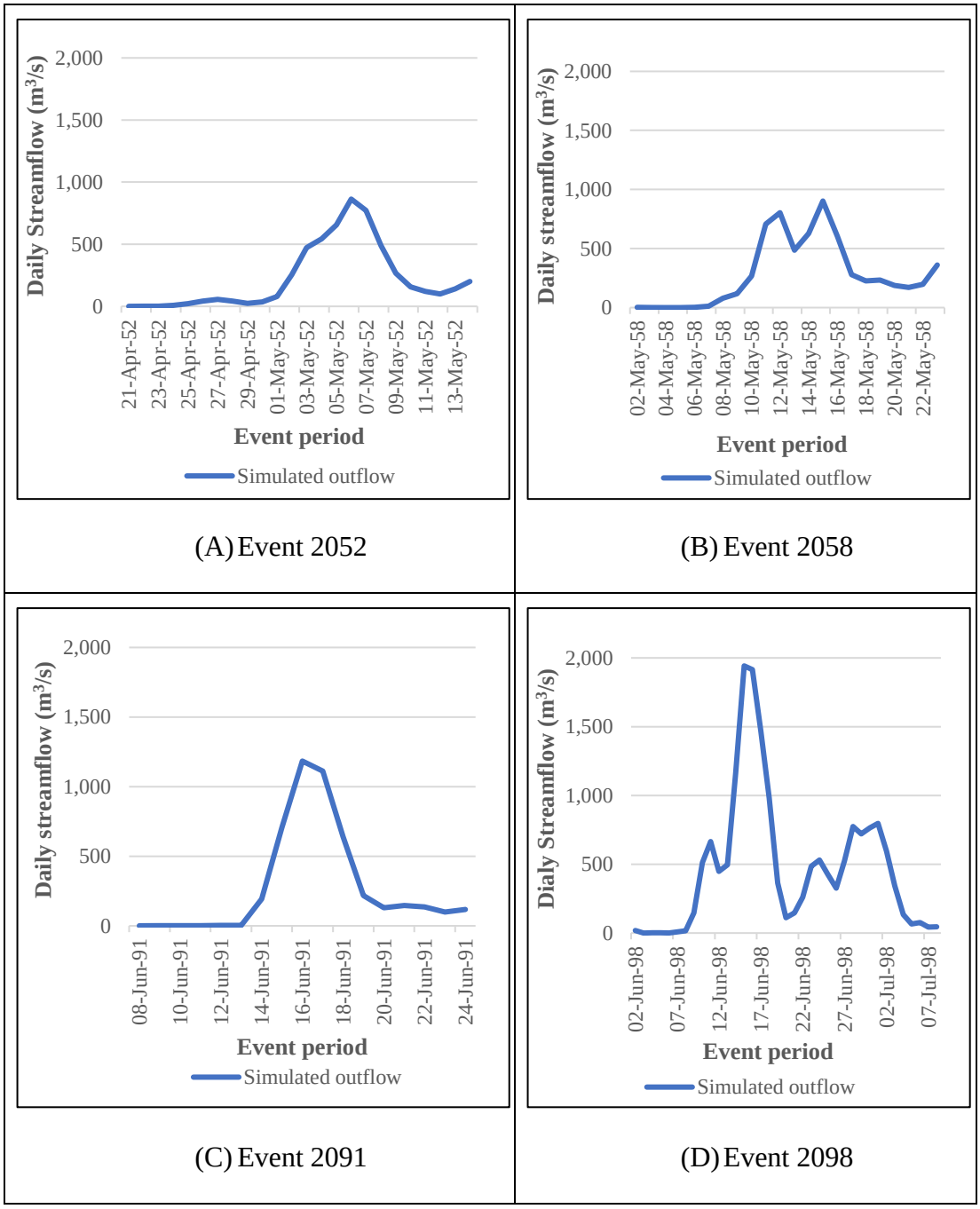

Figure 6-5 HEC-HMS simulation for future events

For future events HEC-HMS was run for the selected event using the optimized parameter as mentioned in Table 6-3 and Table 6-4. The model outflow peak observed

for events 2052, 2058, 2091, 2098 was estimated as 863.6 m^3/s, 902.6 m^3/s, 1184.1 m^3/s, 1942 m^3/s respectively as shown in Figure 6-5.

2. HEC-RAS mid-century and end- century simulation results

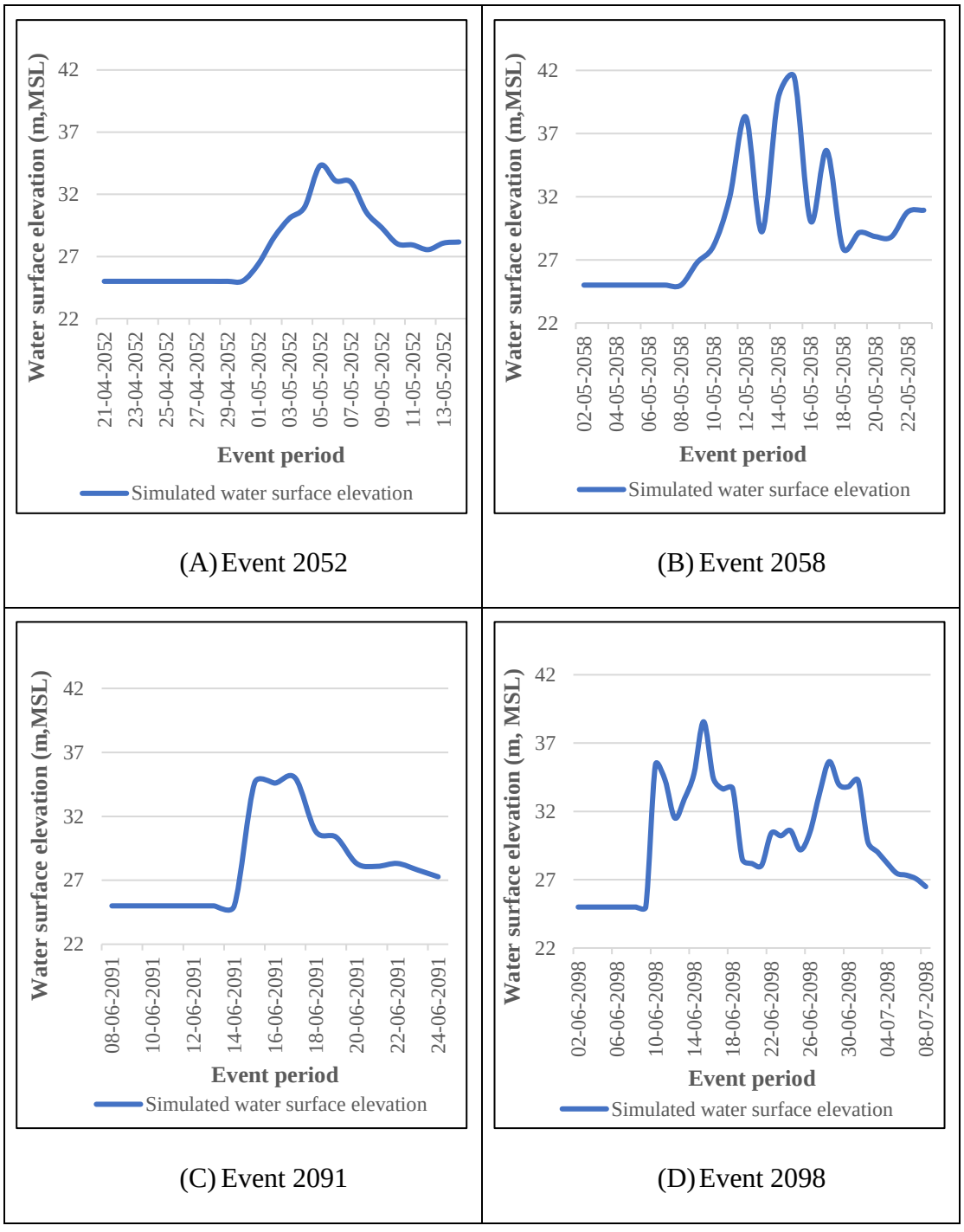

Figure 6-6 HEC-RAS simulation for future events

For future events, HEC-RAS was run for the selected event using the optimized parameter as mentioned in Table 6-8. The model simulated water surface elevation for events 2052, 2058, 2091, 2098 was estimated as 34.31 m, 41.44 m, 34.97 m, 38.56 m respectively as shown in Figure 6-6.

6.3 Flood Inundation Maps

The flood inundation maps were prepared through HEC-RAS for events 1999, 2003, 2052, 2058, 2091, 2098 after calibration and validation of events 2003, 1999 respectively.

The flood inundation maps 12-year return period for different years (2003, 2058, 2098) and 5-year return period for different years (1999, 2052, 2091) were represented separately.

6.3.1 Flood Inundation Map verification of Event 2003

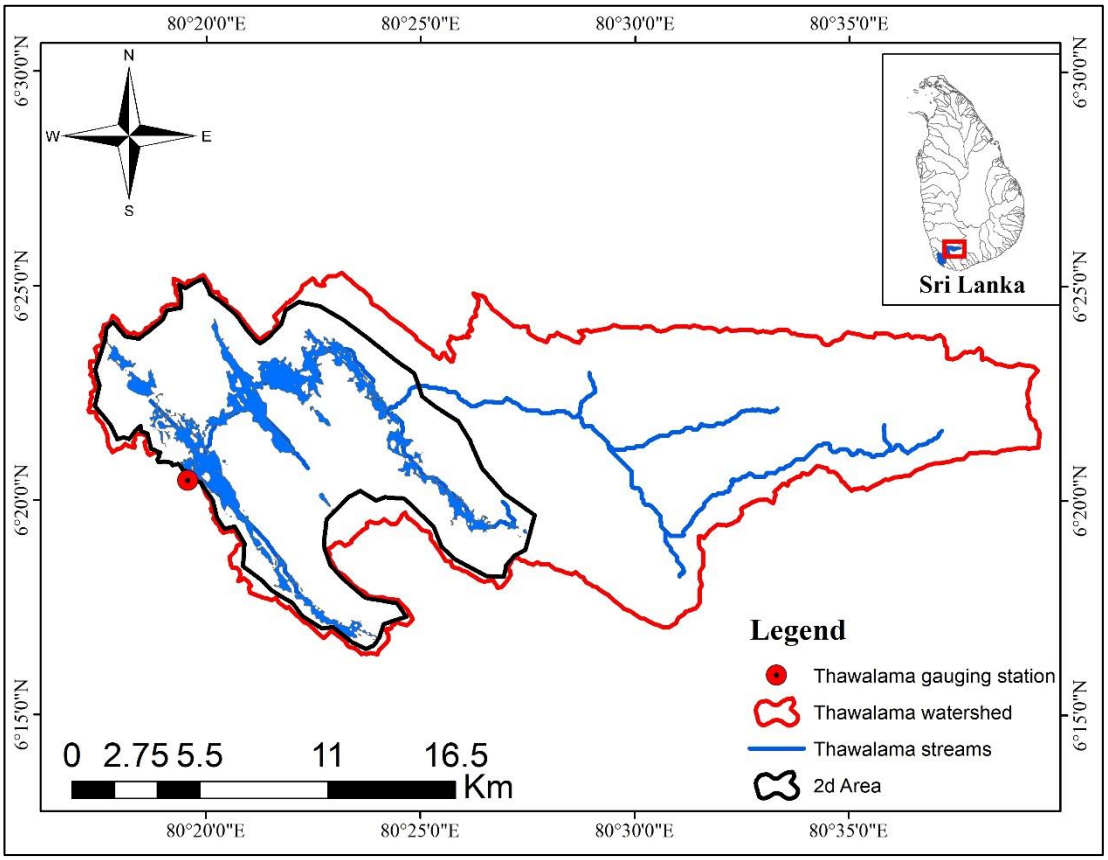

Figure 6-7 Flood Inundation map of the year 2003 event

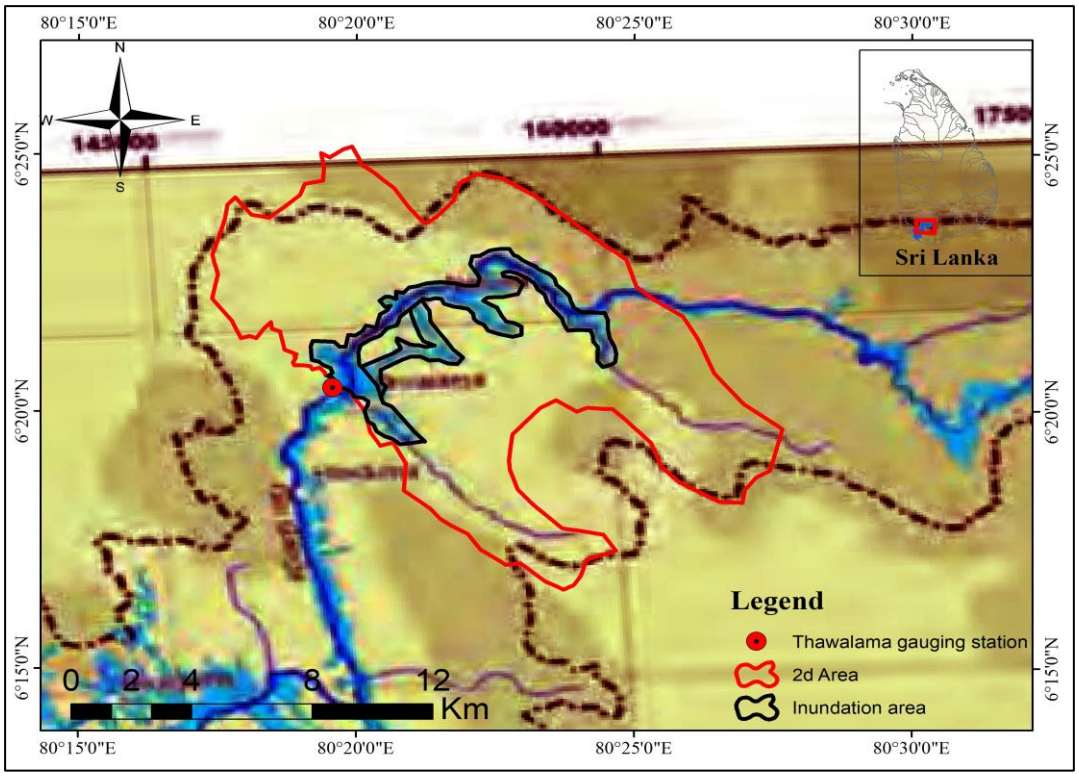

Figure 6-8 Flood Inundation map for event 2003 (Source: JICA, 2009)

From Figure 6-7, the total Inundated area using HEC-RAS was estimated to be 19.55 km² and from Figure 6-8 the total inundated area was estimated to be 16.22 km².

Since the flood inundation for the present modeling is found adequate in comparison to Japan International Cooperation Agency (JICA) report. Therefore, it can be said that the flood inundation area simulated from HEC-RAS is satisfactory.

It can be seen in Japan International Cooperation Agency (JICA) report that there is less flood extent in sub-streams of the catchment which can be because of poor resolution of terrain used during modeling from the present model in HEC-RAS. Also, the catchment edges look very smooth in a document which justifies the quality of terrain to be used may be more than 30 m which is being used in this research study.

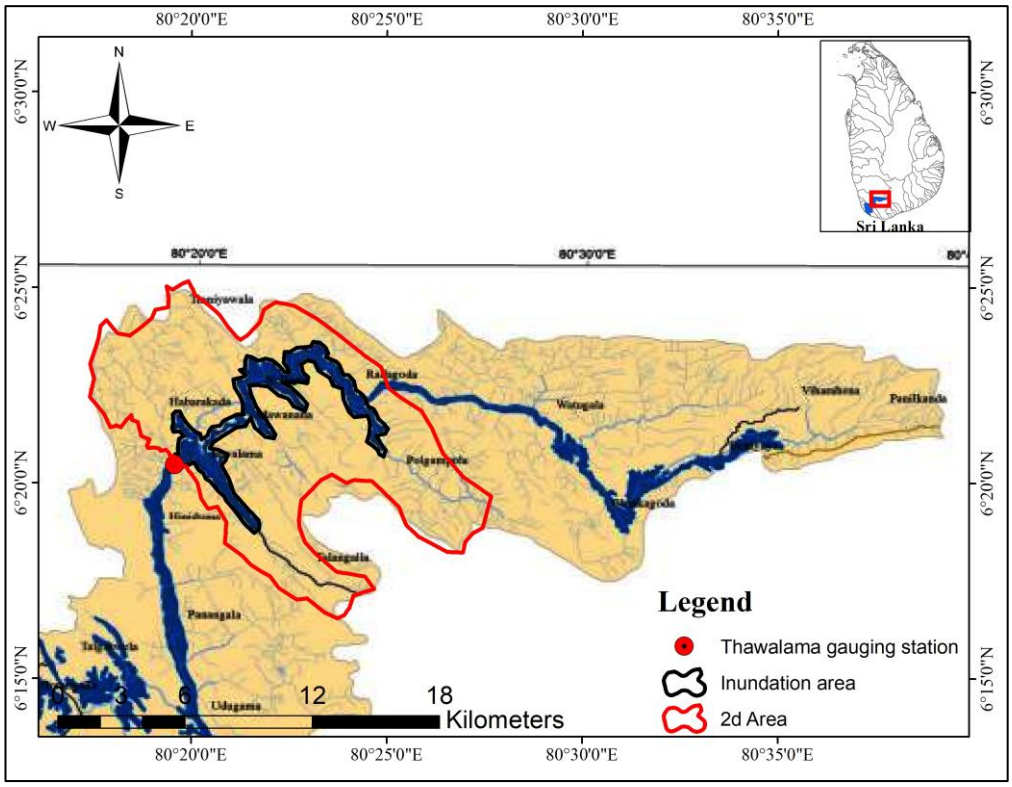

Figure 6-9 Flood Inundation Map for Event 2003 (Source: UNDP, 2010)

The flood extent map shown in Figure 6-9 was prepared by the survey of the actual flood. The ground survey was carried out using GPS monitors.

The total Inundated area using HEC-RAS in the present study and United Nations Development Programme (UNDP) report was estimated to be 19.55 km² 17.97 km² respectively.

It is found that the difference is only 8% in the flood inundation area from Figure 6-7 (2003 flood event simulated by present study) and Figure 6-9 (2003 flood event from UNDP report) inside 2-D area. Hence, the flood inundation for the present modeling is found adequate in comparison to the UNDP report.

6.3.2 12-Year Return Period

(A) Year -2003 Flood Event

From Figure 6-7, the total Inundated area was estimated to be 19.55 km² within the 2-D area of the watershed. The total inundation area was verified by JICA and UNDP report. The UNDP report flood map was found more adequate to match the flood inundation area of the present study using HEC-RAS.

(B) Mid-century Event

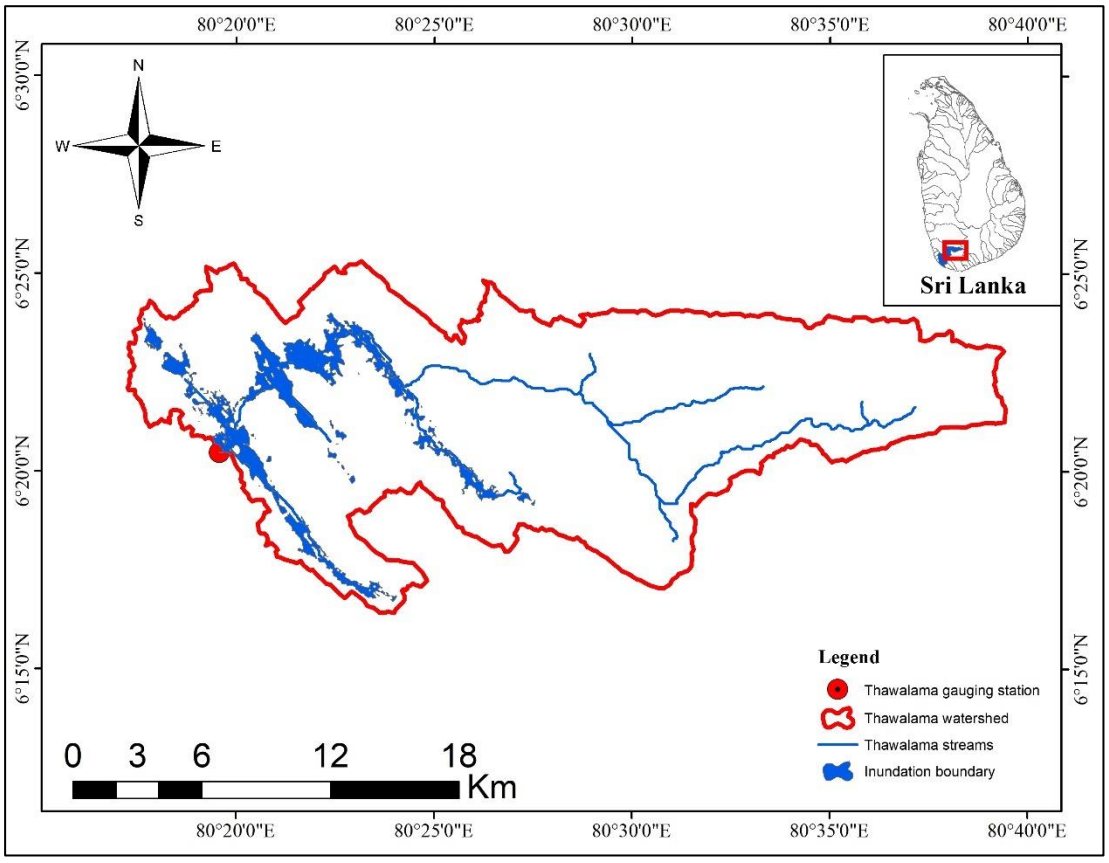

Figure 6-10 Flood Inundation map of mid-century for the 12-year return period

The total Inundated area was estimated to be 20.06 km² within the 2-D area of the Thawalama catchment shown in Figure 6-10. The inundation area was estimated to be increased from event-2003.

(C) End-century Flood Event

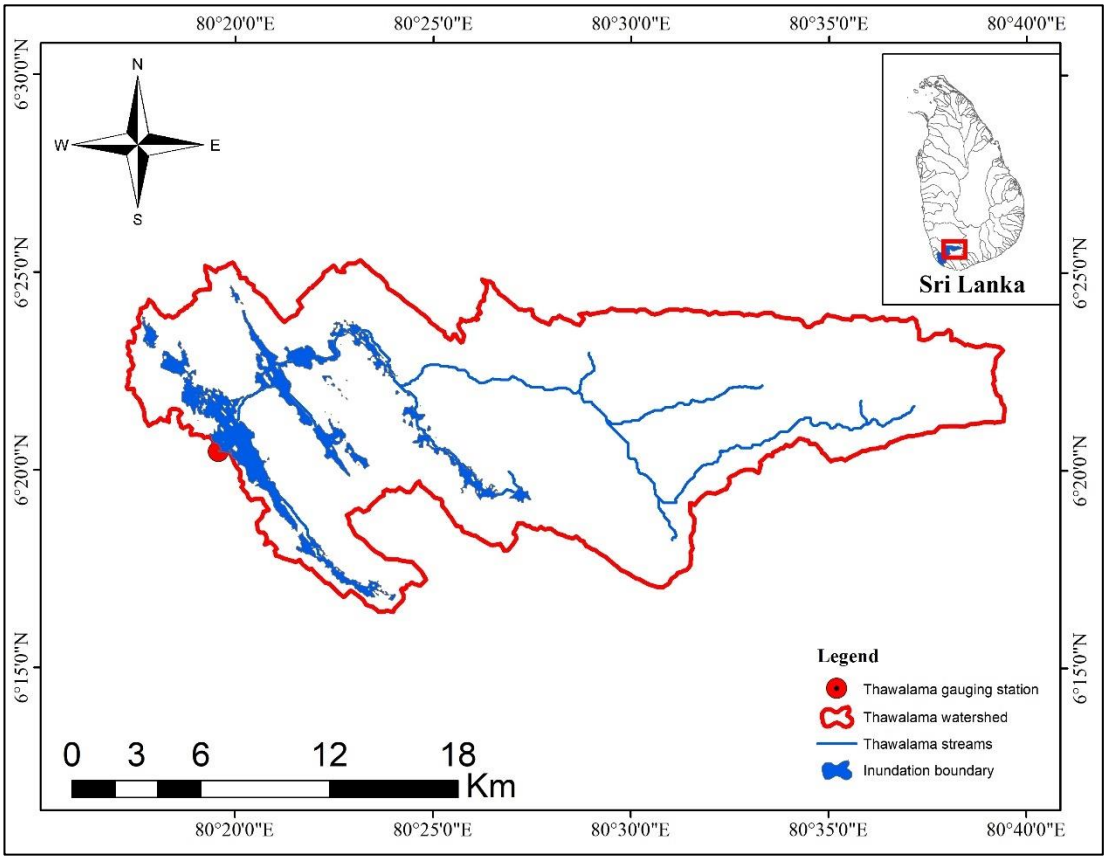

Figure 6-11 Flood Inundation map of end century for the 12-year return period

The total Inundated area was estimated to be 21.18 km² within the 2-D area of the watershed as shown in Figure 6-11. The total inundated area was increased from mid-century due to change in climate as from Figure 6-5 it can be seen that flood discharge peak was estimated to be almost double from mid-century.

6.3.3 5-Year Return Period

(A) Year -1999 Flood Event

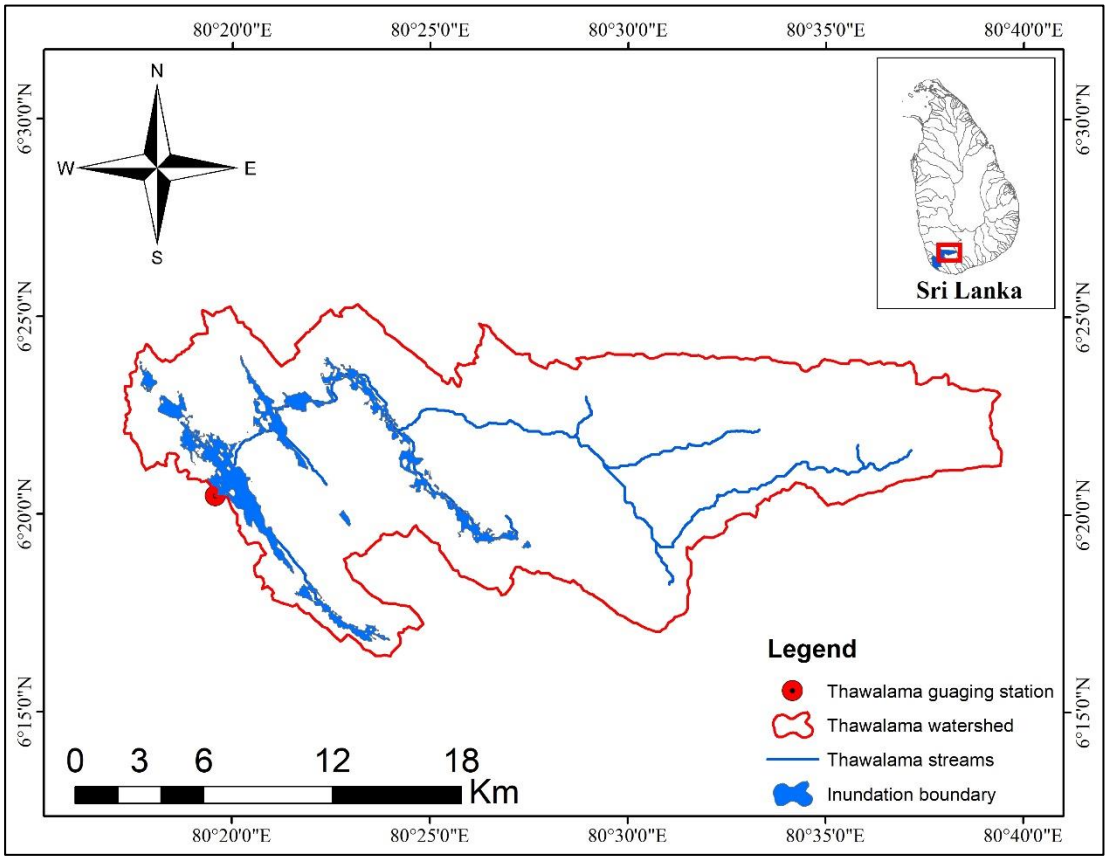

Figure 6-12 Flood Inundation map of the year 1999 event

The total Inundated area was estimated to be 17.36 km² within the 2-D area of the watershed as shown in Figure 6-12

(B) Mid-Century Flood Event

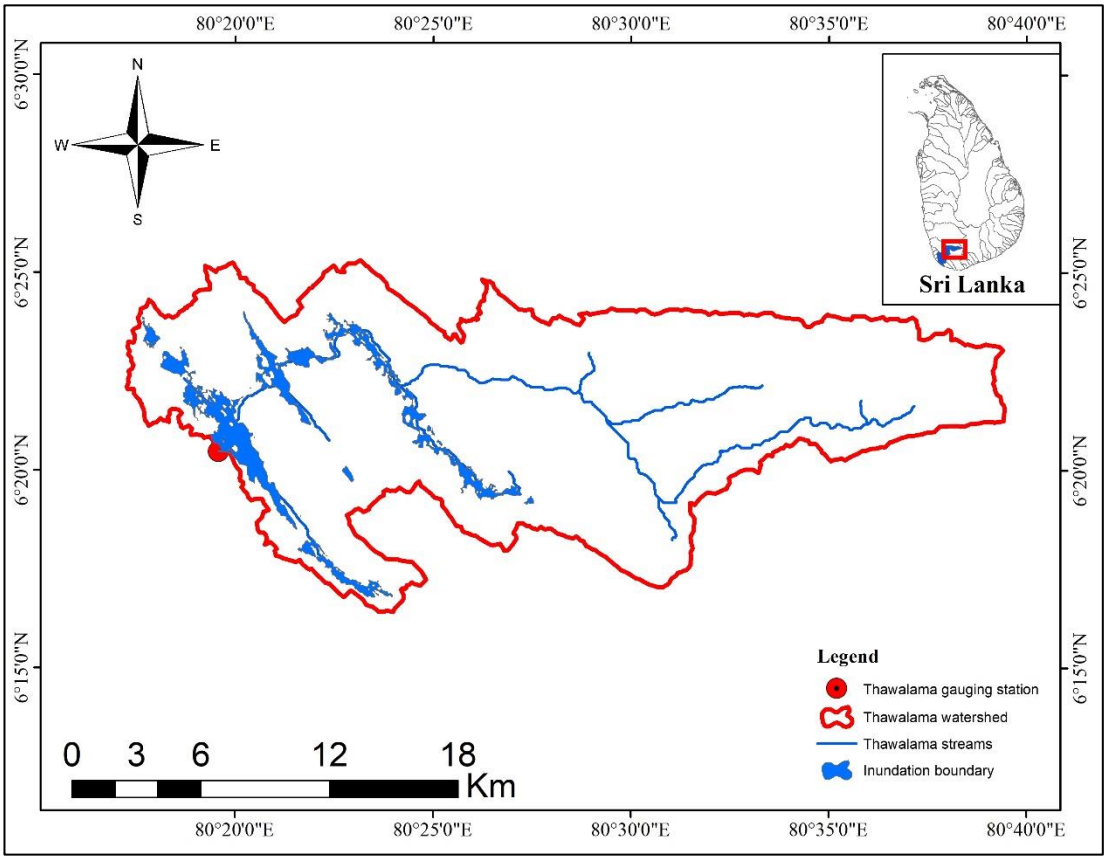

Figure 6-13 Flood Inundation map of mid-century for the 5-year return period

The total Inundated area was estimated to be 17.40 km² within the 2-D area of the watershed as shown in Figure 6-13.

The total inundated area was increased from event-1999 due to change in climate as it was estimated that flood discharge peak was increased from 631 m³/s in year 1999-event to 861 m³/s in the mid-century event.

(C) End-Century Flood Event

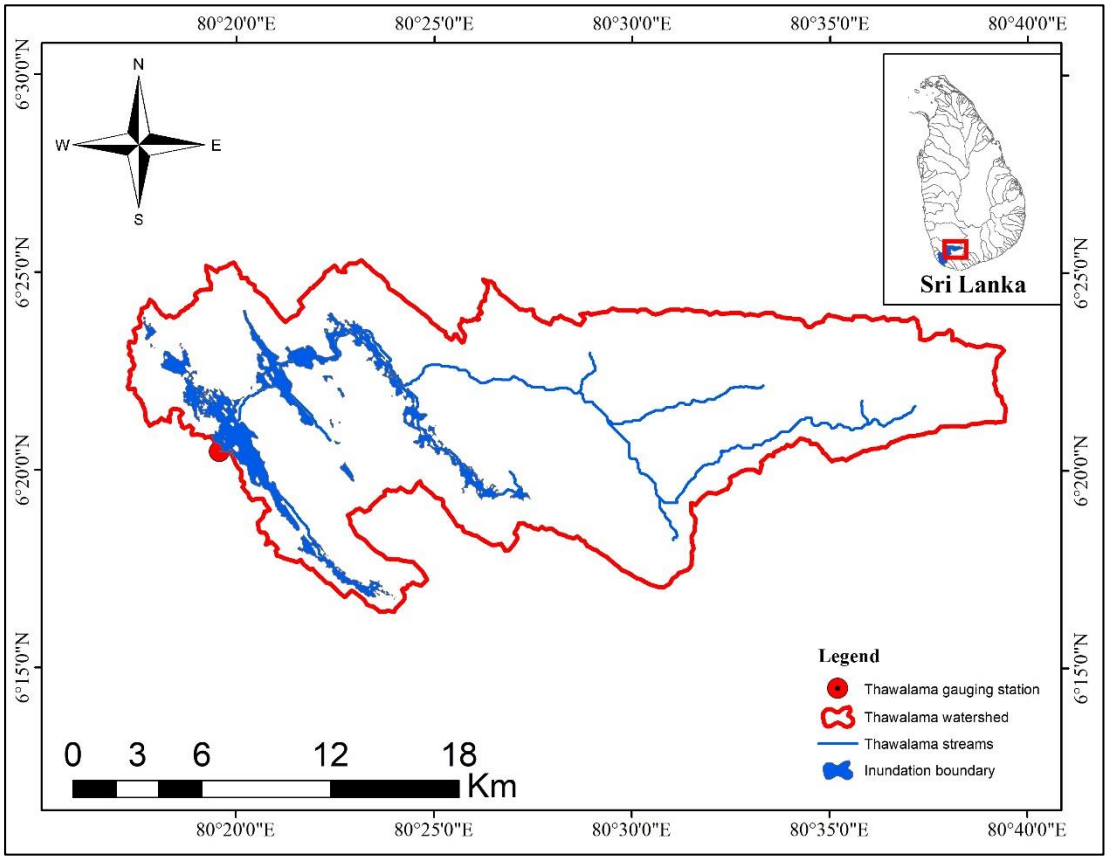

Figure 6-14 Flood Inundation map of End century for the 5-year Return period

The total Inundated area was estimated to be 19.77 km² within the 2-D area of the watershed as shown in Figure 6-14.

The total inundated area was increased from mid-century to end-century due to change in climate as from Figure 6-5 it can be observed that peak flood discharge estimated was increased from 861 m³/s in mid-century to 1184 m³/s in end-century

6.4 Flood Hazard and Vulnerability Map

In this section flood hazard and vulnerability maps, results are presented which were generated from HEC-RAS in the form of Raster. Further raster was imported to Arc-Map and thereafter, hazard maps and vulnerability maps were developed using GIS operations.

For the flood hazard and vulnerability mapping, a 12-year return period for different years (2003, 2058, 2098), and a 5-year return period for different years (1999, 2052, 2091) were represented separately.

6.4.1 Flood hazard maps

For flood hazard mapping, the flood depth and the flood velocity were adopted as hazardous parameters. These parameter maps are obtained from HEC-RAS in raster format and thereafter have been imported to ARC-GIS for obtaining flood hazard maps. To obtain flood hazard maps, flood depth and flood velocity maps were superimposed using GIS operation and further classified into various hazard levels.

A GIS operation used for flood depth and flood velocity mapping-

Step 1- Import flood depth and flood velocity map in Arc GIS from HEC-RAS.

Step 2- Reclassify into the appropriate section.

Step 3- Convert the raster to the polygon.

Step 4- Clip along the catchment boundary.

Step 5- Dissolve Grid code.

Step 6- Union with GND boundary.

The matrix used for Hazard mapping

Level of Hazards/Risk	Zero (0)	Very Low (1)	Low (2)	Moderate (3)	High (4)	Very High (5)
Zero (0)	0	0	0	0	0	0
Very Low (1)	0	1	2	3	4	5
Low (2)	0	2	4	6	8	10
Moderate (3)	0	3	6	9	12	15
High (4)	0	4	8	12	16	20
Very High (5)	0	5	10	15	20	25

Figure 6-15 Matrix for hazard and risk mapping

The hazards, social vulnerability, and risk are each graded in five levels as developed by Liu et al. (2021) in urban areas of Southern Taiwan for flood risk assessment, which is shown in Figure 6-15.

6.4.1.1 12-Year Return Period

(A) Year-2003 Flood Event

Flood Depth

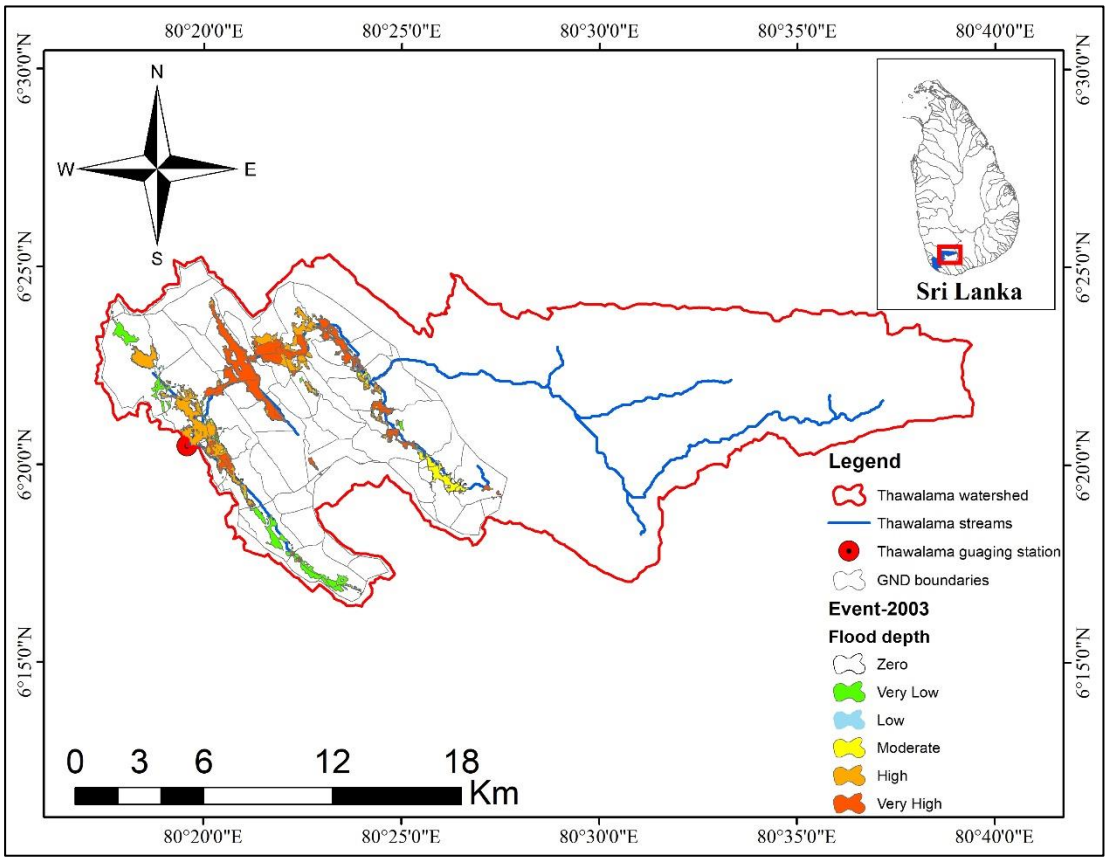

Figure 6-16 Flood depth map of the 2003-year flood event for the 12-year return period

A flood depth map was generated using Arc-GIS for flood event 2003 as shown in Figure 6-16. The hazard level area of event 2003 flood depth is mentioned in Table 6-9.

Table 6-9 Area affected by flood depth according to hazard level in the 2003-year flood event for the 12-year Return period

Hazard Level	Area (km²)
Zero	118.54
Very Low	3.20
Low	0.81
Moderate	2.22
High	6.71
Very High	7.20

Flood Velocity

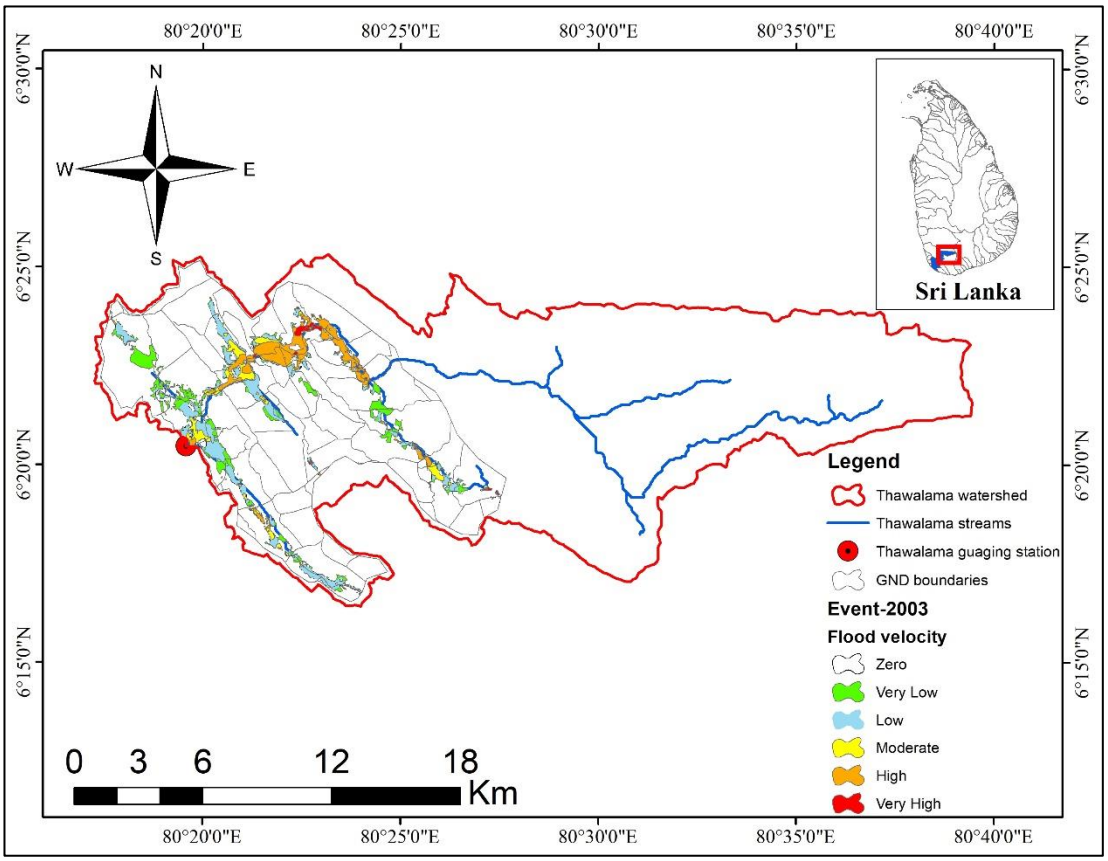

Figure 6-17 Flood velocity map of the 2003 flood event for the 12-year Return period

A flood velocity map was generated using Arc-GIS for flood event 2003 as shown in Figure 6-17. The hazard level area of event 2003 flood velocity is mentioned in Table 6-10.

Table 6-10 Area affected by flood velocity according to hazard level of the 2003 flood event for the 12-year Return period

Hazard Level	Area (km²)
Zero	118.55
Very Low	4.96
Low	6.77
Moderate	2.72
High	5.13
Very High	0.54

Flood Hazard Map

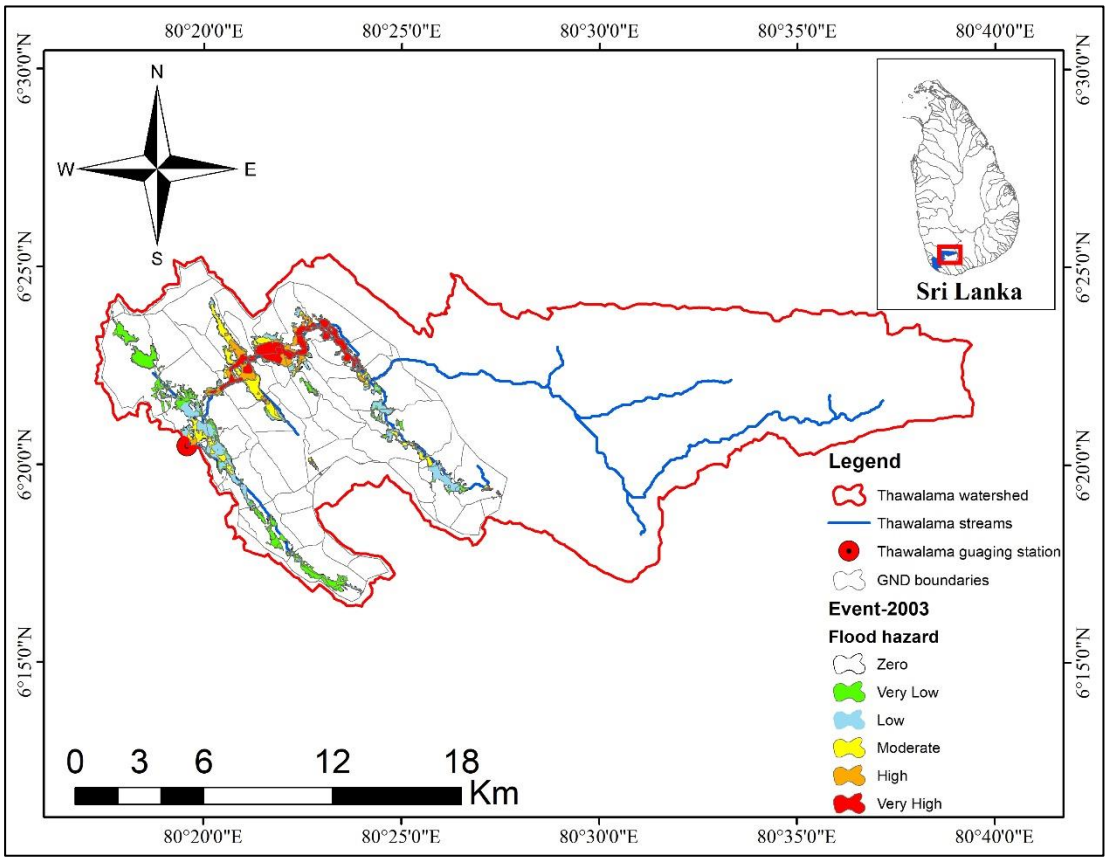

Figure 6-18 Flood hazard map of the 2003 flood event for the 12-year return period

A flood hazard map was generated using Arc-GIS for flood event 2003 as shown in Figure 6-18. The hazard level area of event 2003 flood hazard is mentioned in Table 6-11.

Table 6-11 Area affected by flood hazard according to hazard level in the 2003 flood event for the 12-year return period

Hazard Level	Area (km²)
Zero	119.04
Very Low	6.20
Low	4.26
Moderate	3.38
High	2.28
Very High	3.51

(B) Mid-Century flood event

Flood Depth

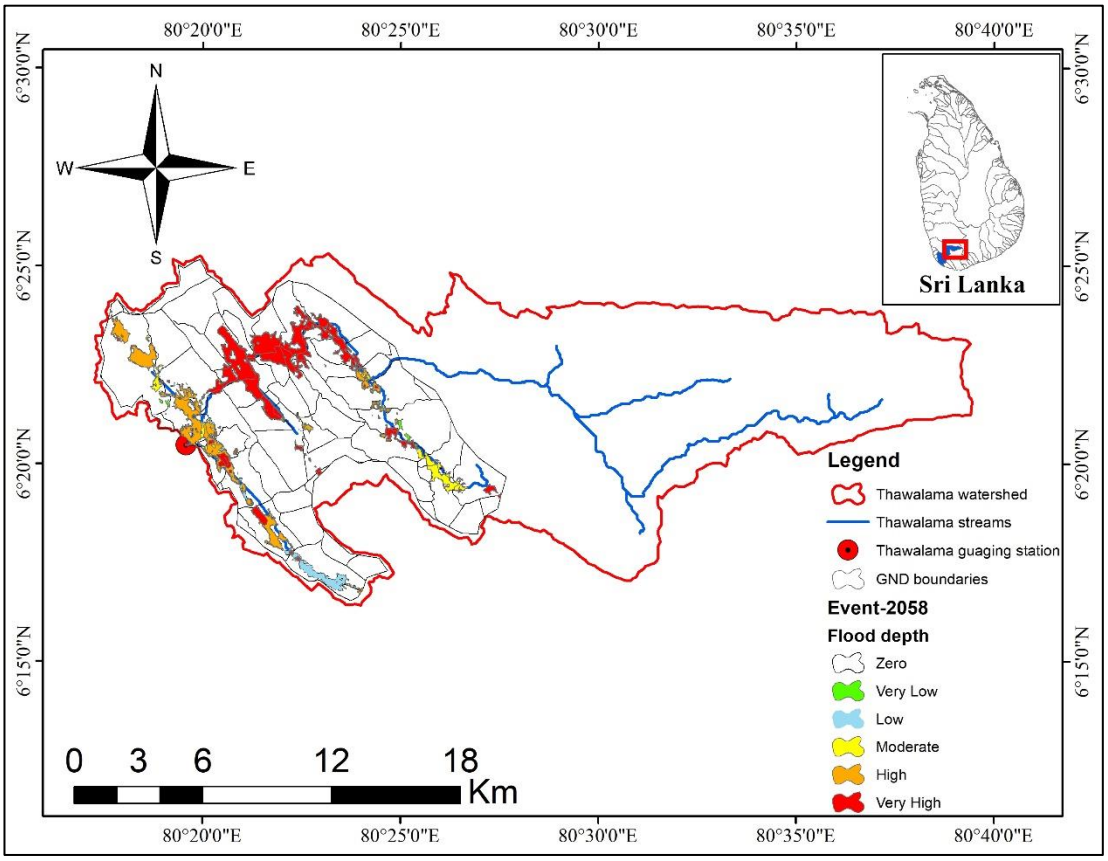

Figure 6-19 Flood depth map of the mid-century flood event for the 12-year return period

A flood depth map of mid-century was generated using Arc-GIS for flood events of 12-year return period as shown in Figure 6-19.

Table 6-12 Area affected by flood depth according to hazard level in the mid-century flood event for the 12-year return period

Hazard Level	Area (km²)
Zero	118.14
Very Low	0.91
Low	1.73
Moderate	2.64
High	6.10
Very High	9.15

The hazard level area by flood depth of mid-century flood event for the 12-year return period is mentioned in Table 6-12.

Flood Velocity

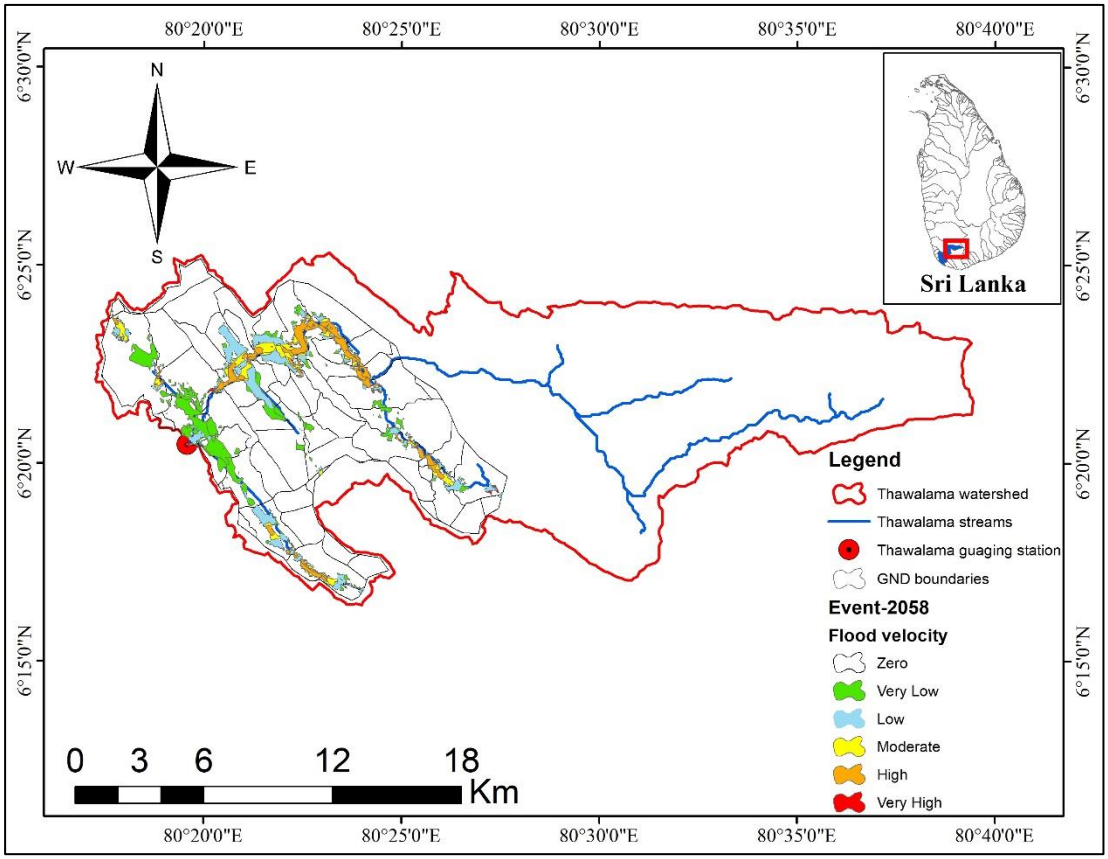

Figure 6-20 Flood velocity map of the mid-century flood event for the 12-year return period

Flood velocity map of mid-century was generated using Arc-GIS for flood event of 12-year return period as shown in Figure 6-20. The hazard level area by flood velocity of mid-century flood events for the 12-year return period is mentioned in Table 6-13.

Table 6-13 Area affected by flood velocity according to hazard level in the mid-century flood event for the 12-year return period

Hazard Level	Area (km²)
Zero	118.10
Very Low	7.26
Low	5.92
Moderate	3.04
High	4.24
Very High	0.13

Flood Hazard Map

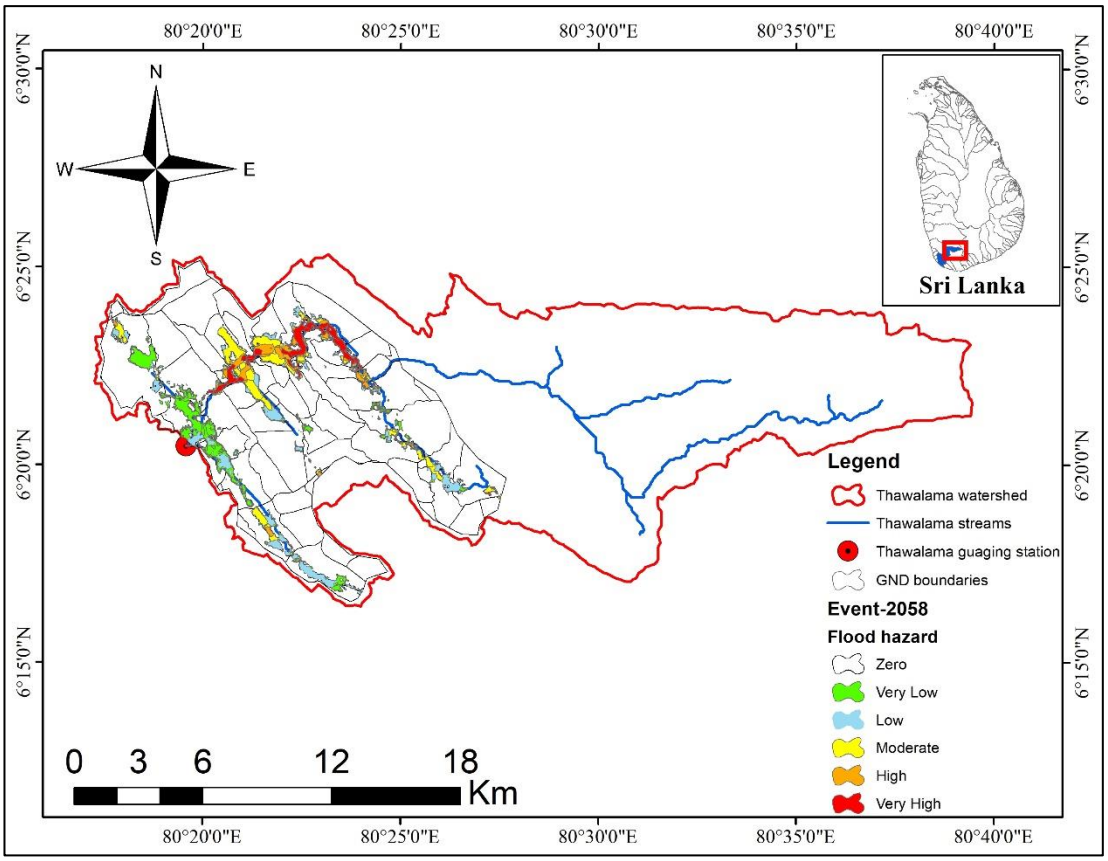

Figure 6-21 Flood hazard map of the mid-century flood event for the 12-year Return period

Flood hazard map of mid-century was generated using Arc-GIS for flood event of 12-year return period as shown in Figure 6-21. The hazard level area by flood hazard map of mid-century flood events for the 12-year return period is mentioned in Table 6-13.

Table 6-14 Area affected by flood hazard according to hazard level in the mid-century flood event for the 12-Year Return period

Hazard Level	Area (km²)
Zero	118.19
Very Low	6.77
Low	4.19
Moderate	4.68
High	2.34
Very High	2.50

(C) End-Century Flood Event

Flood Depth

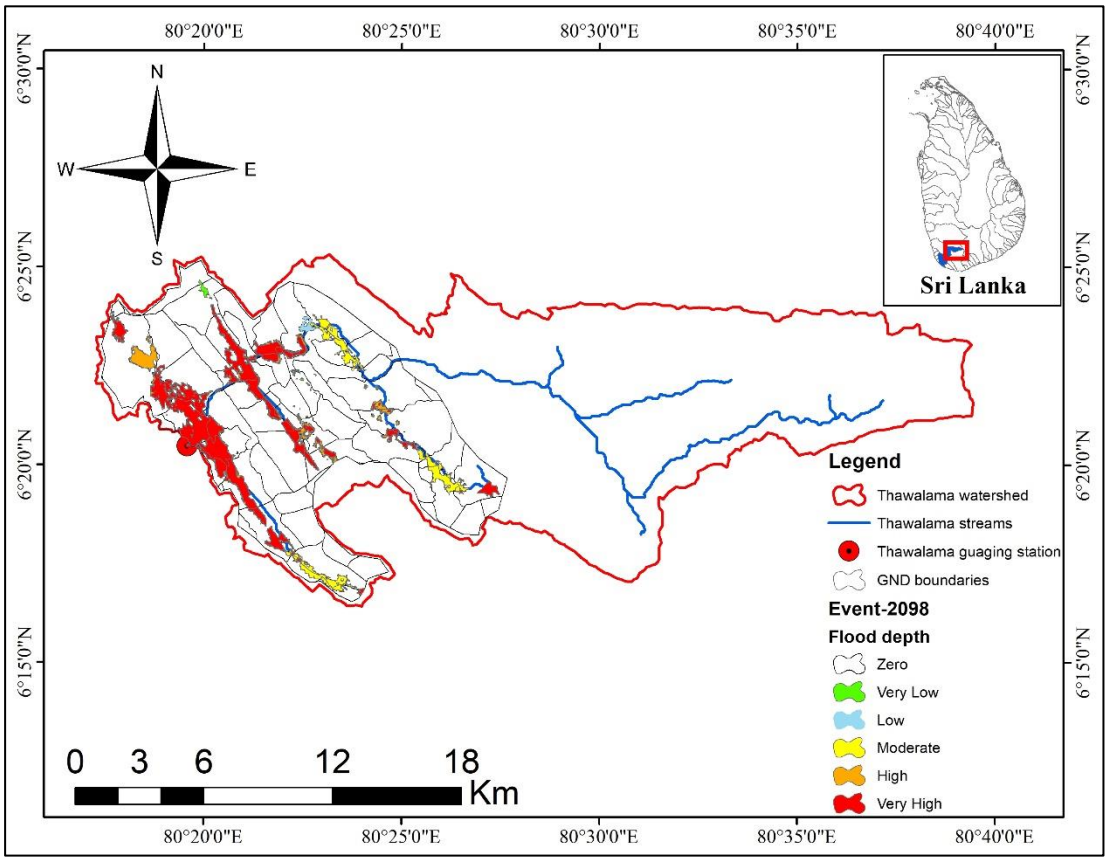

Figure 6-22 Flood depth map of end-century flood event for the 12-year return period

Flood depth map of end-century was generated using Arc-GIS for flood event of 12-year return period as shown in Figure 6-22. The hazard level area by flood depth map of mid-century flood events for the 12-year return period is mentioned in Table 6-15.

Table 6-15 Area affected by flood depth according to hazard level in end-century flood event for the 12-year return period

Hazard Level	Area (km²)
Zero	117.09
Very Low	0.78
Low	0.88
Moderate	3.90
High	3.19
Very High	12.84

Flood Velocity

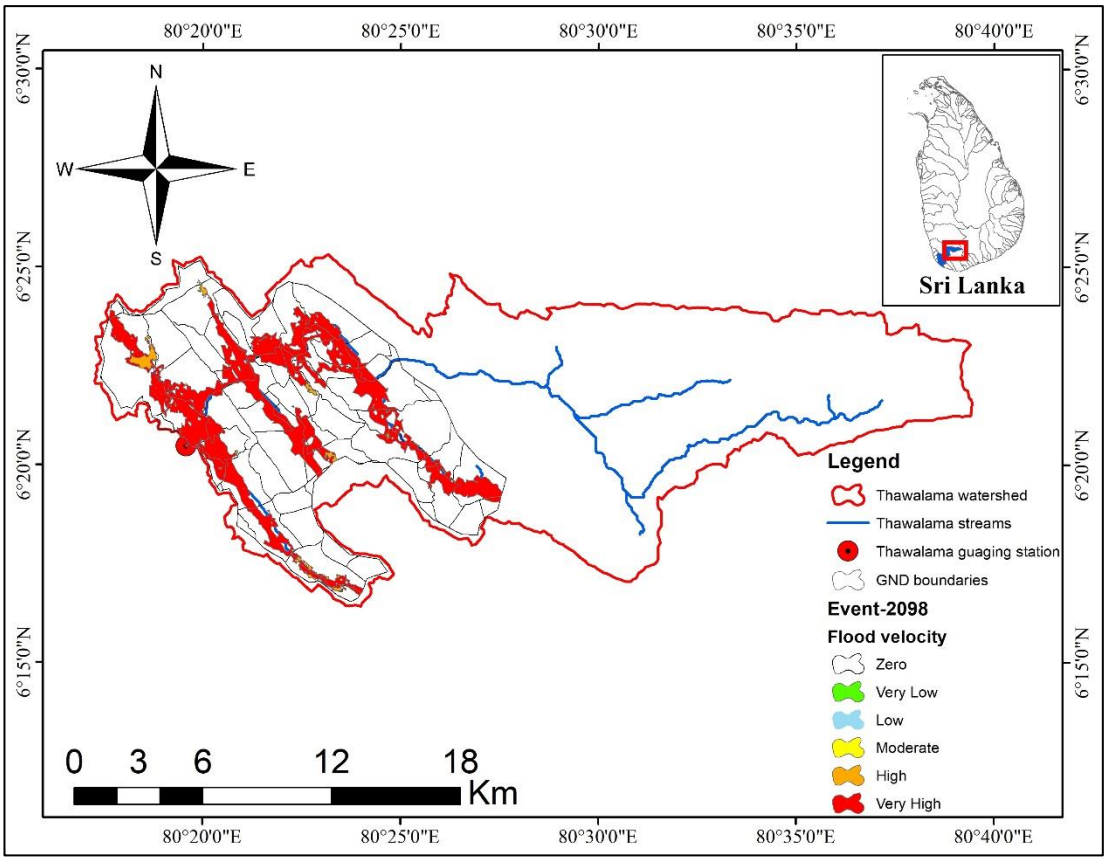

Figure 6-23 Flood velocity map of end-century flood event for the 12-year Return period

Flood velocity map of end-century was generated using Arc-GIS for flood event of 12-year return period as shown in Figure 6-23. The hazard level area by flood velocity of end-century flood event for the 12-year return period is mentioned in Table 6-16.

Table 6-16 Area affected by flood velocity according to hazard level in end-century flood event for the 12-year return period

Hazard Level	Area (km²)
Zero	104.23
Very Low	0.01
Low	0.04
Moderate	0.06
High	1.33
Very High	33.01

Flood Hazard Map

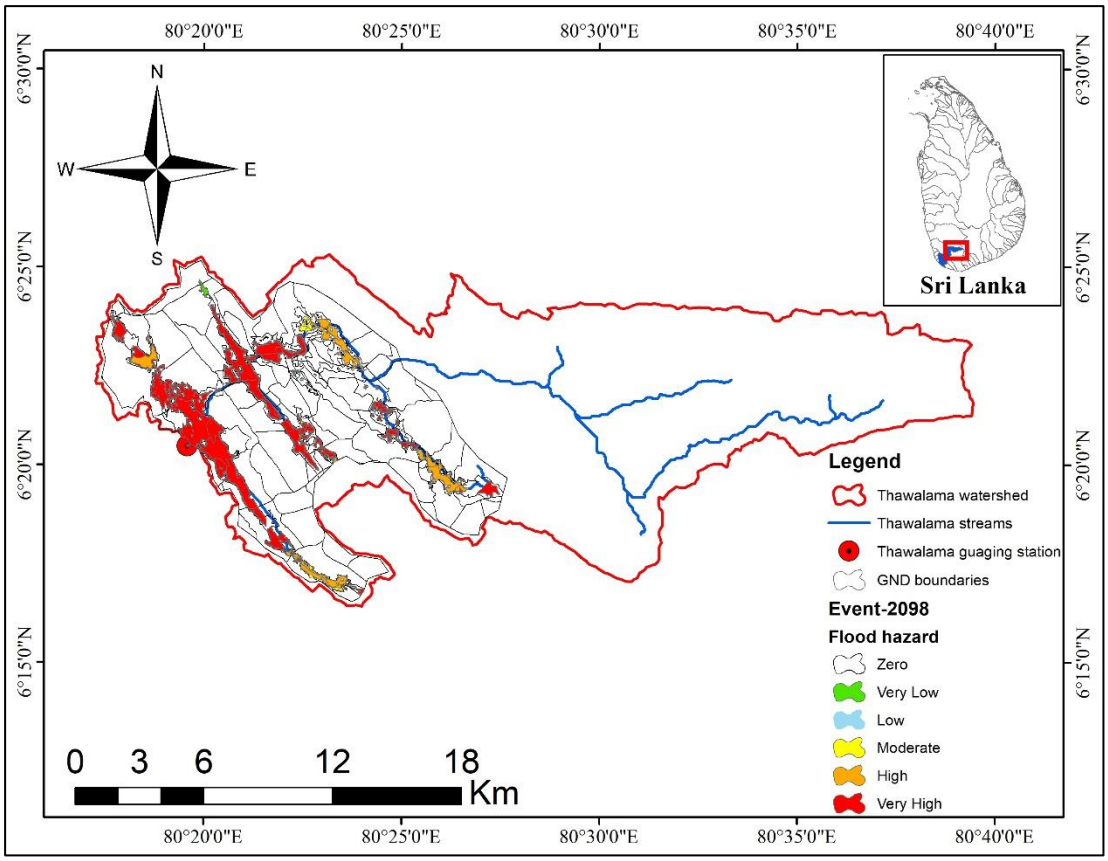

Figure 6-24 Flood hazard map of end-century flood event for the 12-year return period

Flood hazard map of end-century was generated using Arc-GIS for flood event of 12-year return period as shown in Figure 6-24. The hazard level area by flood hazard map of end-century flood events for the 12-year return period is mentioned in Table 6-17.

Table 6-17 Area affected by flood hazard according to hazard level in end-century flood event for the 12-year return period

Hazard Level	Area (km²)
Zero	117.20
Very Low	0.18
Low	0.62
Moderate	1.02
High	4.29
Very High	15.36

6.4.1.2 *5-Year Return period*

(A) The 1999-Year Flood event

Flood Depth

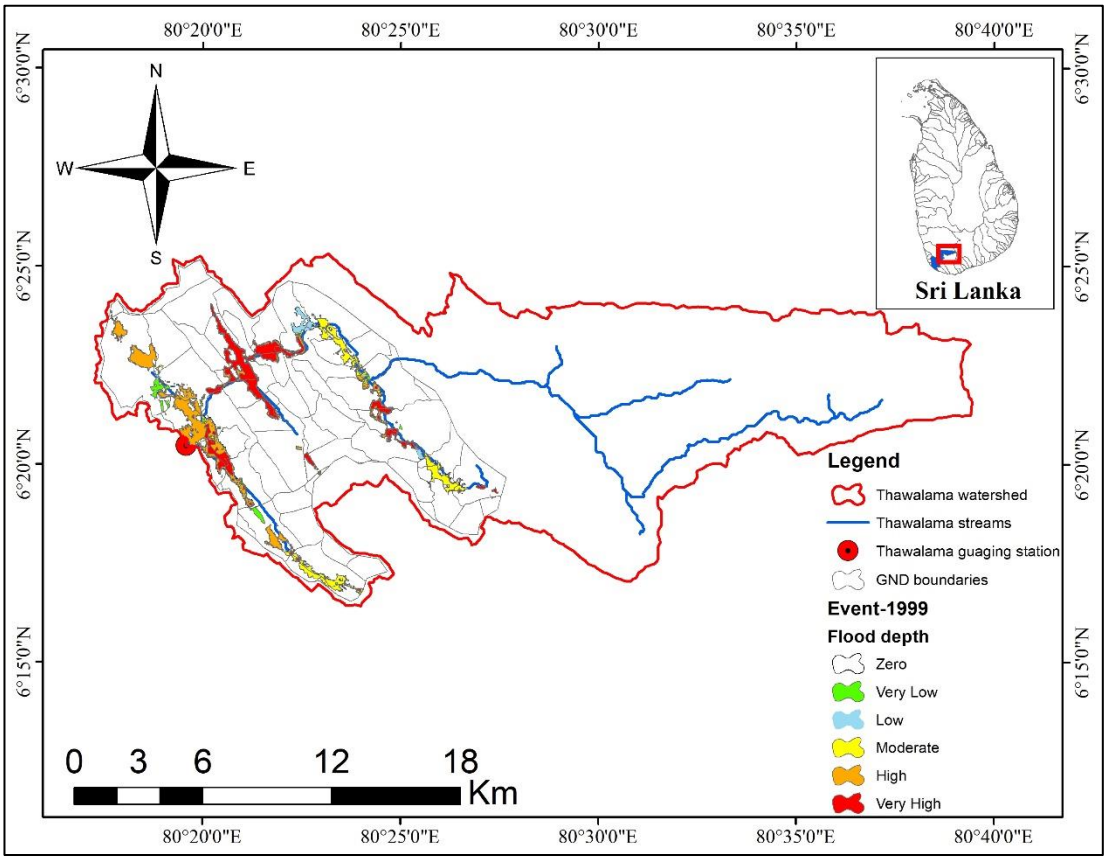

Figure 6-25 Flood depth map of 1999 flood event for the 5-year return period

Table 6-18 Area affected by flood depth according to hazard level in the 1999 year flood event for the 5-year return period

Hazard Level	Area (km²)
Zero	121.35
Very Low	1.44
Low	1.32
Moderate	3.87
High	5.78
Very High	4.91

A flood depth map was generated using Arc-GIS for flood event 1999 as shown in Figure 6-25. The hazard level area of event 1999 flood depth is mentioned in Table 6-18.

Flood Velocity

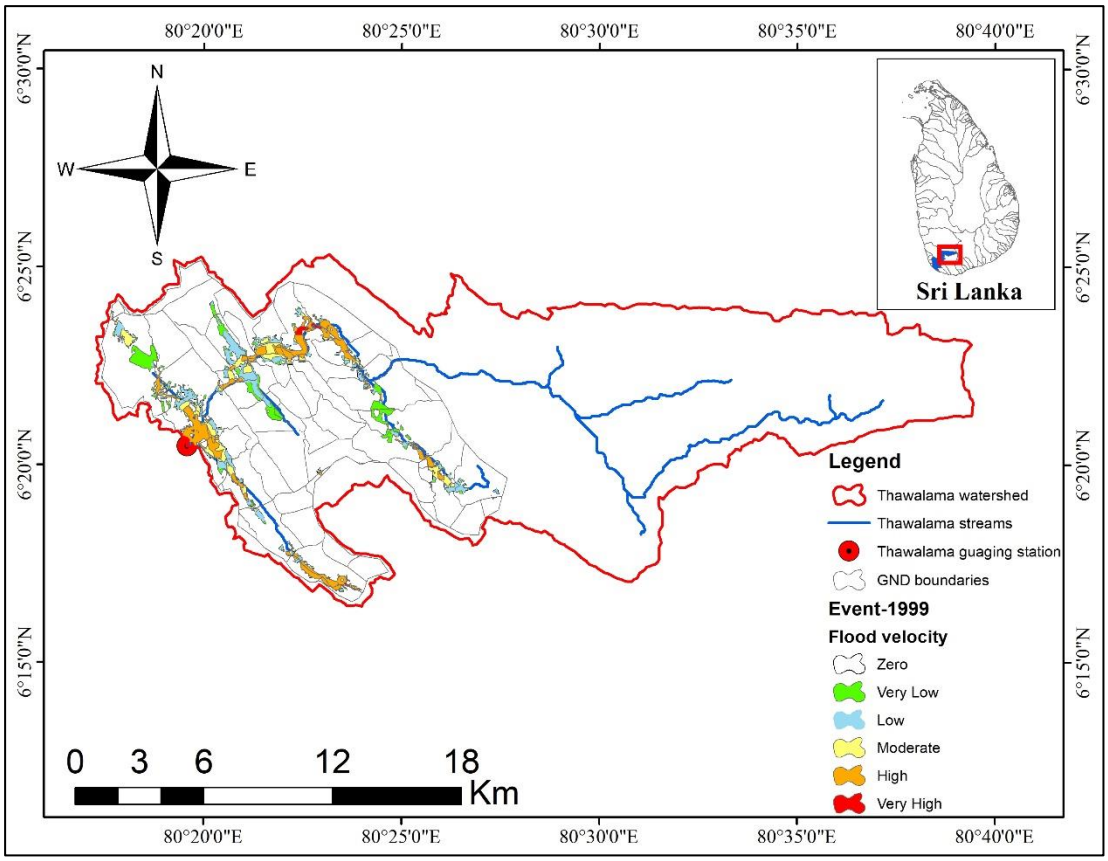

Figure 6-26 Flood velocity map of 1999 flood event for the 5-year return period

Table 6-19 Area affected by flood velocity according to hazard level in the 1999 year flood event for the 5-year return period

Hazard Level	Area (km²)
Zero	120.52
Very Low	3.63
Low	4.78
Moderate	3.61
High	5.82
Very High	0.32

A flood velocity map was generated using Arc-GIS for flood event 1999 as shown in Figure 6-26. The hazard level area of the event 1999 flood velocity map is mentioned in Table 6-19.

Flood Hazard Map

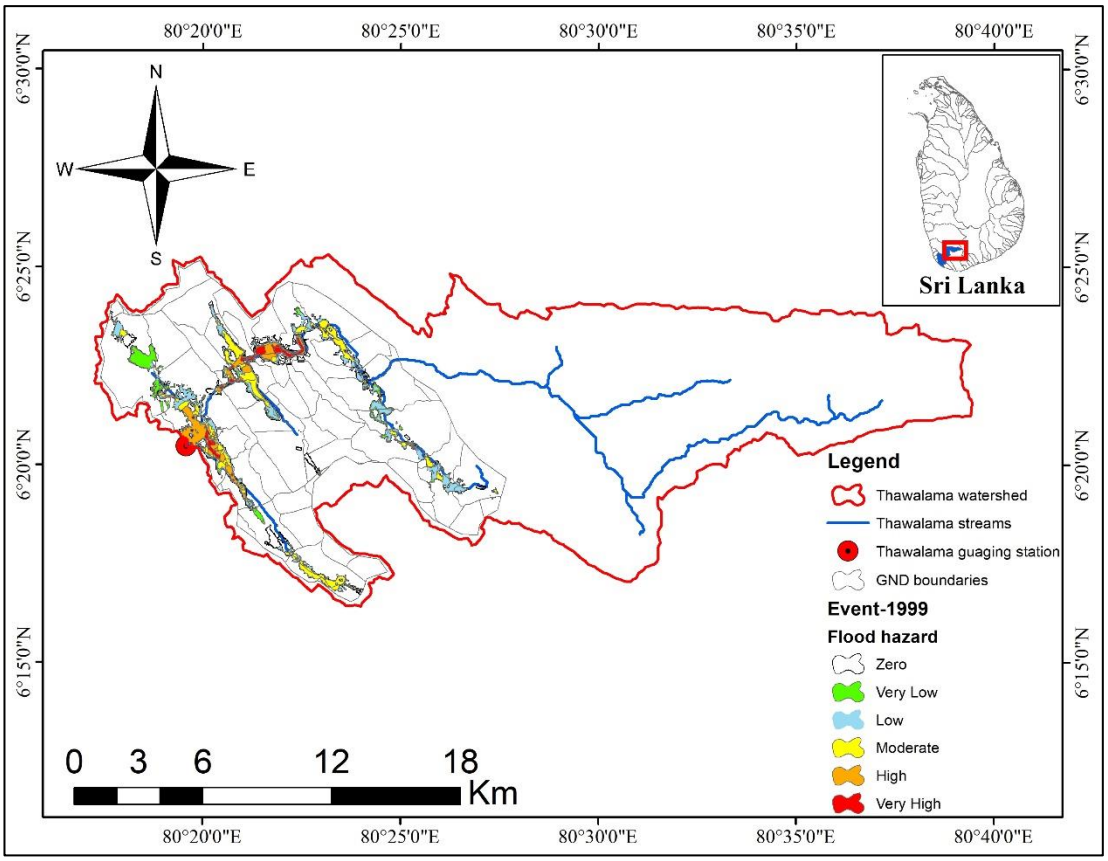

Figure 6-27 Flood hazard map of the 1999-year flood event for the 5-year return period

A flood hazard map was generated using Arc-GIS for flood event 1999 as shown in Figure 6-27. The hazard level area of event 1999 flood hazard map is mentioned in Table 6-20.

Table 6-20 Area affected by flood hazard according to hazard level in 1999 flood event for the 5-year return period

Hazard Level	Area (km²)
Zero	122.90
Very Low	3.14
Low	4.15
Moderate	4.68
High	2.78
Very High	1.04

(B) Mid Century

Food Depth

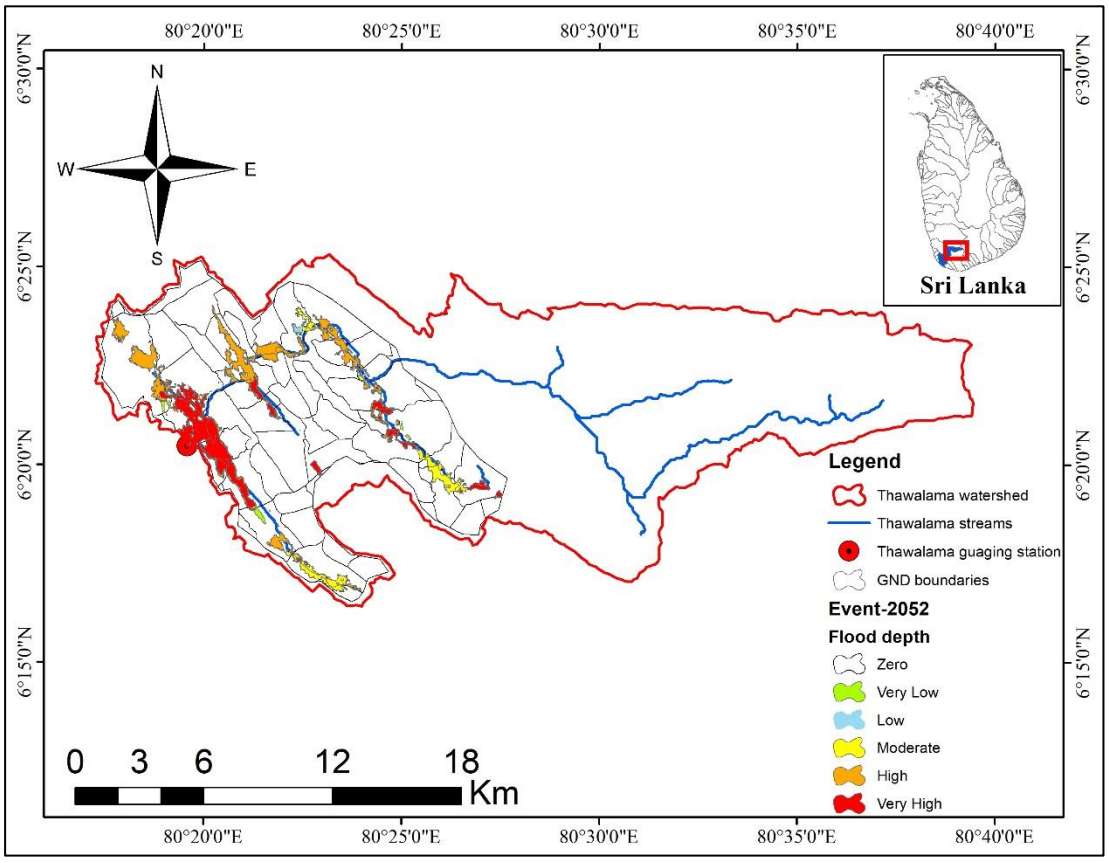

Figure 6-28 Flood depth map of the mid-century flood event for the 5-year return period

Flood depth map of mid-century was generated using Arc-GIS for flood event of 5-year return period as shown in Figure 6-28. The hazard level area by flood hazard map of end-century flood event for the 12-year return period is mentioned in Table 6-21.

Table 6-21 Area affected by flood depth according to hazard level in mid-century flood event for the 5-year return period

Hazard Level	Area (km²)
Zero	120.79
Very Low	0.89
Low	0.86
Moderate	3.39
High	6.69
Very High	6.06

Flood Velocity

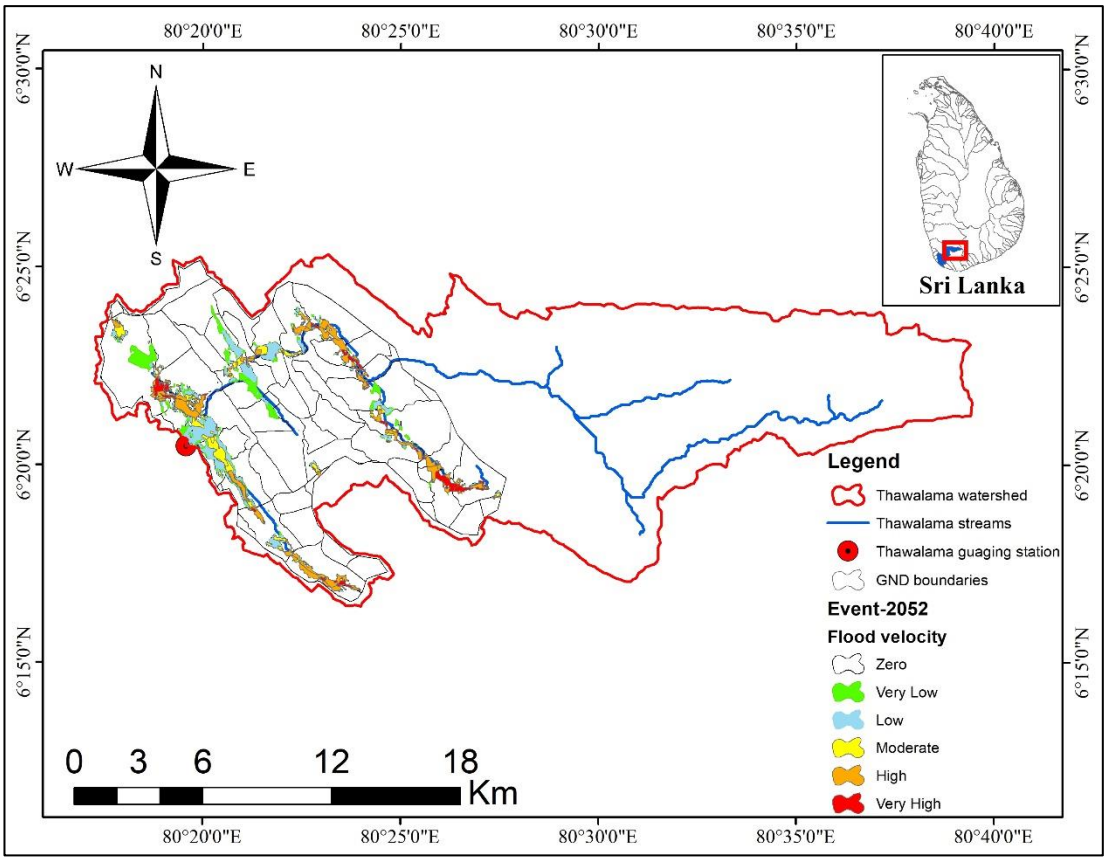

Figure 6-29 Flood velocity map of the mid-century flood event for the 5-year return period

Flood velocity map of mid-century was generated using Arc-GIS for flood event of 5-year return period as shown in Figure 6-29. The hazard level area by flood velocity map of mid-century flood events for the 5-year return period is mentioned in Table 6-22.

Table 6-22 Area affected by flood velocity according to hazard level in mid-century flood event for the 5-year return period

Hazard Level	Area (km²)
Zero	120.81
Very Low	3.03
Low	5.11
Moderate	2.66
High	5.45
Very High	1.62

Flood Hazard Map

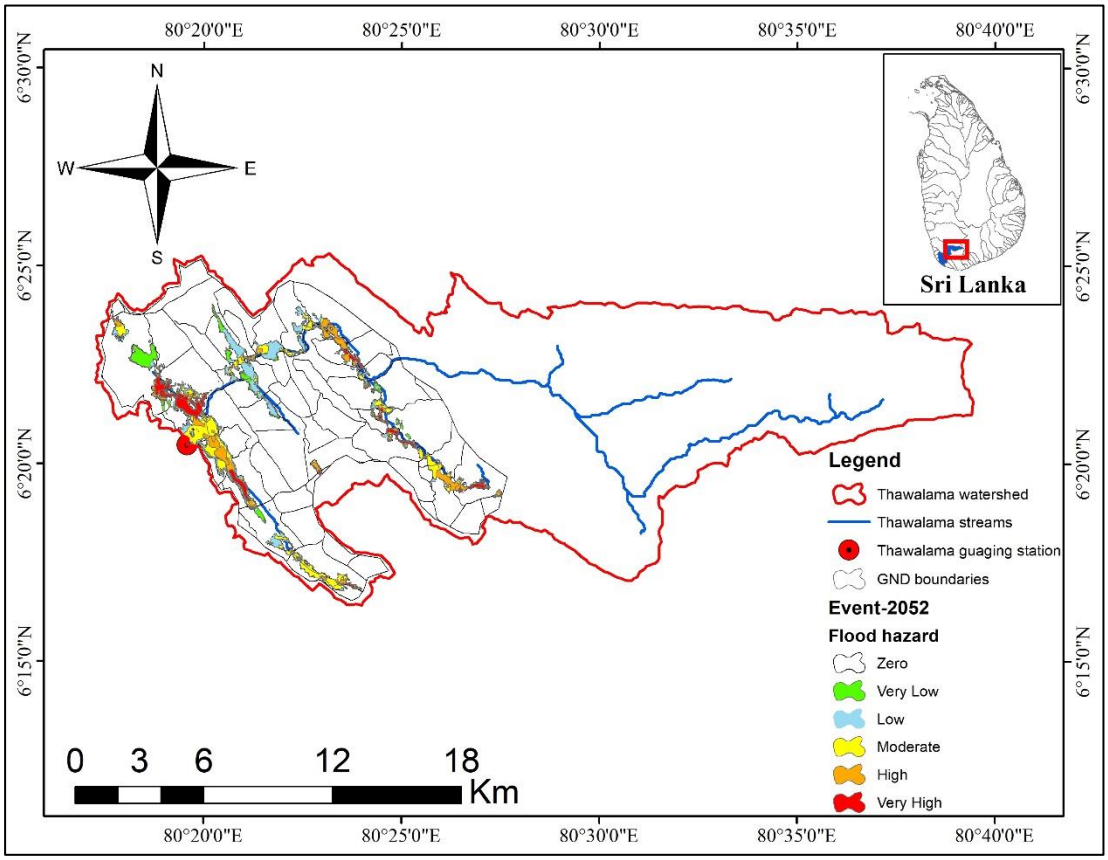

Figure 6-30 Flood hazard map of the mid-century flood event for the 5-year return period

Flood hazard map of mid-century was generated using Arc-GIS for flood event of 5-year return period as shown in Figure 6-30. The hazard level area by flood hazard of mid-century flood event for the 5-year return period is mentioned in Table 6-23.

Table 6-23 Area affected by flood hazard according to hazard level in mid-century flood event for the 5-year return period

Hazard Level	Area (km²)
Zero	121.22
Very Low	2.85
Low	3.70
Moderate	5.06
High	3.71
Very High	2.14

(C) End- Century

Flood Depth

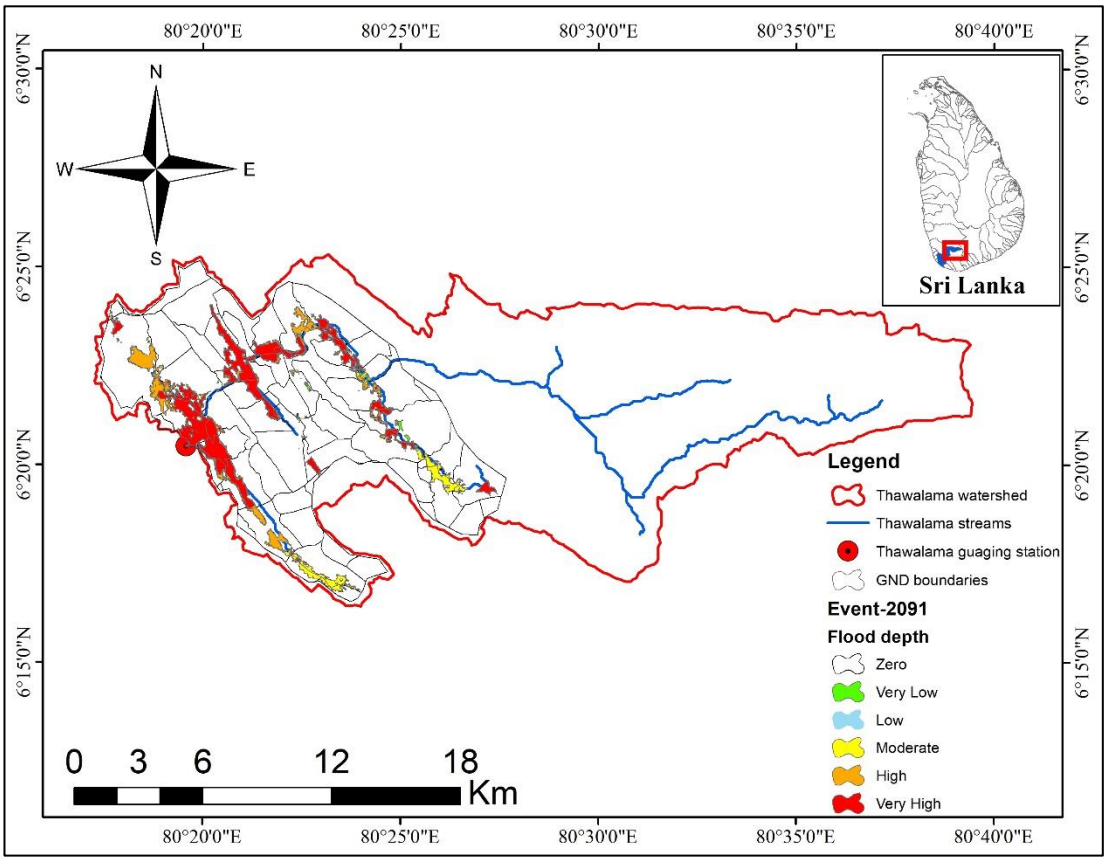

Figure 6-31 Flood depth map of end-century flood event for the 5-year return period

Flood depth map of end-century was generated using Arc-GIS for flood event of 5-year return period as shown in Figure 6-31. The hazard level area by flood depth map of end-century flood events for the 5-year return period is mentioned in Table 6-24.

Table 6-24 Area affected by flood depth of end-century flood event for the 5-year return period

Hazard Level	Area (km²)
Zero	118.60
Very Low	0.80
Low	0.65
Moderate	3.13
High	5.22
Very High	10.28

Flood Velocity

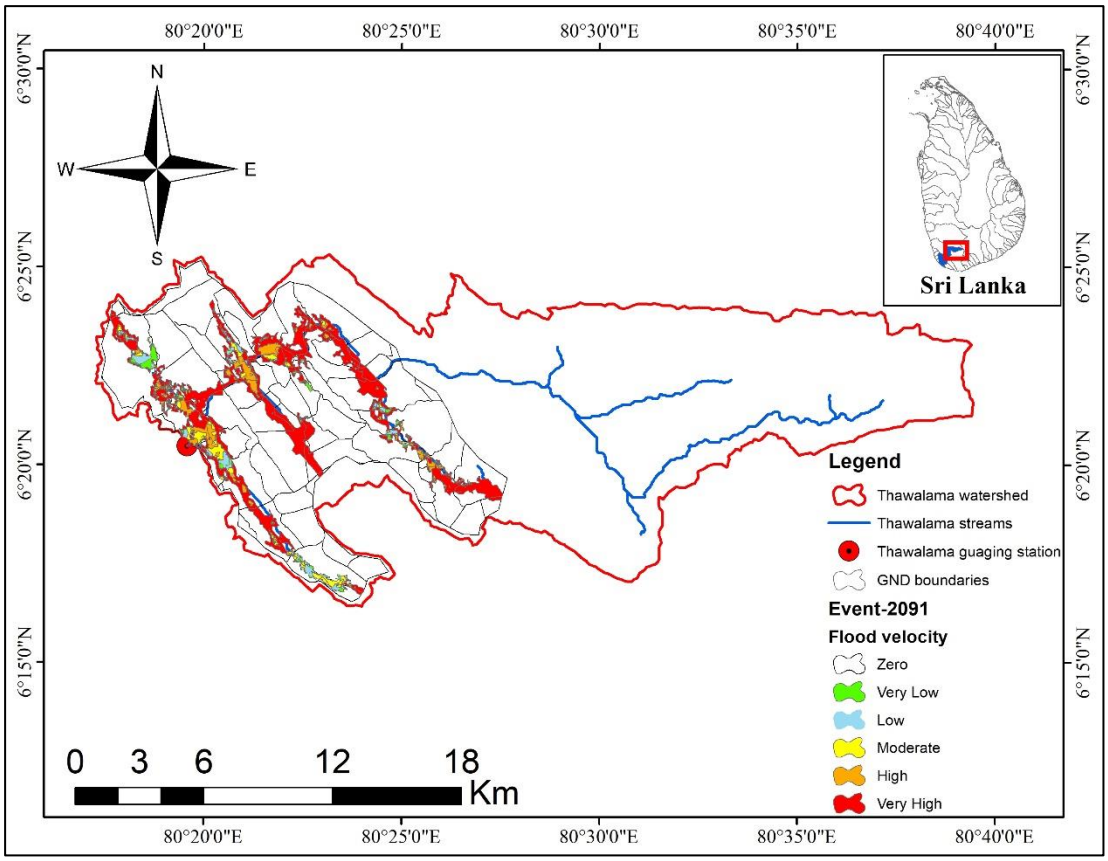

Figure 6-32 Flood velocity map of end-century flood event for the 5-year return period

Flood velocity map of end-century was generated using Arc-GIS for flood event of 5-year return period as shown in Figure 6-32. The hazard level area by flood velocity of end-century flood event for the 5-year return period is mentioned in Table 6-25.

Table 6-25 Area affected by flood velocity according to hazard level of end-century flood event for the 5-year return period

Hazard Level	Area (km²)
Zero	110.09
Very Low	1.12
Low	1.77
Moderate	2.65
High	3.82
Very High	19.22

Flood Hazard Map

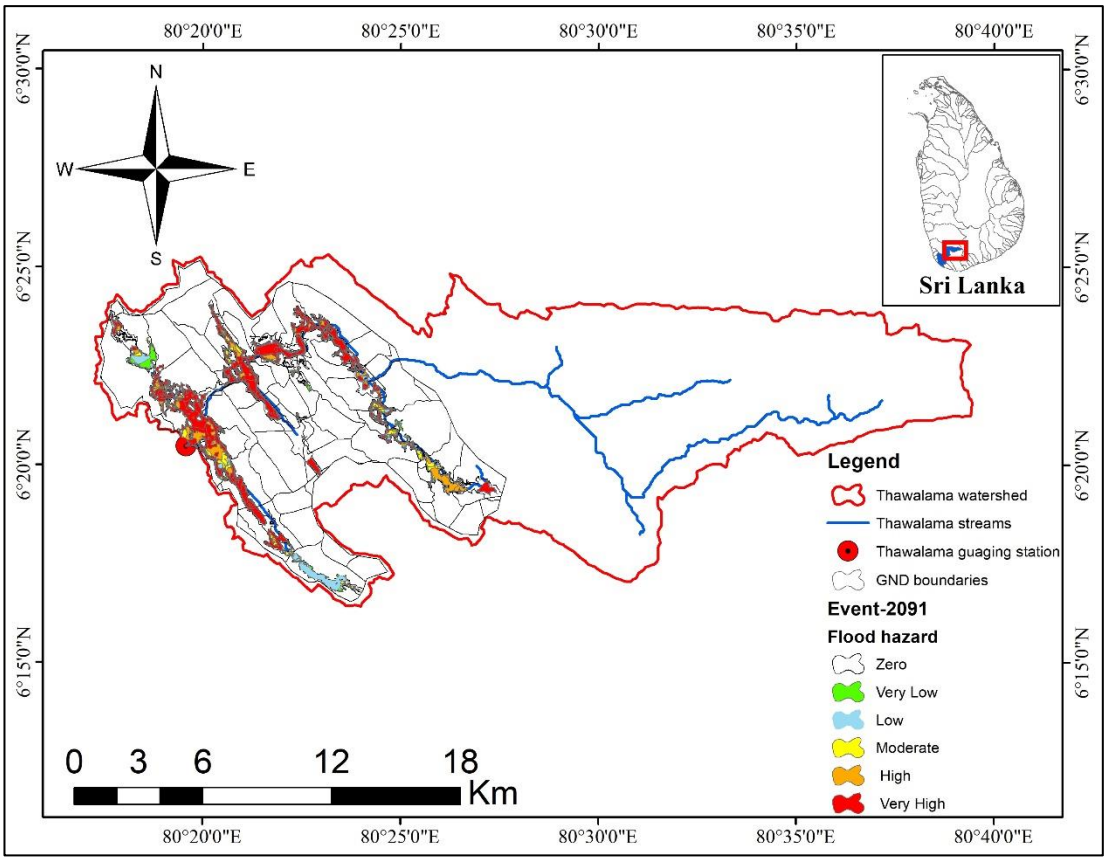

Figure 6-33 Flood hazard map of end-century flood event for the 5-year return period

Flood hazard map of end-century was generated using Arc-GIS for flood event of 5-year return period as shown in Figure 6-33. The hazard level area by flood hazard map of end-century flood event for the 5-year return period is mentioned in Table 6-26.

Table 6-26 Area affected by flood hazard according to hazard level of end-century flood event for the 5-year return period

Hazard Level	Area (km^2)
Zero	118.72
Very Low	0.89
Low	2.15
Moderate	1.99
High	3.64
Very High	11.30

6.4.2 Flood Vulnerability Map

In this section, Flood vulnerability map results are presented which were prepared through Arc-Map. Population data were forecasted as per chapter 4.5. Further vulnerability map was prepared through GIS operation.

A GIS operation used for generating flood vulnerability maps-

Step-1 Clip 2-D area across the GND

Step-2 Import population statistics through table operation

Step-3 Calculate population density in the attribute table

Step-4 Classify into vulnerability category-Very Low, Low, Moderate, High and, Very High using table operation in GIS.

The matrix used for Vulnerability mapping

Level of Vulnerability	Very Low (1)	Low (2)	Moderate (3)	High (4)	Very High (5)
Very Low (1)	1	2	3	4	5
Low (2)	2	4	6	8	10
Moderate (3)	3	6	9	12	15
High (4)	4	8	12	16	20
Very High (5)	5	10	15	20	25

Figure 6-34 Matrix for vulnerability mapping

The vulnerability of each graded in five levels was developed by Liu et al. (2021) which is shown in Figure 6-34.

6.4.2.1 *12-Year Return Period*

(A) Historical Event

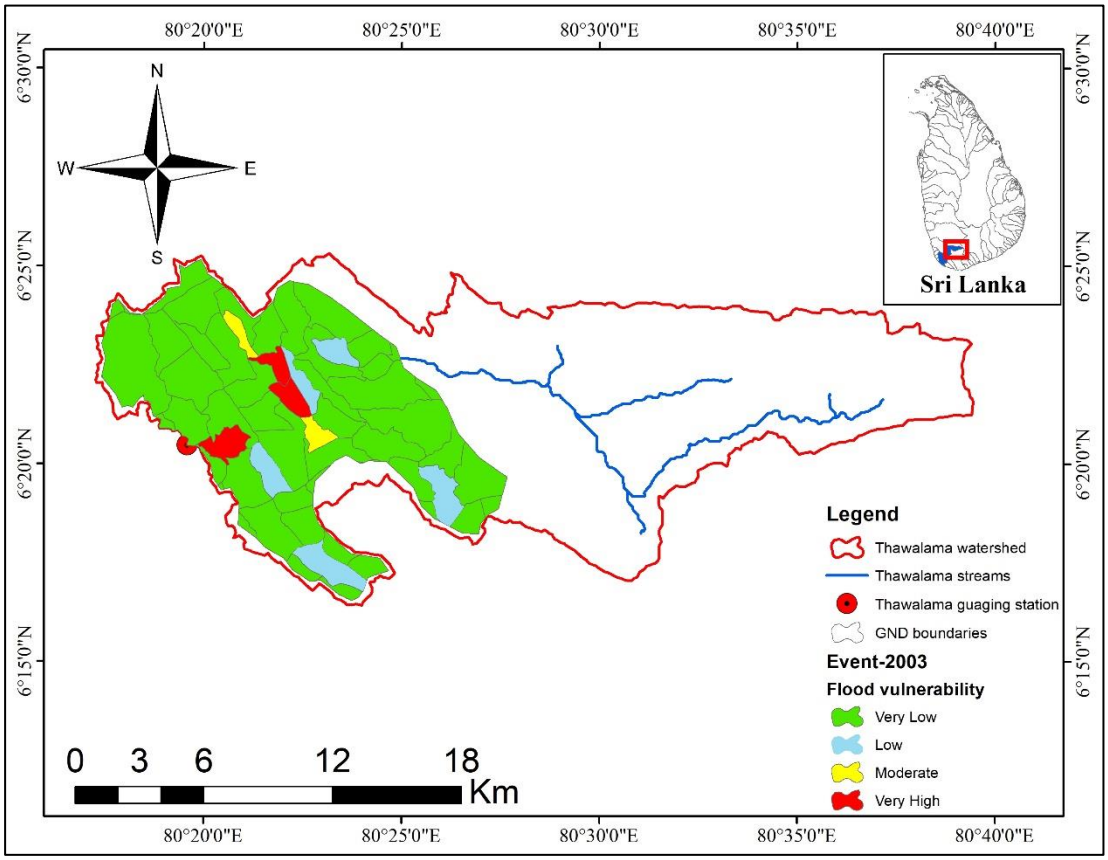

Figure 6-35 Flood vulnerability map of the 2003-year flood event for the 12-year return period

Flood vulnerability map was generated using Arc-GIS for the year 2003 as shown in Figure 6-35. The flood vulnerable area of the year 2003 is mentioned in Table 6-27.

Table 6-27 Area affected by flood vulnerability according to the vulnerable level of the 2003-year flood event for the 12-year return period

Vulnerable Level	Area (km²)
Very Low	118.55
Low	12.02
Moderate	2.59
High	0.00
Very High	5.51

(B) Mid-Century Event

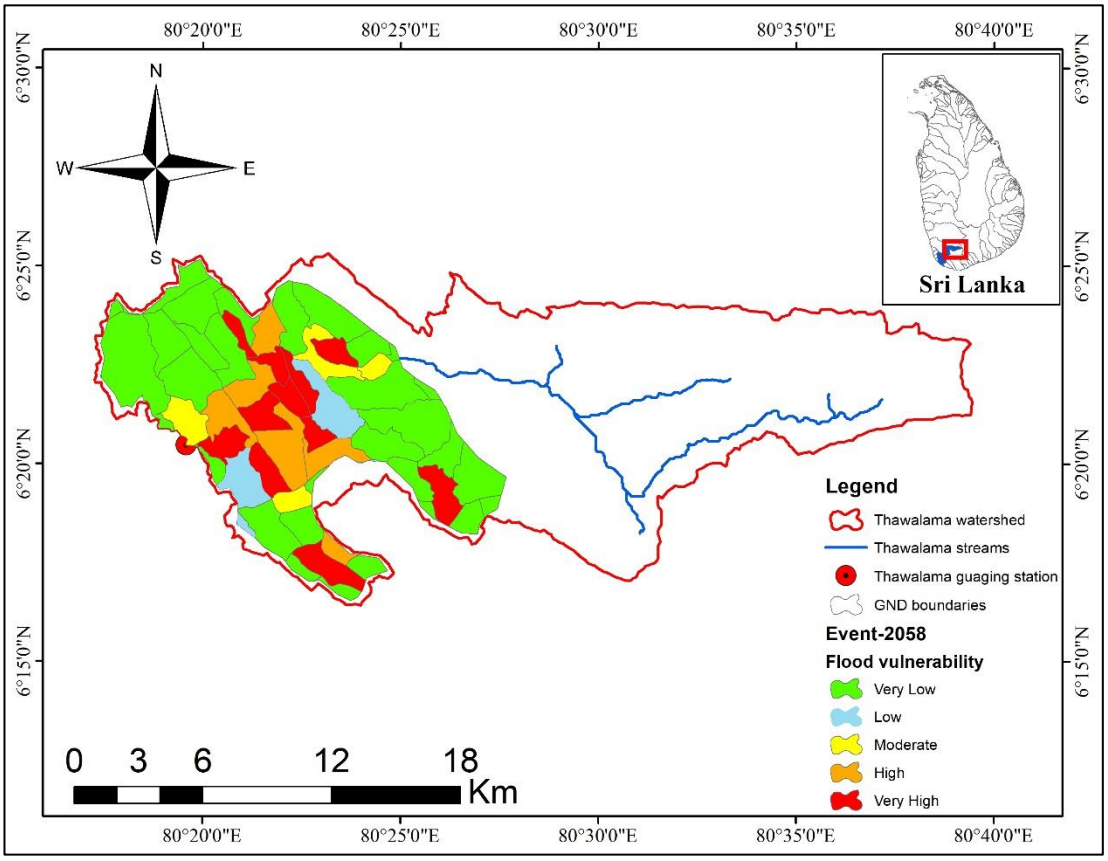

Figure 6-36 Flood vulnerability map of mid-century flood event for the 12-year return period

Flood vulnerability map was generated using Arc-GIS for mid-century of 12-year return period as shown in Figure 6-36. The flood vulnerable area for mid-century of 12-year return period is mentioned in Table 6-28.

Table 6-28 Area affected by flood vulnerability according to the vulnerable level of mid-century flood event for the 12-year return period

Vulnerable Level	Area (km²)
Very Low	81.43
Low	8.63
Moderate	8.52
High	17.44
Very High	22.66

(C) End-Century Event

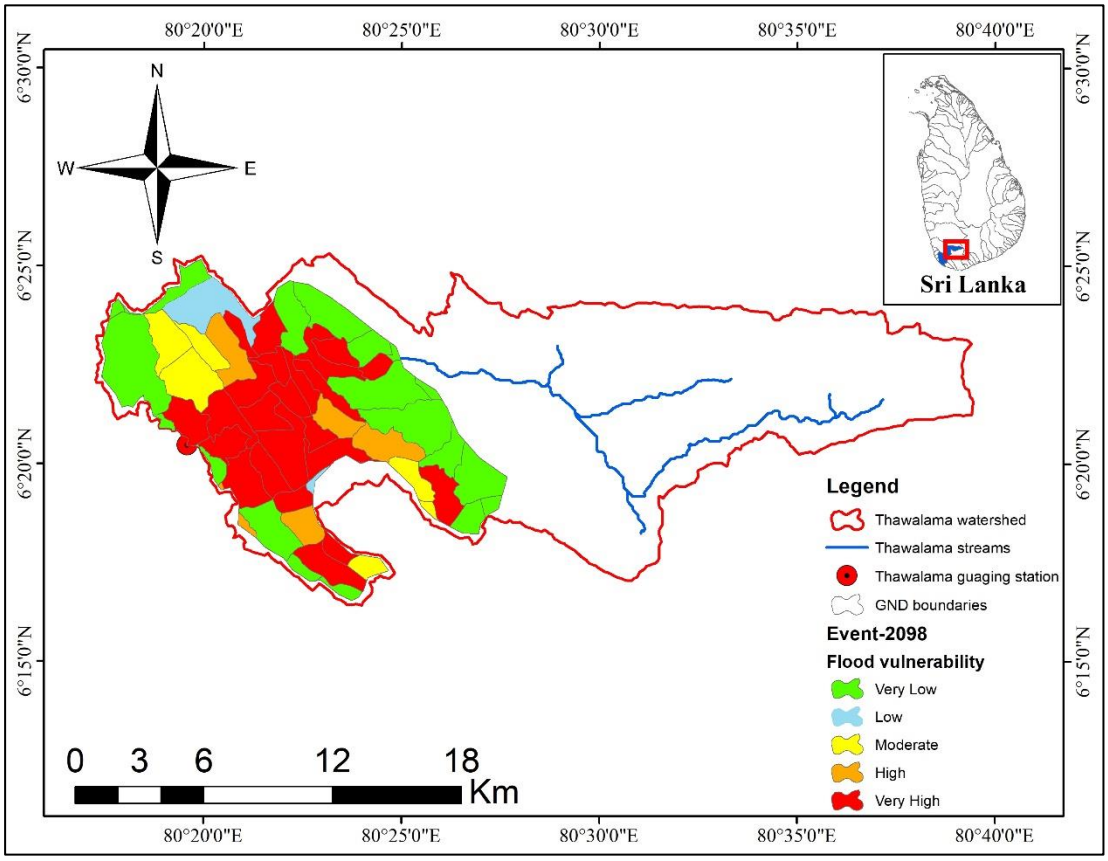

Figure 6-37 Flood vulnerability map of end-century flood event for the 12-year return period

Flood vulnerability map was generated using Arc-GIS for end-century of 12-year return period as shown in Figure 6-37. The flood vulnerable area for the end-century of the 12-year return period is mentioned in Table 6-29.

Table 6-29 Area affected by flood vulnerability according to the vulnerable level of end-century flood event for the 12-year return period

Vulnerable Level	Area (km²)
Very Low	51.58
Low	6.13
Moderate	14.04
High	12.50
Very High	54.42

6.4.2.2 *5-Year Return Period*

(A) Historical Event

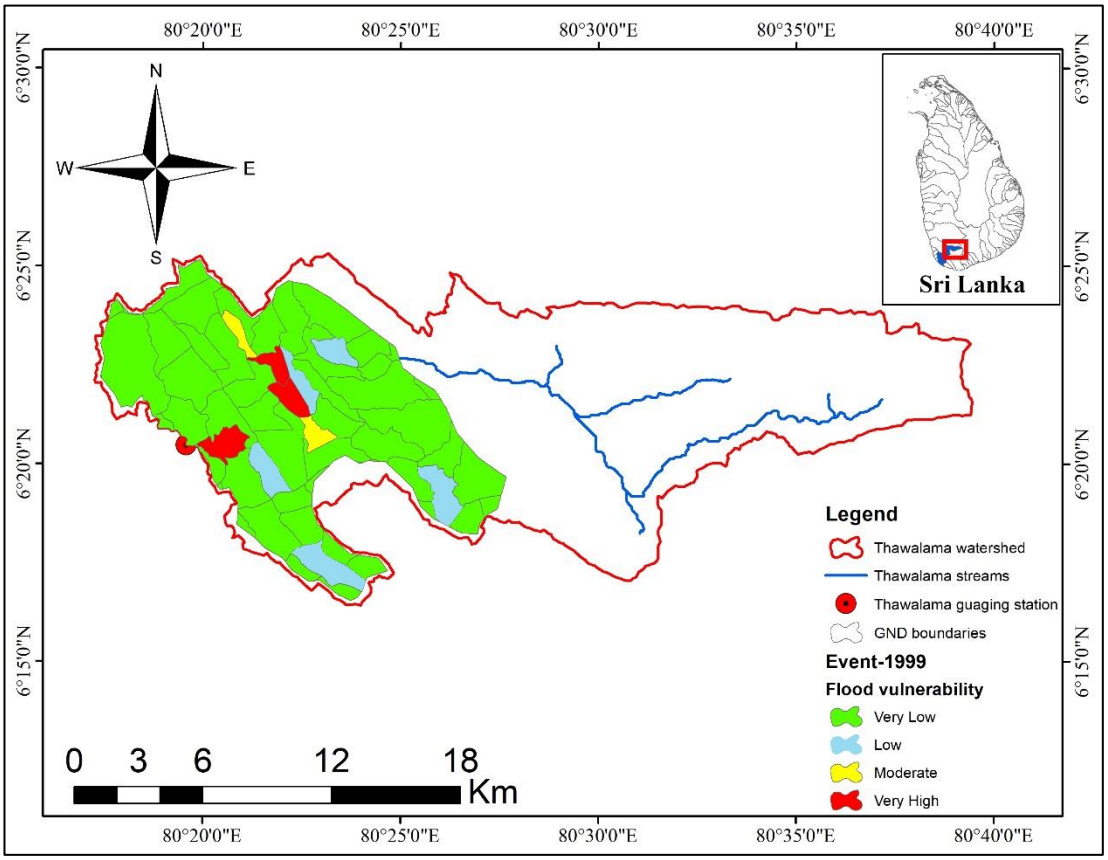

Figure 6-38 Flood vulnerability map of 1999 flood event for the 5-year return period

Flood vulnerability map was generated using Arc-GIS for the year 1999 as shown in Figure 6-38. The flood vulnerable area of the year 2003 is mentioned in Table 6-30.

Table 6-30 Area affected by flood vulnerability according to the vulnerable level of 1999 flood event for the 5-year return period

Vulnerable Level	Area (km^2)
Very Low	118.55
Low	12.02
Moderate	2.59
High	0.00
Very High	5.51

(B) Mid Century Event

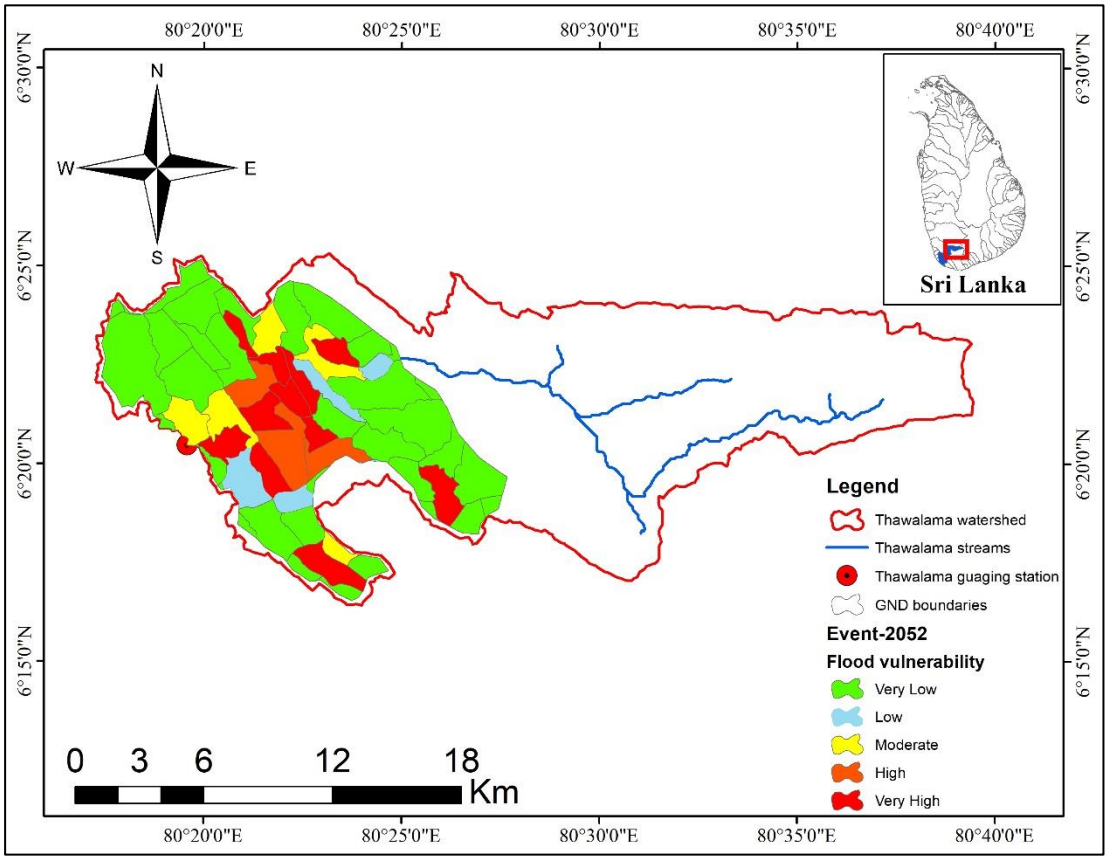

Figure 6-39 Flood vulnerability map of mid-century flood event for the 5-year return period

Flood vulnerability map was generated using Arc-GIS for mid-century of 5-year return period as shown in Figure 6-39. The flood vulnerable area for mid-century of 5-year return period is mentioned in Table 6-31.

Table 6-31 Area affected by flood vulnerability according to the vulnerable level of mid-century flood event for the 5-year return period

Vulnerable Level	Area (km²)
Very Low	84.25
Low	8.56
Moderate	12.47
High	10.73
Very High	22.66

(C) End-Century Event

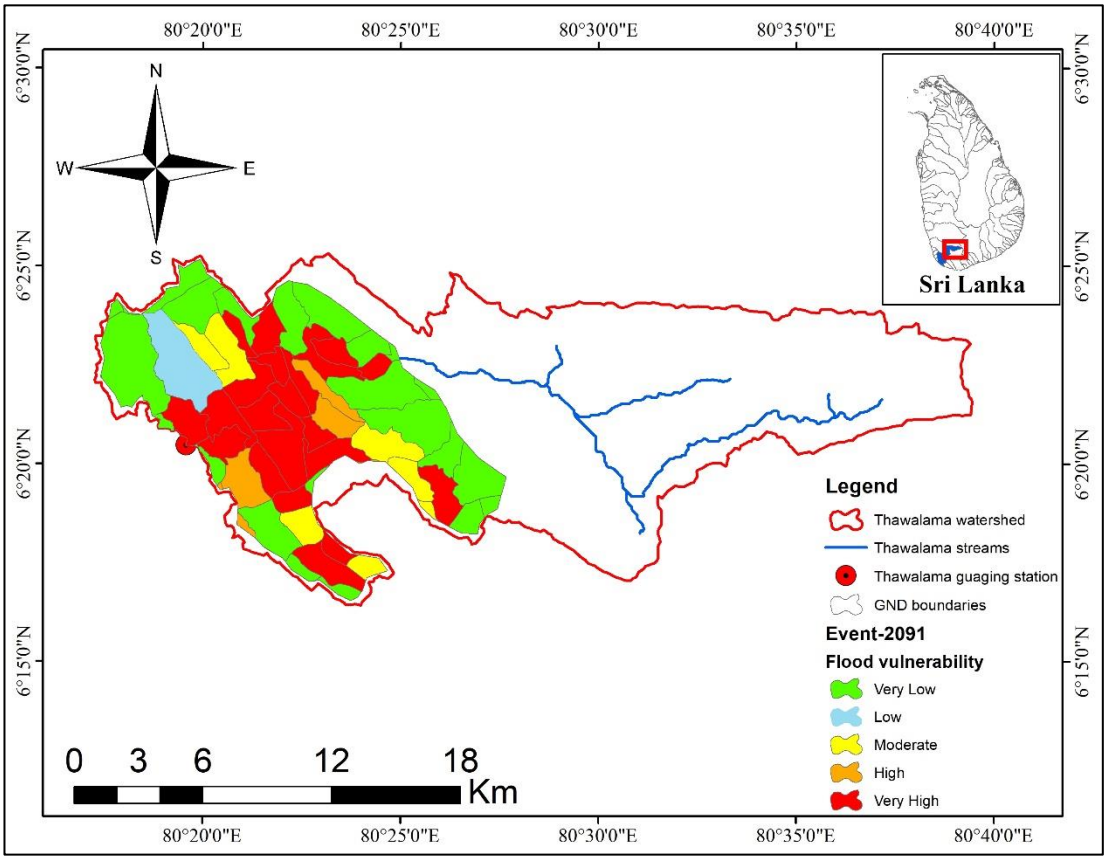

Figure 6-40 Flood vulnerability map of end-century flood event for the 5-year return period

Flood vulnerability map was generated using Arc-GIS for end-century of 5-year return period as shown in Figure 6-40. The flood vulnerable area for the end-century of the 5-year return period is mentioned in Table 6-32.

Table 6-32 Area affected by flood vulnerability according to the vulnerable level of end-century flood event for the 5-year return period

Vulnerable Level	Area (km^2)
Very Low	57.71
Low	8.32
Moderate	15.40
High	8.63
Very High	48.62

6.5 Flood Risk Map

In this section, flood risk map results are presented which were prepared through Arc-Map 10.3. The following equation was used to prepare the flood risk map through Arc map 10.3.

Flood Risk = Flood hazard X Vulnerability

Flood hazard and vulnerability maps were combined through an overlay tool (Union) and further categorized into High, Moderate, Low, etc. using GIS table operation.

The matrix for the flood risk map is according to Figure 6-15.

For the flood risk mapping, a 12-year return period for different years (2003, 2058, 2098), and a 5-year return period for different years (1999, 2052, 2091) were represented separately.

6.5.1 12-Year Return Period

(A) 2003-Year Flood Event

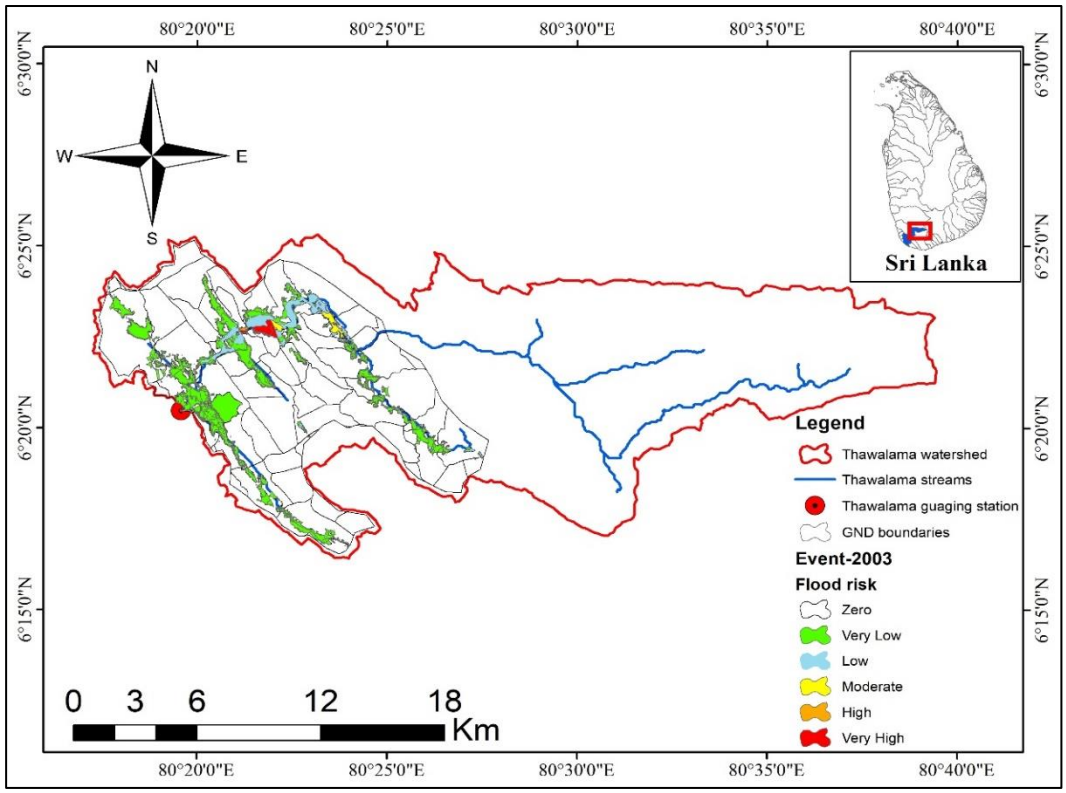

Figure 6-41 Flood risk map of 2003-year flood event for the 12-year return period

Table 6-33 Area affected by flood risk according to the risk level of 2003-year flood event for the 12-year return period

Risk Level	Area (km²)
Zero	117.58
Very Low	17.09
Low	2.82
Moderate	0.55
High	0.07
Very High	0.57

A flood risk map was generated using Arc-GIS for the year 2003 as shown in Figure 6-41. The flood risk area of the year 2003 is mentioned in Table 6-33.

(B) Mid-Century

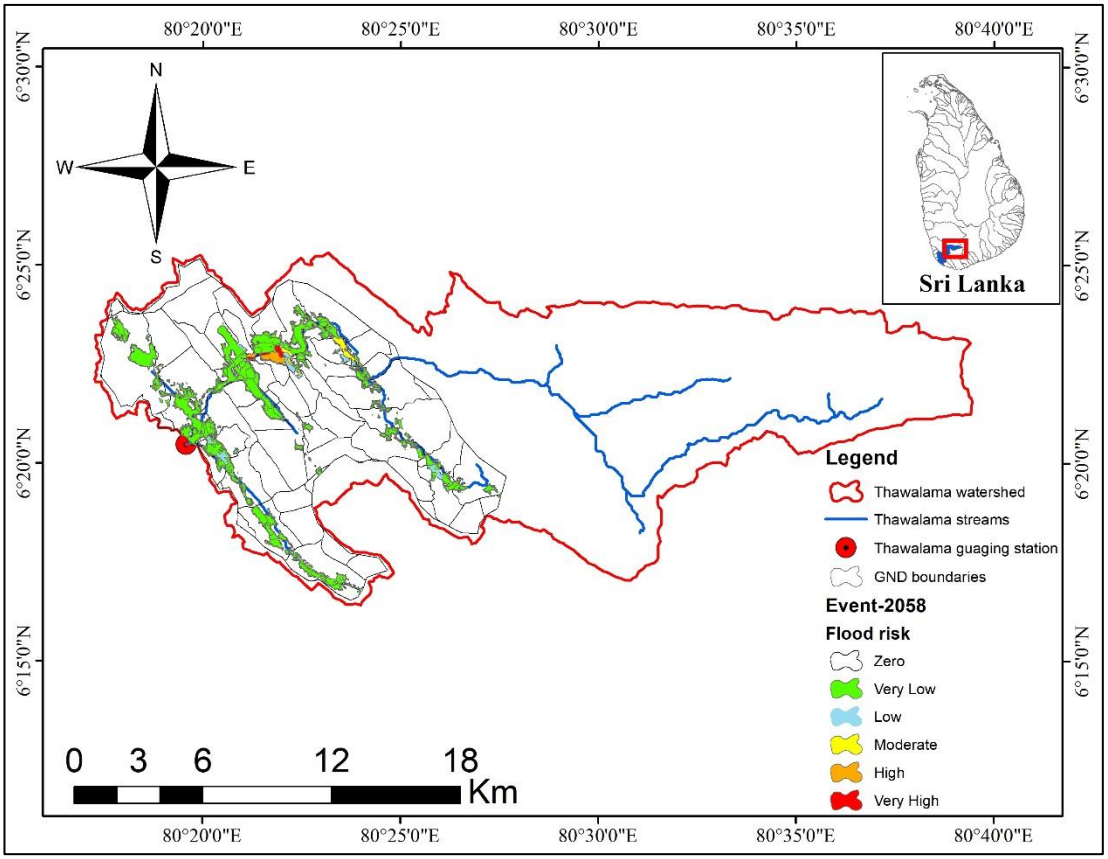

Figure 6-42 Flood risk map of mid-century flood event for the 12-year return period

Table 6-34 Area affected by flood risk according to the risk level of mid-century flood event for the 12-year return period

Risk Level	Area (km²)
Zero	118.19
Very Low	18.44
Low	0.85
Moderate	0.54
High	0.44
Very High	0.21

A flood risk map was generated using Arc-GIS for mid-century of 12-year return period as shown in Figure 6-42. The flood risk area for mid-century of 12-year return period is mentioned in Table 6-34.

(C) End Century

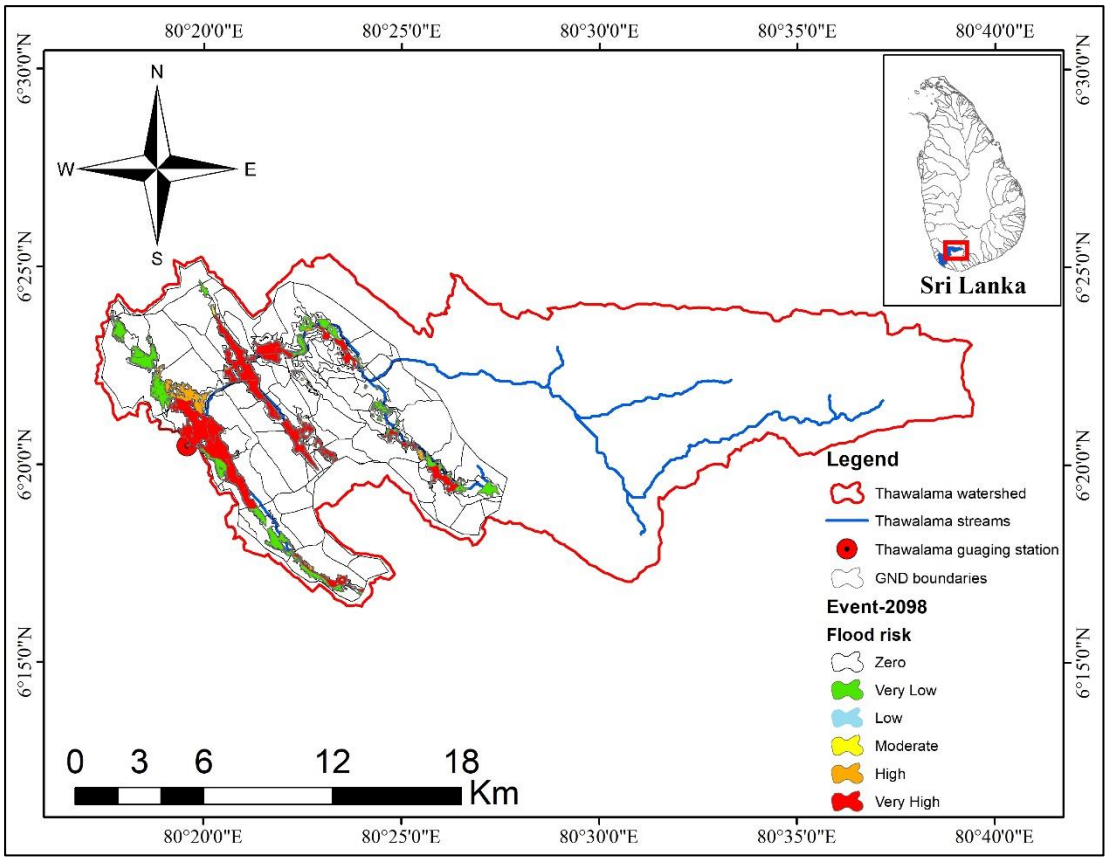

Figure 6-43 Flood risk map of end-century flood event for the 12-year return period

Table 6-35 Area affected by flood risk according to the risk level of end-century flood event for the 12-year return period

Risk Level	Area (km²)
Zero	117.20
Very Low	6.87
Low	0.12
Moderate	0.47
High	1.85
Very High	12.17

A flood risk map was generated using Arc-GIS for the end-century of the 12-year return period as shown in Figure 6-43. The flood risk area for the end-century of the 12-year return period is mentioned in Table 6-35.

6.5.2 5-Year Return Period

(A) Historical Event

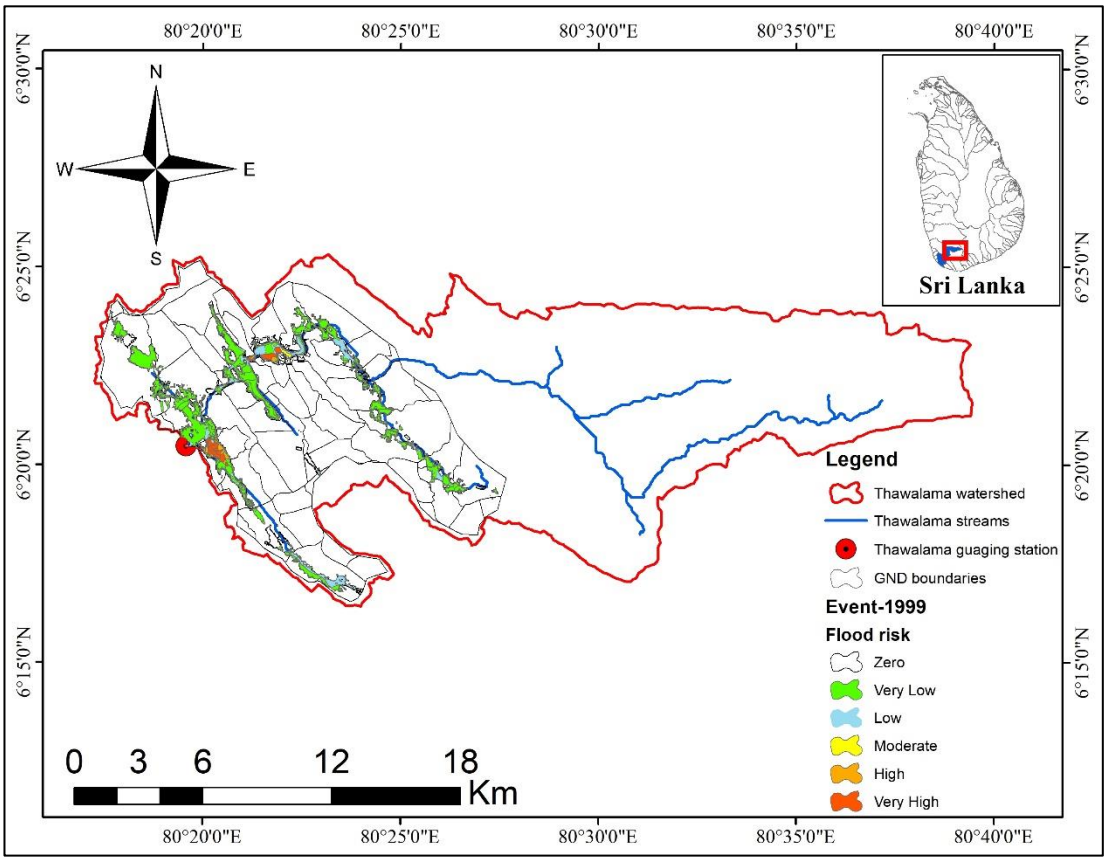

Figure 6-44 Flood risk map of 1999-year flood event for the 5-year return period

Table 6-36 Area affected by flood risk according to the risk level of 1999-year flood event for the 5-year return period

Risk Level	Area (km²)
Zero	122.90
Very Low	13.08
Low	1.49
Moderate	0.10
High	0.37
Very High	0.74

A flood risk map was generated using Arc-GIS for the year 1999 as shown in Figure 6-44. The flood risk area of the year 2003 is mentioned in Table 6-36.

(B) Mid-century

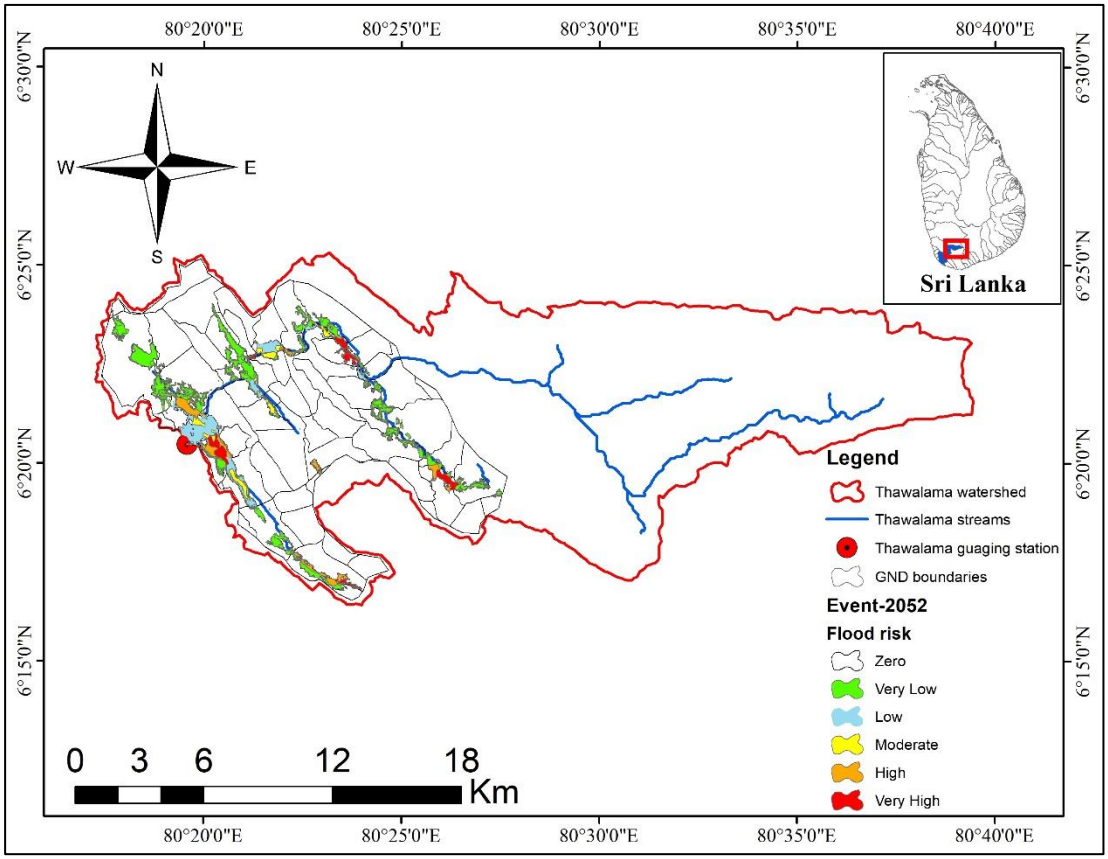

Figure 6-45 Flood risk map of mid-century flood event for the 5-year return period

Table 6-37 Area affected by flood risk according to the risk level of mid-century flood event for the 5-year return period

Risk Level	Area (km²)
Zero	121.22
Very Low	10.11
Low	2.67
Moderate	1.50
High	1.70
Very High	1.48

A flood risk map was generated using Arc-GIS for mid-century of 5-year return period as shown in Figure 6-45. The flood risk area for mid-century of 5-year return period is mentioned in Table 6-37.

(C) End Century

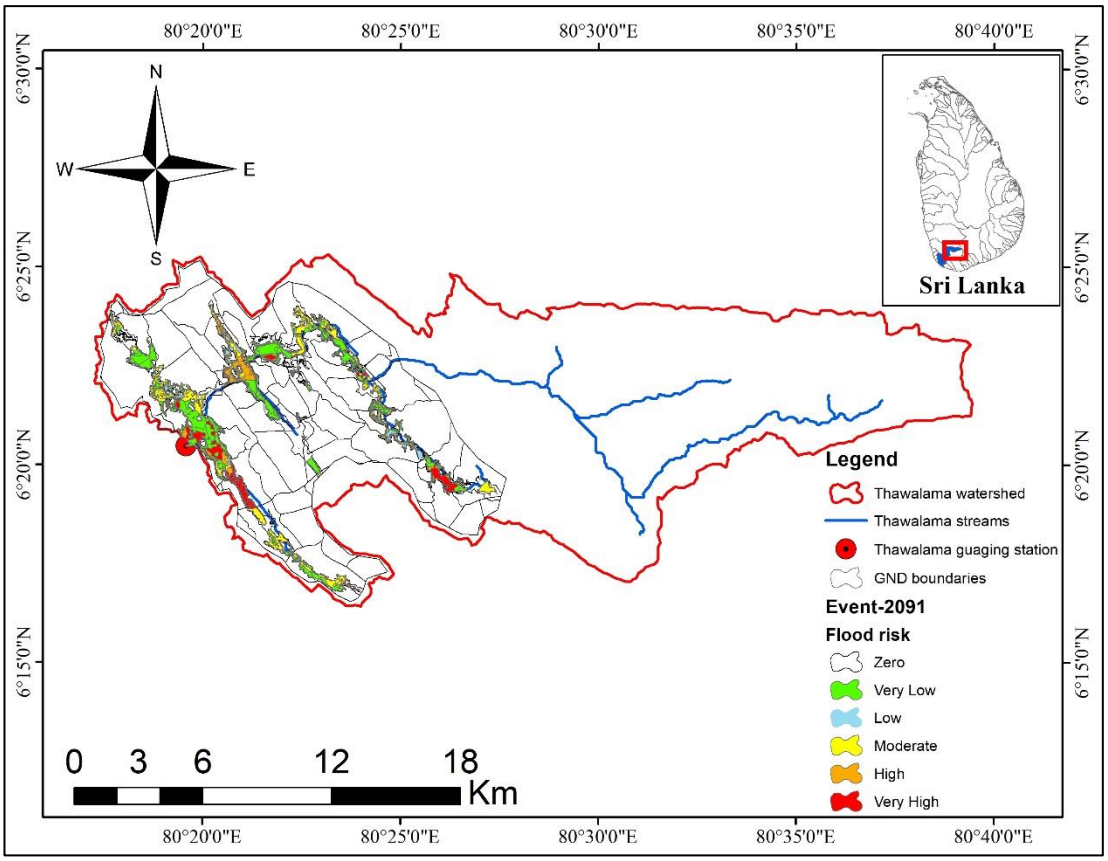

Figure 6-46 Flood risk map of end-century flood event for the 5-year return period

A flood risk map was generated using Arc-GIS for end-century of 5-year return period as shown in Figure 6-46. The flood risk area for the end-century of the 5-year return period is mentioned in Table 6-38.

Table 6-38 Area affected by flood risk according to the risk level of end-century flood event for the 5-year return period

Risk Level	**Area (km^2)**
Zero	118.72
Very Low	9.07
Low	0.80
Moderate	5.41
High	2.12
Very High	2.55

CHAPTER 7

7 DISCUSSION

The following discussion is given based on the study's findings.:

For event modeling, the SCS Curve Number (CN), SCS Unit Hydrograph, and Muskingum method were adopted. The selection of simulation methods for each model component in event-based modeling was covered in Chapter 2.6.1.

7.1 Data Period for Bias correction

According to World Meteorological Organization (WMO), the minimum period of rainfall required for bias correction is 30 years. But due to data unavailability, economy, and data accuracy 15-year data (1990-2005) was used as a baseline for bias correction. But still, this data period is enough, according to (Sirisena et al., 2021).

7.2 HEC-RAS Model Parameter Selection

Since, there was no significant difference in model performance when different mesh sizes (25, 50, and 75 m) were compared in Yesil (Ishim) River in Kazakhstan to generate flood hazard maps (Ongdas et al., 2020).

Hence, the two-dimensional mesh size adopted for this research work was 60 m according to chapter 2.6.2.

The Yesil (Ishim) River in Kazakhstan, for its superior stability and computation speed, the Diffusion Wave equation was used exclusively in simulations. Trial simulations have revealed that utilizing a Full Momentum equation necessitates a simulation duration that is more than 21 times longer than employing a Diffusion Wave equation. As a result, it was deemed unsuitable for practical purposes (doing sensitivity analysis and calibration) (Ongdas et al., 2020).

7.3 Flood Hazard and vulnerability

Flood hazard maps are valuable sources of information for flood preparedness as well as planning and implementing flood mitigation methods, including vulnerability assessments of impacted areas. Several parameters are frequently taken into account while creating flood hazard maps, including water depth, water velocity, flood duration, flood extent, and the rate at which water rises. Flood depth and velocity maps are extremely important for future planning and raising public awareness of flood hazard risks in locations designated as vulnerable to high flood water velocities (Marqueso et al., 2016).

There may be many parameters for vulnerability assessment of flood-like social, economic, and, agriculture, etc. Among those population density is an important parameter in flood vulnerability analysis since it is directly related to humans and is proportional to the amount of flood susceptibility (Nguyen et al., 2021).

The study demonstrates the methodical procedure of creating flood vulnerability and hazard maps using the two-dimensional model HEC RAS and Arc-GIS. The use of these models and techniques yields effective results in less time and with fewer resources. The model's output as graphical output (maps) for different flood return periods might aid in decision making.

A flood risk study of a flood-prone location greatly assists decision-makers in making the appropriate decisions at the right time. It is beneficial in all stages of a flood-related disaster, namely before, after, and during the event. During a disaster in Sri Lanka, all aid operations are always conducted out at the GN division level; therefore, flood risk analysis done for GN divisions is the most appropriate. The hydrodynamic model was found to be particularly useful in calculating flood inundation regions in the Thawalama basin.

7.4 12-Year Return Period

1) Hazard

Flood Depth

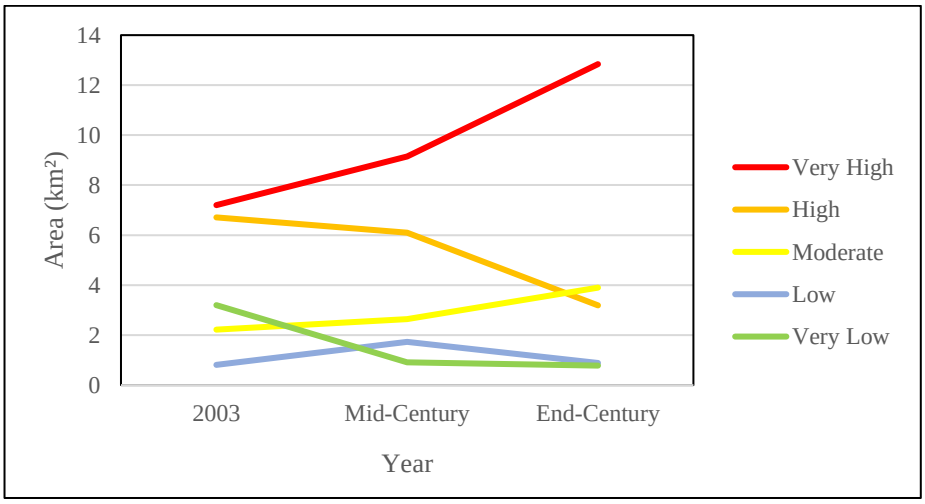

Figure 7-1 Hazardous area at various periods due to flood depth for 12 years return period

The depth hazard increases gradually in the very high hazard zone, whereas it decreases in the high hazard zone as shown in Figure 7-1. This demonstrates that the very high zone is expanding while the high zone is contracting, which shows how climate change is affecting flood depth with respect to time. As a result, the depth hazard will become more hazardous.

Flow Velocity

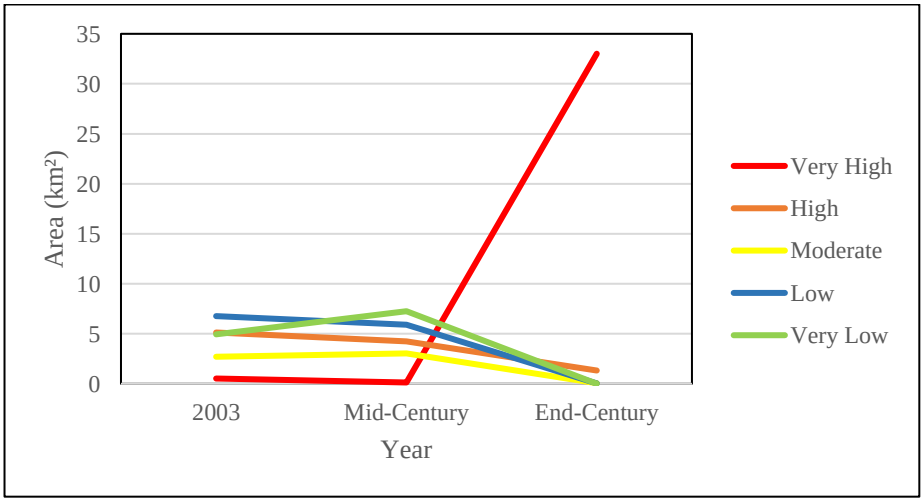

Figure 7-2 Hazardous area at various periods due to flood velocity for 12 years return period

The flow velocity increases after the mid-century in the very high hazard zone, whereas it decreases in the high hazard zone as shown in Figure 7-2. This demonstrates that the very high zone is expanding after the mid-century while the high zone is contracting gradually, which shows that after the mid-century there will be the effect of climate change in flow velocity. As a result, the flow velocity will become more hazardous after mid-century.

Flood Hazard

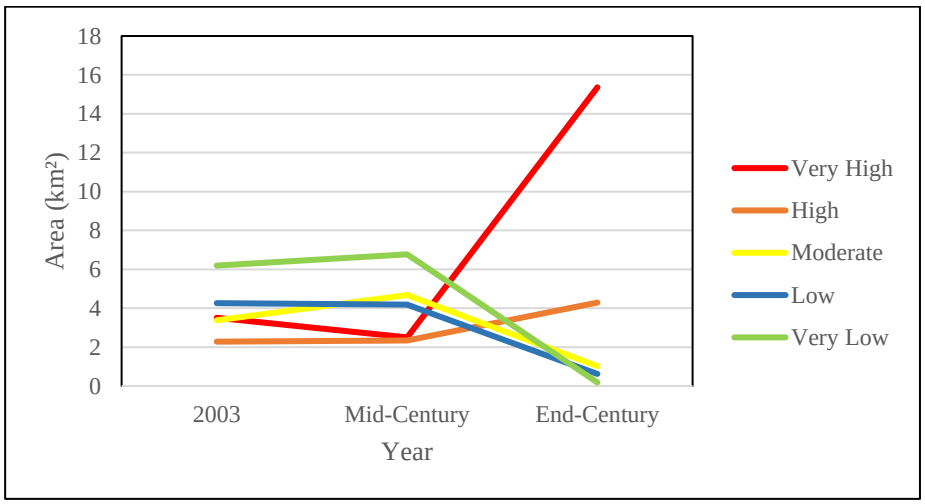

Figure 7-3 Hazardous area at various periods due to flood hazard for 12 years return period

The flood hazard increases after the mid-century in the very high hazard zone, whereas it has gradual or very little incremental in the high hazard zone as shown in Figure 7-3. This demonstrates that the very high zone and the high zone are expanding after Mid-Century while the moderate, low and very low zone are contracting. Hence, climate change will have a high impact after mid-century as flood hazard will become more hazardous in terms of flood depth and flood velocity.

2) Flood Vulnerability

The population vulnerability for flood, area percentage is increasing concerning time for the 12-year Return period.

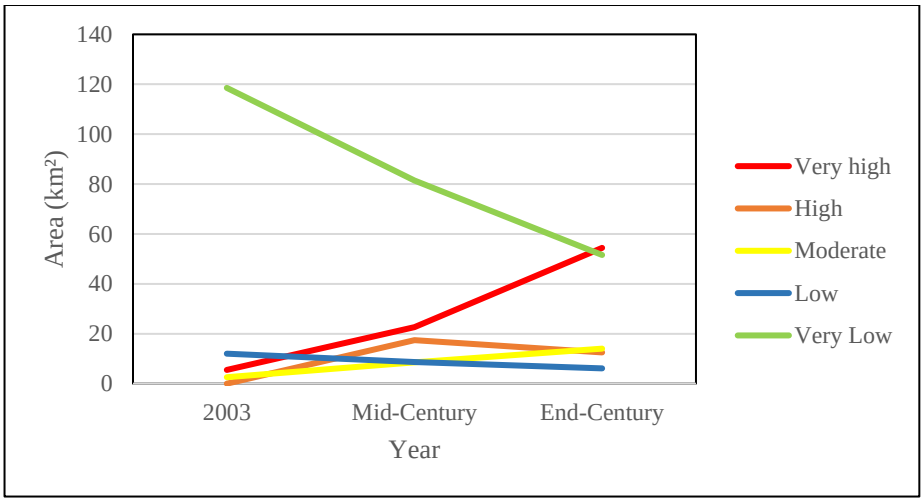

Figure 7-4 Vulnerable area at various periods due to flood for 12 years return period

Figure 7-4 illustrates that the population density vulnerability for the area is increasing for high hazard zone whereas high vulnerability zone for population density is decreasing after mid-century and the very low zone is sharply decreasing. Hence, as the population increases the impact on population density increases for the flood vulnerability.

3) Flood Risk

The Flood risk for a 12-year return period is becoming hazardous after Mid-Century

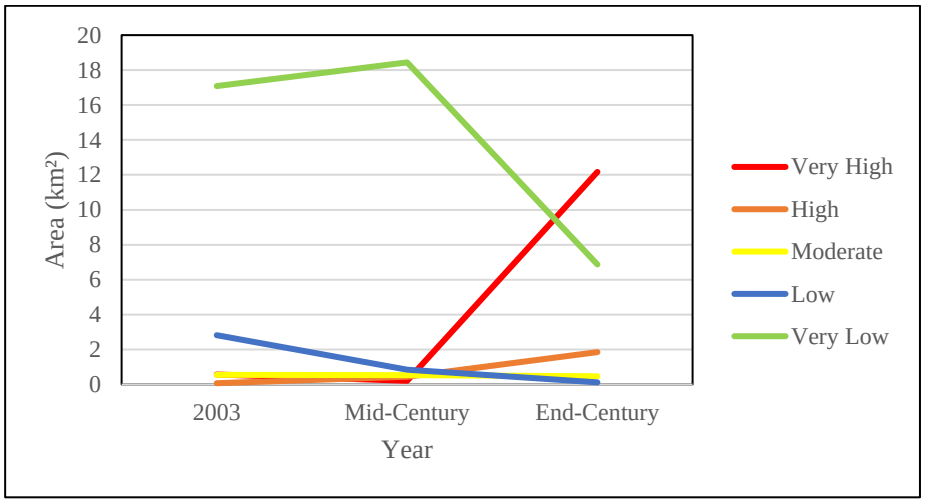

Figure 7-5 Risk area at various periods due to flood for 12 years return period

Figure 7-5 illustrates that the high-risk area is gradually increasing with respect to time whereas, the very high-risk area is suddenly increasing after mid-century and the very low-risk area is suddenly decreasing. The low-risk area is gradually decreasing with respect to time. Hence, it can be predicted that due to changes in climate flood area is more at risk after mid-century.

Number of Grama Niladhari Division (GND) at a various Risk level

Table 7-1 Number of GND affected by various Risk level in 12-year return period

Risk level/Year	(2003)	Mid-Century	End-century
Very High	1	1	22
High	2	2	21
Moderate	3	4	28
Low	21	6	8
Very Low	41	42	21

Table 7-1 illustrates that the risk level at the GND level is increasing after mid-century which is because of the very high peak as compared to the mid-century and historical events.

Risk Classification

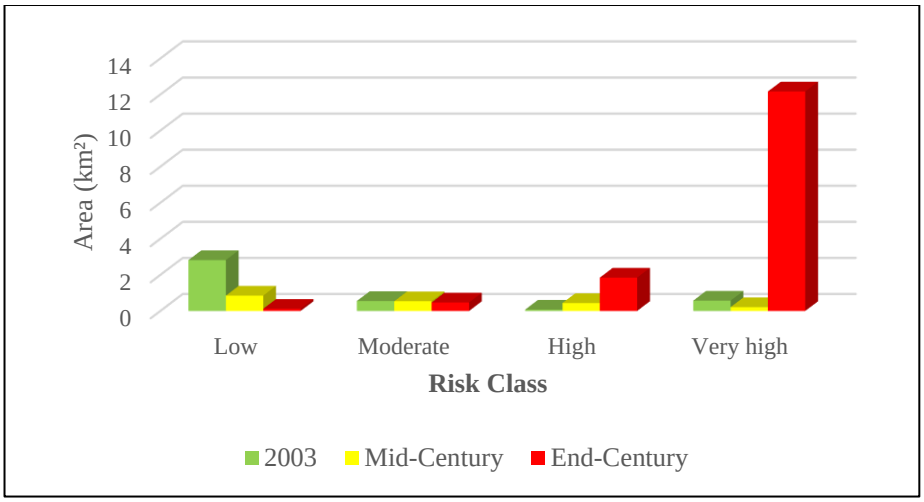

Figure 7-6 Area facing flood risk at a 12-year Return period

Figure 7-6 illustrates that at the end century, the high flood risk is due to the high magnitude of rainfall, and variation of flood risk is showing an increasing trend in high and very high-risk categories as a variation of risk is decreasing in the low category.

7.5 5-Year Return Period

1) Flood Hazard

Flood Depth-

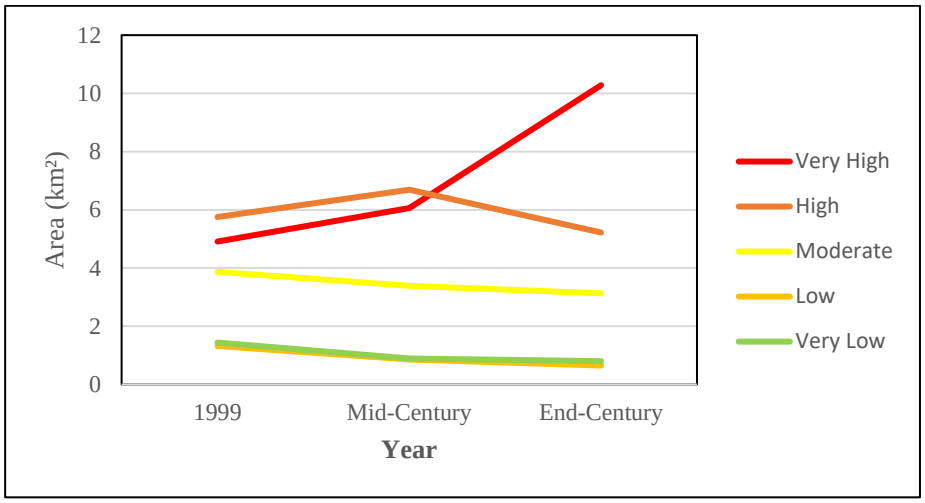

Figure 7-7 Hazardous area at various periods due to flood depth for a 5-year return period

Figure 7-7 illustrates that the depth hazard increases practically gradually in the very high hazard zone, whereas it decreases in the high hazard zone after mid-century. This demonstrates that the very high zone is expanding while the high zone is contracting after mid-century. As a result, the depth hazard will become more hazardous due to climate change.

Flow Velocity-

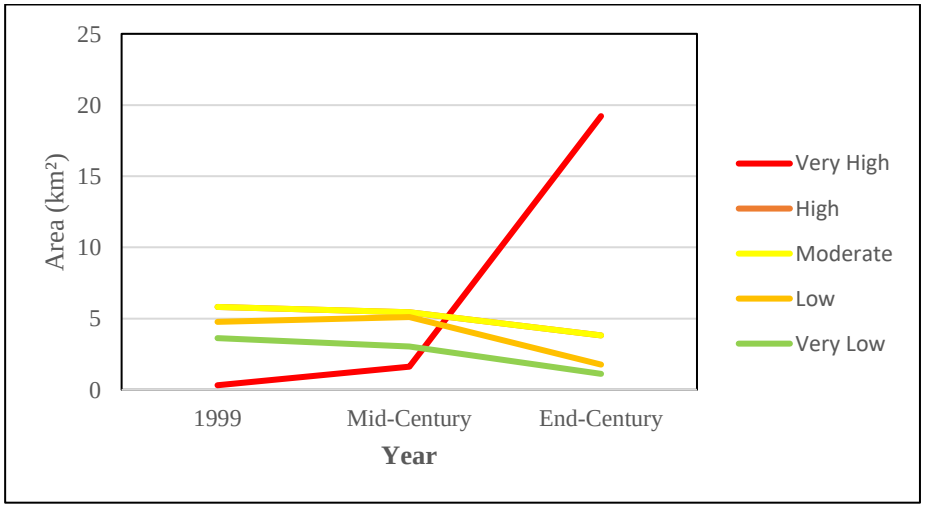

Figure 7-8 Hazardous area at various periods due to flood velocity for a 5-year return period

Figure 7-8 illustrates that the flow velocity increases after the mid-century in the very high hazard zone, whereas it decreases in the high hazard zone. This demonstrates that the very high zone is expanding while the high zone is contracting gradually. As a result, the velocity hazard will become more hazardous after the mid-century due to climate change.

Flood Hazards-

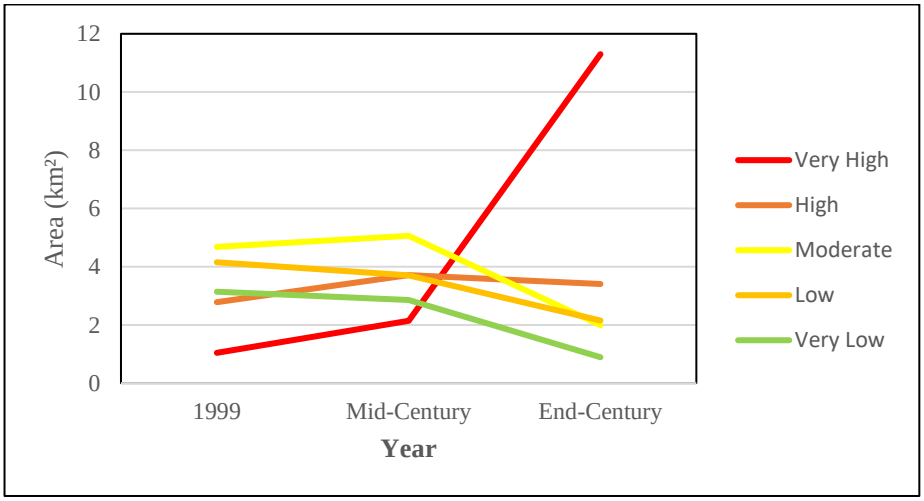

Figure 7-9 Hazardous area at various periods due to flood hazard for a 5-year return period

Figure 7-9 illustrates that the flood hazard increases gradually till mid-century and after a mid-century sudden increase in the very high hazard zone, whereas it has gradual or very little incremental in high hazard. This demonstrates that the very high zone is expanding after the mid-century while the high zone is expanding but with less quantity till mid-century then start decreasing. As a result, overall hazards will become more hazardous after the mid-century due to climate change.

2) Flood Vulnerability-

The population vulnerability for flood, area percentage is increasing with respect to time for the 5-year return period.

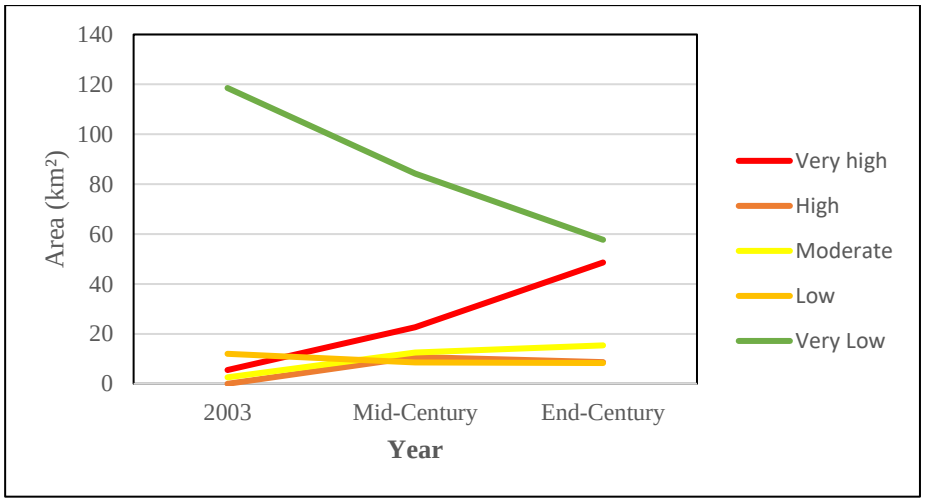

Figure 7-10 Vulnerable area at various periods due to flooding for a 5-year return period

Figure 7-10 illustrates that the flood vulnerability for the area is increasing for very high hazard zone whereas the high vulnerability zone for population density is decreasing after mid-century due to an increase in population with respect to time.

3) Flood Risk

The flood risk for a 5-year return period is becoming hazardous and shows almost the same variation for the very high-risk category, and high-risk category

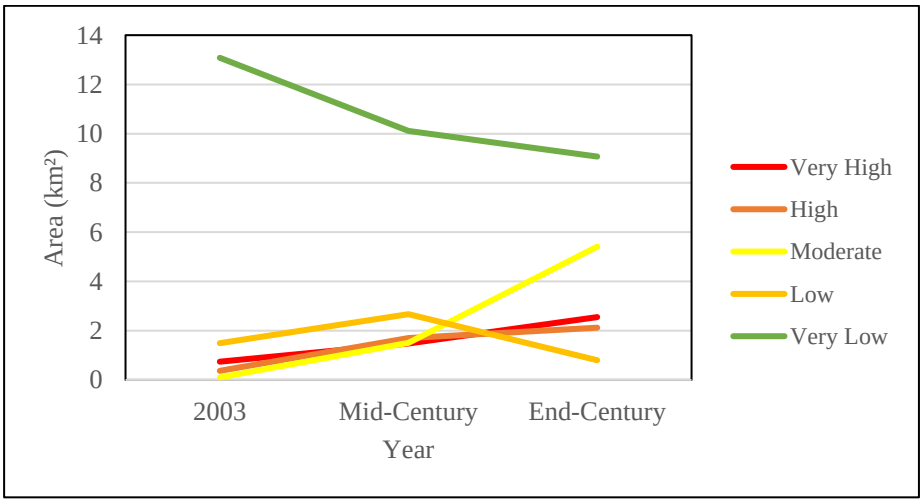

Figure 7-11 Risk area at various periods due to flood for a 5-year return period

Figure 7-11 illustrates that the very high-risk area is increasing after the 2003 event whereas, the very low-risk area is suddenly decreasing after mid-century which states how climate change is increasing flood risk after mid-century.

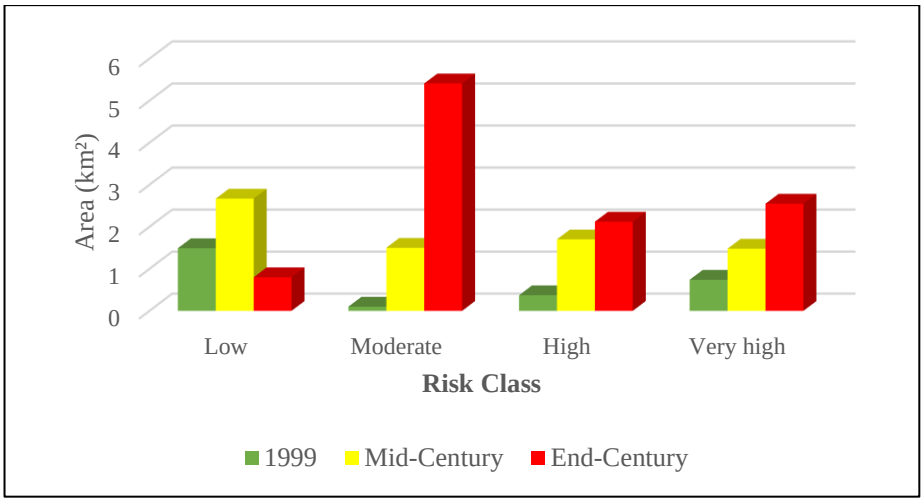

Figure 7-12 Area facing flood risk in 5-year Rteun period

Figure 7-12 illustrates that in the mid-century the high flood risk is there due to the high magnitude of rainfall and variation of risk is showing an increasing trend in moderate, high, and very high risk.

Table 7-2 illustrates that the risk level at the GND level is increasing after mid-century which is because of the very high peak as compared to the mid-century and historical events.

The No. of Grama Niladhari (GND) at various Risk level

Table 7-2 Number of GND affected at various Risk levels in 5-year return period

Risk/Year	1999	Mid-Century	End-Century
Very High	2	8	19
High	3	13	23
Moderate	3	16	42
Low	23	9	8
Very Low	40	39	39

CHAPTER 8

8 CONCLUSIONS

- The flood hazard, vulnerability, and risk maps were generated using HEC RAS 2-D modeling. The flood depth and flood velocity were adopted as flood hazard parameters whereas the population density was adopted to develop flood vulnerability maps.
- For the 5-year return period and the 12-year return periods, about 4.98% and 5.50% of the area were found to be inundated, respectively in the historical period.
- At the end of the century, 12-year return period, the number of GNDs discovered to be at very high risk was 22, whereas in the 5-year return period, the number of GNDs discovered to be at very high risk was 19.
- The very high and high hazardous area was discovered to be rising mostly after mid-century. At the end of the century, almost 11.30 km^2 in the 5-year return period and 15.36 km^2 area in the 12-year return period were discovered to be at very high risk.
- Among the various statistical approaches Gumbel, Log-Pearson Type III, and Log normal distribution, the Gumbel method was adopted to be the best method to identify Return periods.
- The simulated flood magnitude was obtained from HEC-HMS. The mid-century event of the 12-year return period simulates smaller magnitude than the year 2003 event and the mid-century event of the 12-year return period is more hazardous than the year 2003 event due to two simultaneous peaks in the mid-century event of 12-year return period ie.,797 m^3/sec and 902 m^3/sec.

- The climate model of 25 km resolution, MPI-M-MPI-ESM-MR, ICHEC-EC-EARTH, MIROC-MIROC5, and NCC-NorESM1-M was bias-corrected with observed rainfall data to obtain the best climate model based on the coefficient of determination (R^2).
- MPI-M-MPI-ESM-MR was selected as an agreeable correlation among the other climate models.
- One of the most difficult challenges that remain is generating an accurate digital elevation model (DEM). In this study DEM of 30 m resolution obtained from Survey Department, Sri Lanka was used which shows better results from 30 m (Shuttle Radar Topography Mission) SRTM DEM which is insufficient for the hydrological modeling in a small catchment like this. As a result, the availability of high-resolution DEM is required to achieve more precise findings. These kinds of models are extremely valuable and vital for disaster preparation as well as proper land use, land development, and settlement planning.
- From a disaster reduction viewpoint, the information derived from this study can contribute to assessing the possibility of flood damage for the local population.

CHAPTER 9

9 RECOMMENDATIONS

The following recommendations for further research are based on the study's findings:

- In the study, DEM resolution 30-meter from the Survey Department, Sri Lanka has been used for flood hazard mapping. In a future study, better resolution data can be used for the flood hazard mapping
- The flood depth and flood flow velocity were employed as hazard parameters in this investigation. More hazard characteristics, such as duration of flood and floodwater recession, may be employed for a more thorough hazard calculation.
- In this study, only population indicators were utilized to evaluate the level of vulnerability of the studied region to flooding. Incorporating data relating to household income, housing types, agriculture, literacy rate, and so on would offer a more sensible assessment of the research area's sensitivity, adaptive ability, and exposure.

BIBLIOGRAPHY

Ahbari, A., Stour, L., Agoumi, A., & Serhir, N. (2018). Estimation of initial values of the HMS model parameters: Application to the basin of Bin El Ouidane (Azilal, Morocco). *Journal of Materials and Environmental Science*, *9*(1), 305–317. https://doi.org/10.26872/jmes.2018.9.1.34

Armanuos, A. M., Al-Ansari, N., & Yaseen, Z. M. (2020). Cross assessment of twenty-one different methods for missing precipitation data estimation. *Atmosphere*, *11*(4), 1–35. https://doi.org/10.3390/ATMOS11040389

Baky, M. A. Al, Islam, M., & Paul, S. (2020). Flood Hazard, Vulnerability and Risk Assessment for Different Land Use Classes Using a Flow Model. *Earth Systems and Environment*, *4*(1), 225–244. https://doi.org/10.1007/s41748-019-00141-w

Becker, A., & Grünewald, U. (2003). Disaster management: Flood risk in Central Europe. *Science*, *300*(5622), 1099. https://doi.org/10.1126/science.1083624

Birmah, M. N., Kigun, P. A., Alfred, Y. B., St, M., & Surajo, L. A. (2021). *International Journal of Research Publication and Reviews Flood Assessment in Suleja Local Government Area , Niger State , Nigeria*. *2*, 219–239.

Booij, M. J. (2005). Impact of climate change on river flooding assessed with different spatial model resolutions. *Journal of Hydrology*, *303*(1–4), 176–198. https://doi.org/10.1016/j.jhydrol.2004.07.013

Brunner, G. W. (2021). *HEC-RAS HEC-RAS 2D User ' s Manual*. *January*, 171.

Buslima, F. S., Omar, R. C., Jamaluddin, T. A., & Taha, H. (2018). Flood and flash flood geo-hazards in Malaysia. *International Journal of Engineering and Technology(UAE)*, *7*(4), 760–764. https://doi.org/10.14419/ijet.v7i4.35.23103

Campozano, L., Sánchez, E., Avilés, Á., & Samaniego, E. (2014). Evaluación de métodos de relleno para series temporales de precipitación y temperatura diarias: el caso de los Andes ecuatorianos. *Maskana*, *5*(1 SE-Artículos científicos), 99–

115.

Chow, V. Te, Maidment, D. R., Mays, L. W., & Ven Te Chow, David R. Maidment, L. W. M. (1998). *Applied Hydrology* (pp. 1–294). http://ponce.sdsu.edu/Applied_Hydrology_Chow_1988.pdf

De Silva, M. M. G. T., Weerakoon, S. B., Herath, S., Ratnayake, U. R., & Mahanama, S. (2012). Flood Inundation Mapping along the Lower Reach of Kelani River Basin under the Impact of Climatic Change. *Engineer: Journal of the Institution of Engineers, Sri Lanka*, *45*(2), 23. https://doi.org/10.4038/engineer.v45i2.6938

Department of Census and Statistics. (2012). Census of Population and Housing 2012 - Final Report, Population by ethnicity and district according to Divisional Secretary's Division, 2012. *Census of Population and Housing*, 52.

Eriyagama, N., & Smakhtin, V. (2009). Observed and projected climatic changes, their impacts and adaptation options for Sri Lanka: A review. *National Conference on Water, Food Security and Climate Change*, *October 2015*, 99–117. http://publications.iwmi.org/pdf/H042863.pdf

Fang, G. H., Yang, J., Chen, Y. N., & Zammit, C. (2015). Comparing bias correction methods in downscaling meteorological variables for a hydrologic impact study in an arid area in China. *Hydrology and Earth System Sciences*, *19*(6), 2547–2559. https://doi.org/10.5194/hess-19-2547-2015

Gawatre, D. W., Kandgule, M. H., & Kharat, S. D. (2016). Comparative Study of Population Forecasting Methods. *IOSR Journal of Mechanical and Civil Engineering*, *13*(04), 16–19. https://doi.org/10.9790/1684-1304051619

Gebre SL, G. Y. (2015). Flood Hazard Assessment and Mapping of Flood Inundation Area of the Awash River Basin in Ethiopia using GIS and HEC-GeoRAS/HEC-RAS Model. *Journal of Civil & Environmental Engineering*, *05*(04). https://doi.org/10.4172/2165-784x.1000179

Hasan, M. M., & Croke, B. F. W. (2013). Filling gaps in daily rainfall data: A statistical approach. *Proceedings - 20th International Congress on Modelling and Simulation, MODSIM 2013*, *December*, 380–386.

https://doi.org/10.36334/modsim.2013.a9.hasan

Hasanpour Kashani, M., & Dinpashoh, Y. (2012). Evaluation of efficiency of different estimation methods for missing climatological data. *Stochastic Environmental Research and Risk Assessment*, *26*(1), 59–71. https://doi.org/10.1007/s00477-011-0536-y

Hoque, M. A. A., Tasfia, S., Ahmed, N., & Pradhan, B. (2019). Assessing spatial flood vulnerability at kalapara upazila in Bangladesh using an analytic hierarchy process. *Sensors (Switzerland)*, *19*(6), 1–19. https://doi.org/10.3390/s19061302

Ibrahim, N. F., Zardari, N. H., Shirazi, S. M., Haniffah, M. R. B. M., Talib, S. M., Yusop, Z., & Yusoff, S. M. A. B. M. (2017). Identification of vulnerable areas to floods in Kelantan River sub-basins by using flood vulnerability index. *International Journal of GEOMATE*, *12*(29), 107–114. https://doi.org/10.21660/2017.29.11110

International Sava River Basin Commission. (2014). *Preliminary Flood Risk Assessment in the Sava River Basin*. *July*.

JICA. (2009). *Ministry of Disaster Management and Human Comprehensive Study on Disaster Management in Comprehensive Study on Disaster Management in* (Issue March).

Liu, W. C., Hsieh, T. H., & Liu, H. M. (2021). Flood risk assessment in urban areas of southern Taiwan. *Sustainability (Switzerland)*, *13*(6). https://doi.org/10.3390/su13063180

Mahmood, R., & Jia, S. (2016). Assessment of impacts of climate change on the water resources of the transboundary Jhelum River Basin of Pakistan and India. *Water (Switzerland)*, *8*(6). https://doi.org/10.3390/W8060246

Marqueso, J. T., Amora, A. M., Santillan, J. R., Makinano-Santillan, M., Gingo, A. L., Cutamora, L. C., Serviano, J. L., & Makinano, R. M. (2016). Flood depth and velocity impact assessment of historical flooding events using lidar and 2d numerical modeling. *37th Asian Conference on Remote Sensing, ACRS 2016*, *3*(December 2014), 2143–2151.

Mihu-pintilie, A., Cîmpianu, I., Stoleriu, C. C., & Paveluc, L. E. (2019). Using High-Density LiDAR Data and 2D Streamflow Hydraulic Modeling to Improve Urban Flood Hazard. *Water*.

Ministry of Mahaweli Development and Environment. (2016). *Climate Change Secretariat, Ministry of Mahaweli Development and Environment*. https://www4.unfccc.int/sites/NAPC/Documents NAP/National Reports/National Adaptation Plan of Sri Lanka.pdf

Mountz, T. W., & Crowley, J. (2009). Comparison of HEC-RAS and infoworks rs a case study in grand prairie, Texas. *Proceedings of World Environmental and Water Resources Congress 2009 - World Environmental and Water Resources Congress 2009: Great Rivers*, *342*, 2853–2862. https://doi.org/10.1061/41036(342)289

Mukherjee, M. K. (2012). *RESEARCH ARTICLE MODEL OF PEAK DISCHARGE (Q P) & RETURN PERIOD (T) OF RIVER SUBERNAREKHA , INDIA*. 3–5.

Nandalal, H. K., & Ratnayake, U. R. (2010). *Setting Up of Indices To Measure Vulnerability of Structures During a Flood*. *December*, 13–14.

Nguyen, H. D., Fox, D., Dang, D. K., Pham, L. T., Viet Du, Q. V., Nguyen, T. H. T., Dang, T. N., Tran, V. T., Vu, P. L., Nguyen, Q. H., Nguyen, T. G., Bui, Q. T., & Petrisor, A. I. (2021). Predicting future urban flood risk using land change and hydraulic modeling in a river watershed in the central province of Vietnam. *Remote Sensing*, *13*(2), 1–24. https://doi.org/10.3390/rs13020262

Ntajal, J., Lamptey, B. L., Mahamadou, I. B., & Nyarko, B. K. (2017). Flood disaster risk mapping in the Lower Mono River Basin in Togo, West Africa. *International Journal of Disaster Risk Reduction*, *23*(March 2020), 93–103. https://doi.org/10.1016/j.ijdrr.2017.03.015

Nur, I., & Shrestha, K. K. (2017). An Integrative Perspective on Community Vulnerability to Flooding in Cities of Developing Countries. *Procedia Engineering*, *198*(September 2016), 958–967. https://doi.org/10.1016/j.proeng.2017.07.141

Ongdas, N., Akiyanova, F., Karakulov, Y., Muratbayeva, A., & Zinabdin, N. (2020). Application of hec-ras (2d) for flood hazard maps generation for yesil (ishim) river in kazakhstan. *Water (Switzerland)*, *12*(10), 1–20. https://doi.org/10.3390/w12102672

Pelling, M. (2006). Editorial board. *Global Environmental Change*, *16*(2), CO2. https://doi.org/10.1016/s0959-3780(06)00031-8

Sah, P. (2015). Flood Frequency Analysis of River Kosi, Uttarakhand, India Using Statistical Approach. *International Journal of Research in Engineering and Technology*, *04*(08), 312–315. https://doi.org/10.15623/ijret.2015.0408053

Samarasinghe, G. B. (2009). Long-range Forecast of Climate Change : Sri Lanka Future Scenario Line-up. *Director*.

Samarasinghea. (2010). Application of Remote Sensing and Gis for Flood Risk Analysis : a Case Study At Kalu- Ganga River , Sri Lanka. *International Archives of the Photogrammetry, Remote Sensing and Spatial Information Science*, *XXXVIII*(8), 110–115.

Sattari, M. T., Rezazadeh-Joudi, A., & Kusiak, A. (2017). Assessment of different methods for estimation of missing data in precipitation studies. *Hydrology Research*, *48*(4), 1032–1044. https://doi.org/10.2166/nh.2016.364

Scawthorn, C., Flores, P., Blais, N., Seligson, H., Tate, E., Chang, S., Mifflin, E., Thomas, W., Murphy, J., Jones, C., & Lawrence, M. (2006). HAZUS-MH Flood Loss Estimation Methodology. II. Damage and Loss Assessment. *Natural Hazards Review*, *7*(2), 72–81. https://doi.org/10.1061/(asce)1527-6988(2006)7:2(72)

Seneviratne, L. W. (2004). *Inter nationales Symposion INTERPRAEVENT 2004 – RIVA / TRIENT*. 281–290.

Shadmehri Toosi, A., Doulabian, S., Ghasemi Tousi, E., Calbimonte, G. H., & Alaghmand, S. (2020). Large-scale flood hazard assessment under climate change: A case study. *Ecological Engineering*, *147*(March), 105765. https://doi.org/10.1016/j.ecoleng.2020.105765

Singh, N., Kumar, M., & Kumar, A. (2019). Hydrological Modeling of Ravi River Catchment Area Using Hec-Hms. *International Journal of Engineering Technology Science and Research*, *6*(7), 30–41. www.ijetsr.com

Sirisena, T. A. J. G., Maskey, S., Bamunawala, J., Coppola, E., & Ranasinghe, R. (2021). Projected streamflow and sediment supply under changing climate to the coast of the kalu river basin in tropical sri lanka over the 21st century. *Water (Switzerland)*, *13*(21). https://doi.org/10.3390/w13213031

Subramanya, K. (2013). *Engineering Hydrology By K Subramanya*.

Tailor, D., & Shrimali, N. J. (2016). Surface runoff estimation by SCS curve number method using gis for Rupen-Khan watershed , Mehsana district , Gujarat soil. *J. Indian Water Resour. Soc.*, *36*(4), 2–6.

Tansar, H., Akbar, H., & Aslam, R. A. (2021). *Type of the Paper (Article) Flood inundation mapping and hazard assessment for mitigation analysis of local adaption measures in Upper Ping River Basin , Thailand*. *2*.

Tenzin, J., & Bhaskar, A. S. (2017). Modeling of the precipitation induced flash flood in Sarpang, Bhutan using HEC-RAS. *Rasayan Journal of Chemistry*, *10*(2), 399–406. https://doi.org/10.7324/RJC.2017.1021648

UNDP. (2010). *UNDP BOOK CHAP 04_ Flood.pdf* (pp. 64–89).

UNDRR. (2019). Disaster risk reduction in Sri Lanka. *UN Disaster Risk Reduction*, 29.

US Army Corps of Engineers. (2018). Hydrologic Modeling System HEC-HMS, Hydrologic Modeling System HEC-HMS, User's Manual. Version 4.3. Hydrologic Engineering Centre. *Hydrologic Engineering Centre*, (Version 4.3), 640. https://www.hec.usace.army.mil/software/hec-hms/documentation/HEC-HMS_Users_Manual_4.3.pdf

USDA-NRCS. (2010). *National Engineering Handbook Chapter 15, Time of Concentration*. 1–15.

Wan Ismail, W. N., & Wan Zin @ Wan Ibrahim, W. Z. (2017). Estimation of rainfall and stream flow missing data for Terengganu, Malaysia by using interpolation

technique methods. *Malaysian Journal of Fundamental and Applied Sciences*, *13*(3), 213–217. https://doi.org/10.11113/mjfas.v13n3.578

Wijesekera, N. T. S., & Perera, L. R. H. (2012). Key Issues of Data and Data Checking for Hydrological Analyses - Case Study of Rainfall Data in the Attanagalu Oya Basin of Sri Lanka. *Engineer: Journal of the Institution of Engineers, Sri Lanka*, *45*(2), 1. https://doi.org/10.4038/engineer.v45i2.6936

Yoshitani, J., Takemoto, N., & Merabtene, T. (2007). *Factor Analysis of Water-related Disasters in Sri Lanka*. *4066*.

ANNEXURE 1

RAINFALL SEASONAL GRAPHS

1. Pallegama station

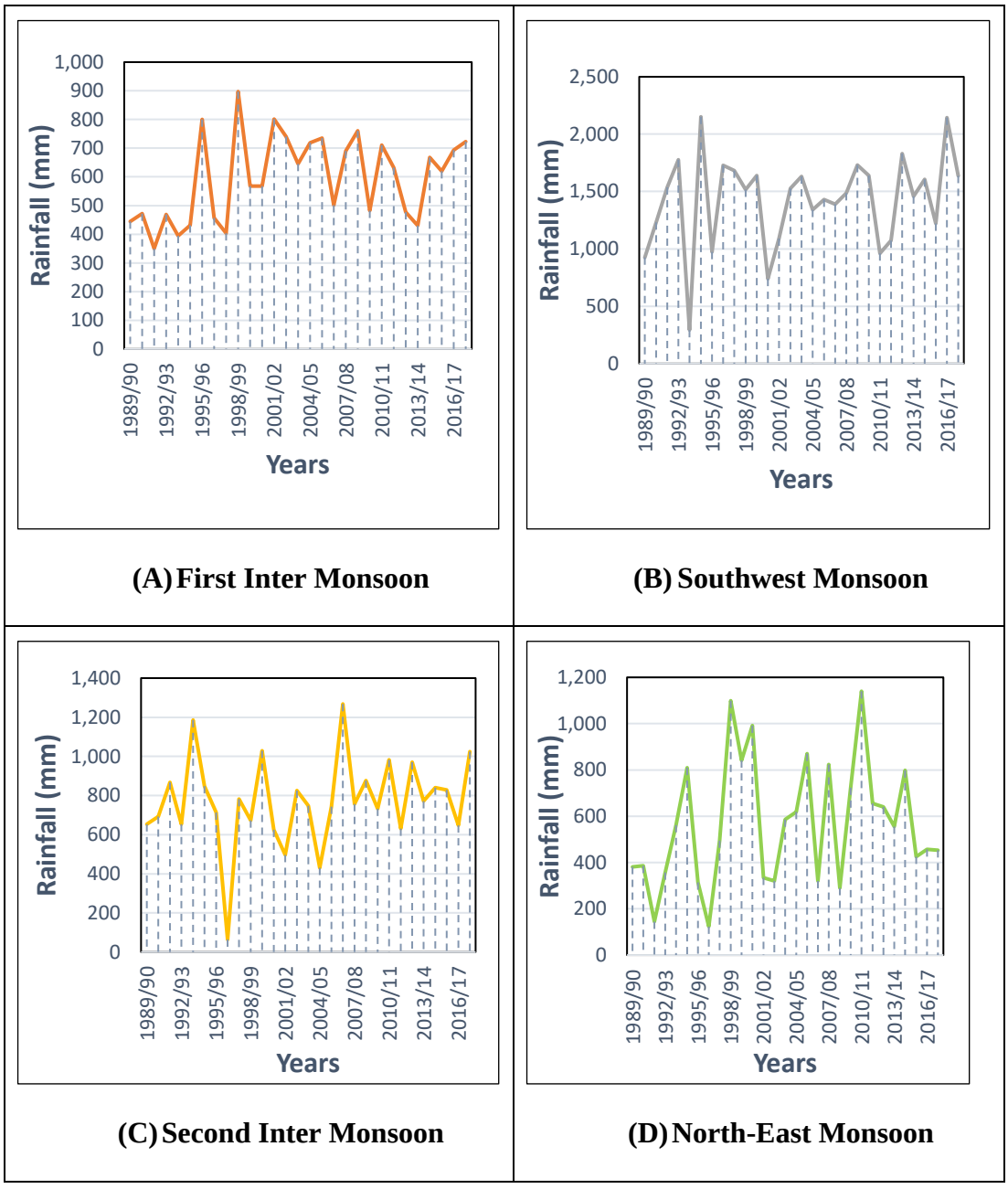

Figure A1- 1: Rainfall Seasonal Variation of Pallegama Rainfall Station

2. Thawalama station

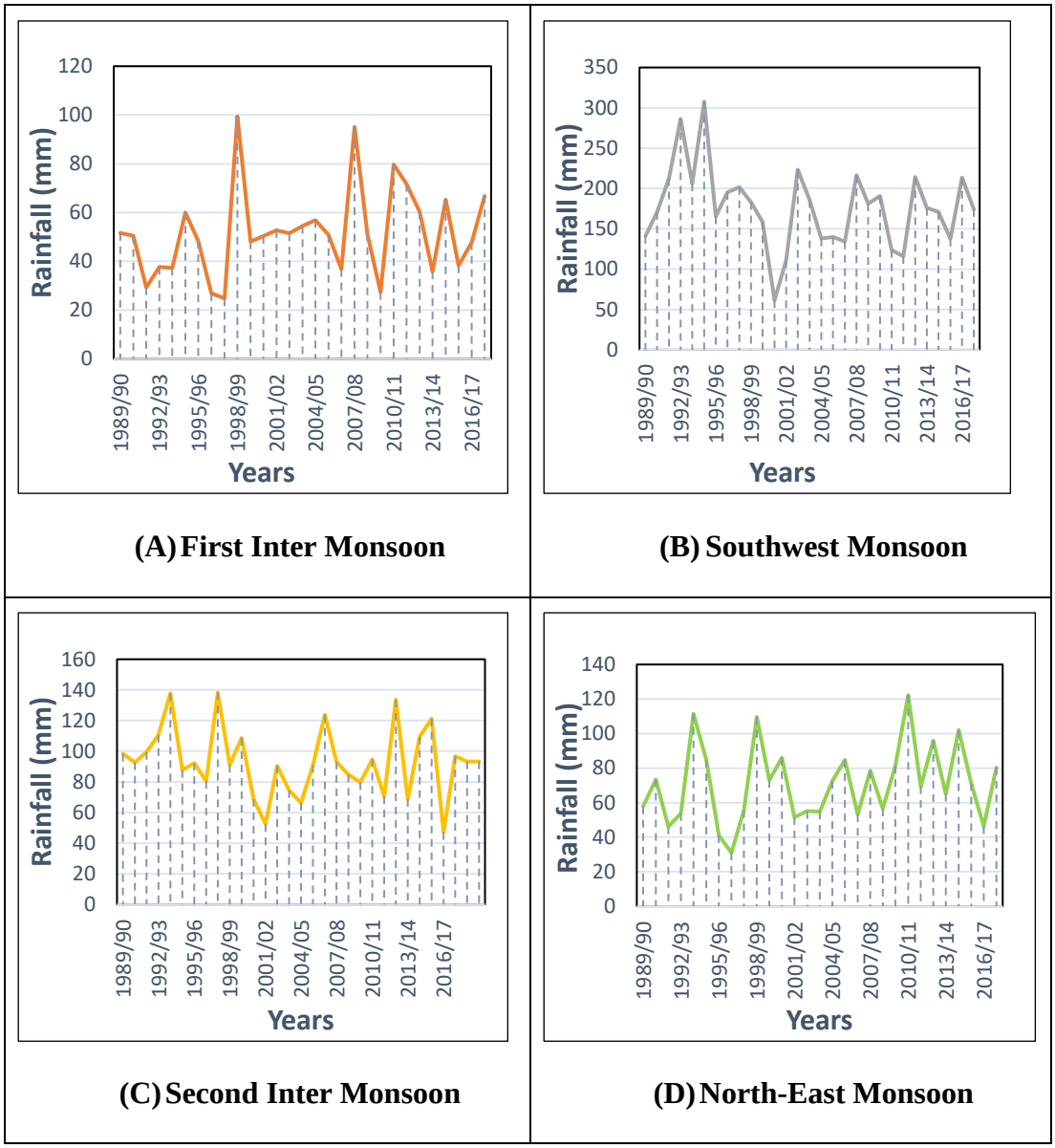

Figure A1- 2: Rainfall Seasonal Variation of Thawalama Rainfall Station

3. Anninkanda station

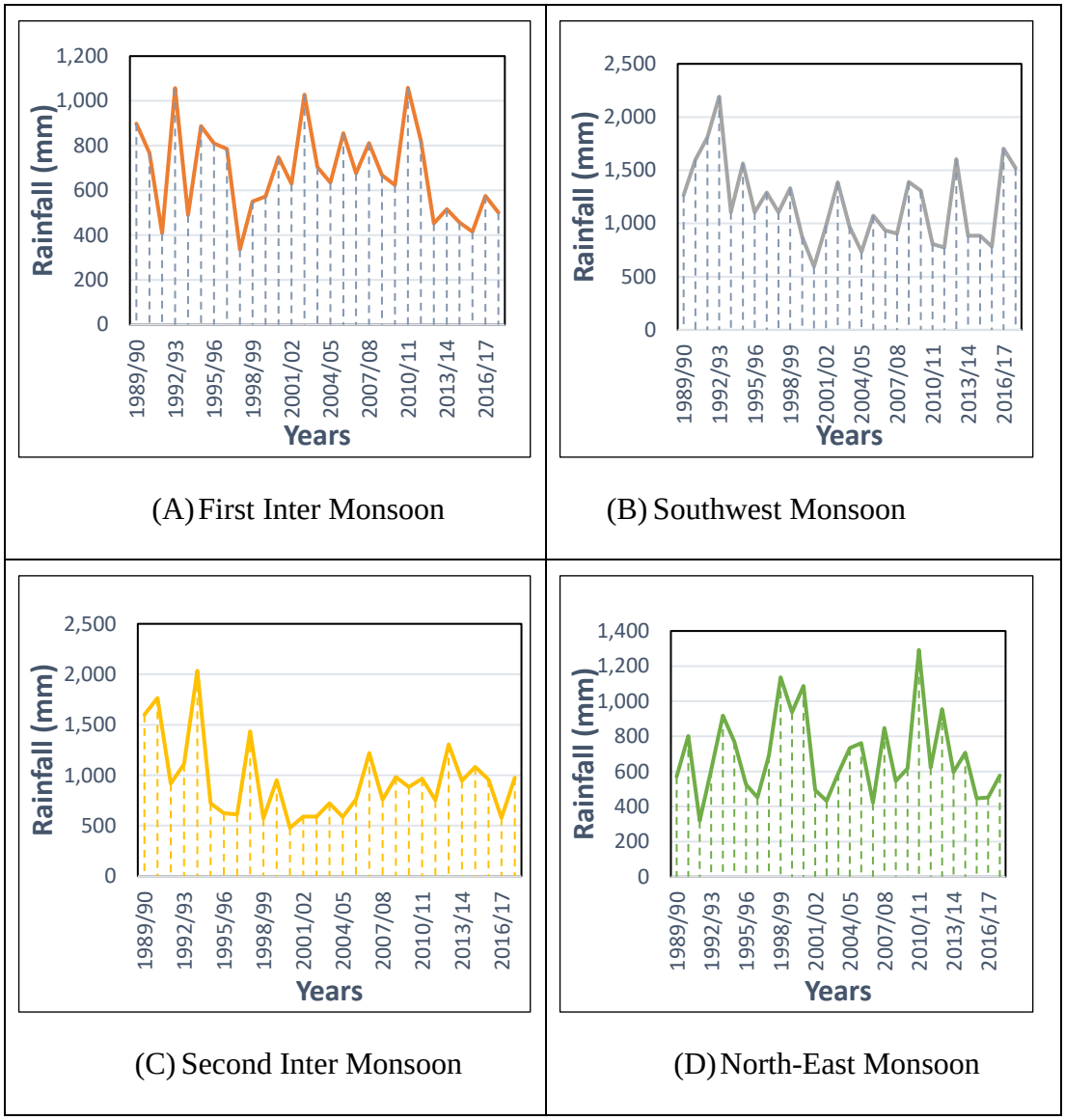

(A) First Inter Monsoon

(B) Southwest Monsoon

(C) Second Inter Monsoon

(D) North-East Monsoon

Figure A1- 3: Rainfall Seasonal Variation of Anninkanda Rainfall Station

4. Kuduwa station

Figure A1- 4: Rainfall Seasonal Variation of Kududwa Rainfall Station

ANNEXURE 2

SINGLE MASS CURVE AND DOUBLE MASS CURVE

1. Single Mass curve after filling missing data

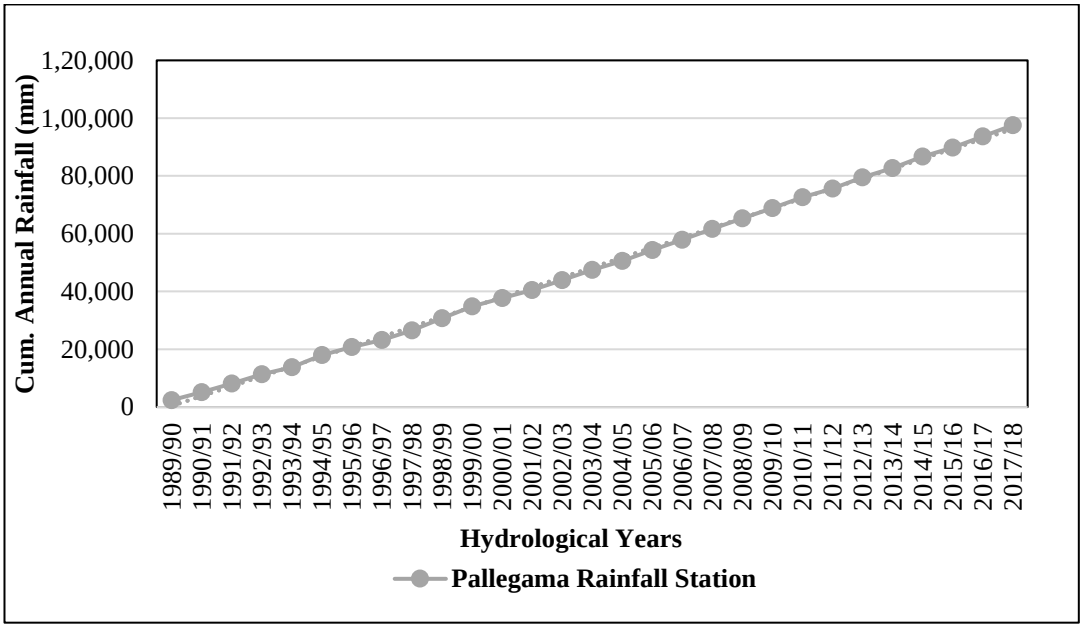

Figure A2- 1: Single Mass Curve for Pallegama Station

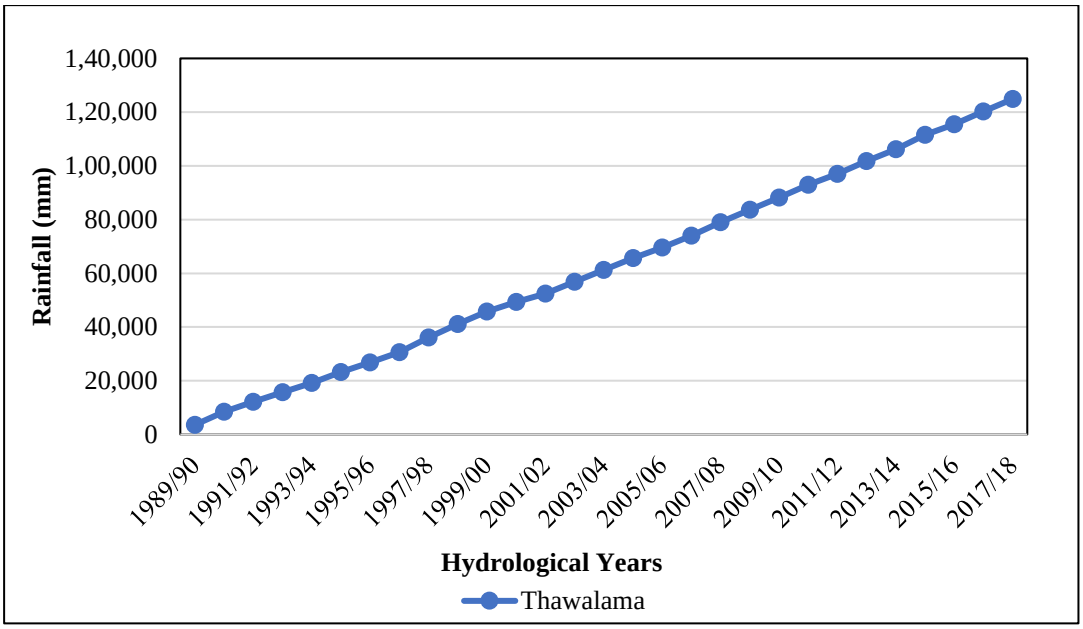

Figure A2- 2: Single Mass Curve for Thawalama Station

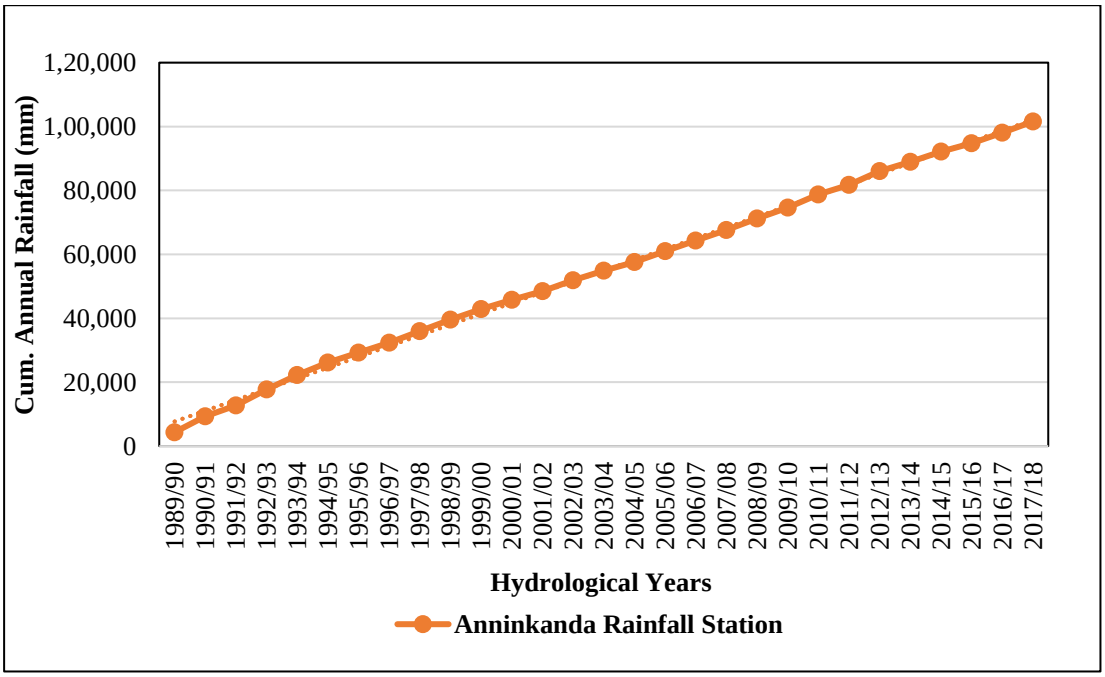

Figure A2- 3: Single Mass Curve for Anninkanda Station

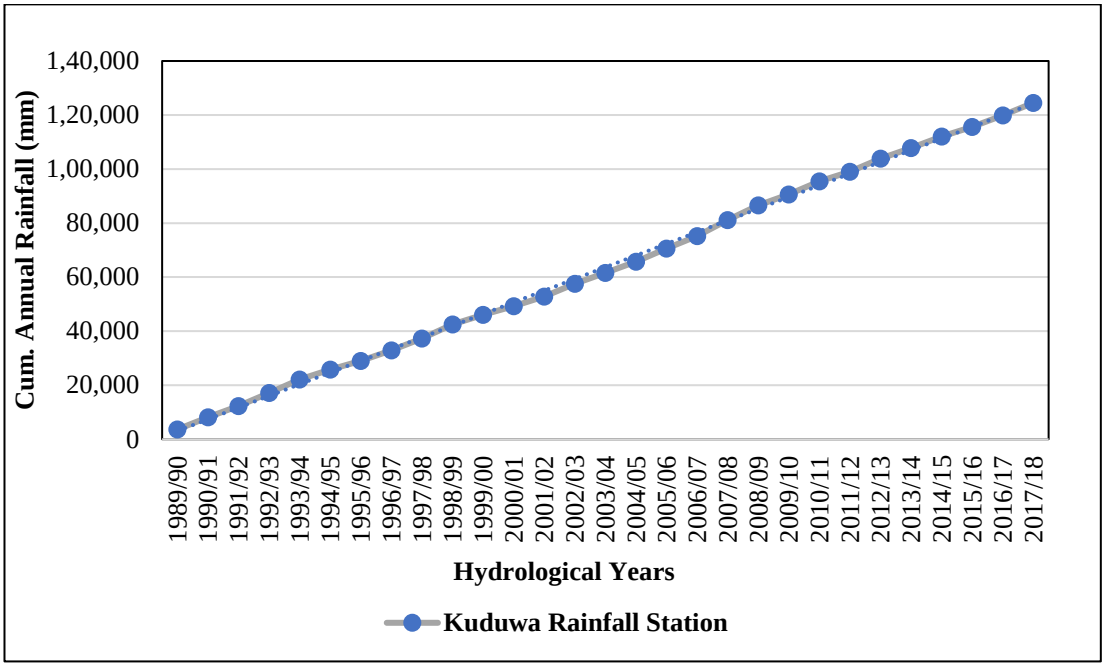

Figure A2- 4: Single Mass Curve for Kuduwa Station

2. Double Mass curve after filling missing data

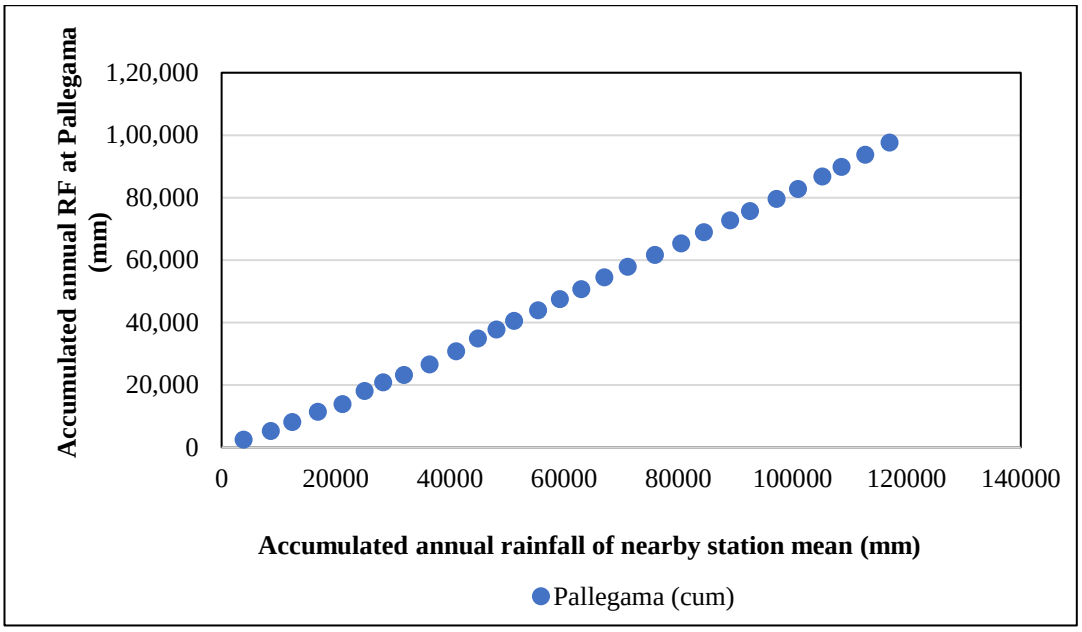

Figure A2- 5: Double Mass Curve of Pallegama rainfall station in the Thawalama Catchment

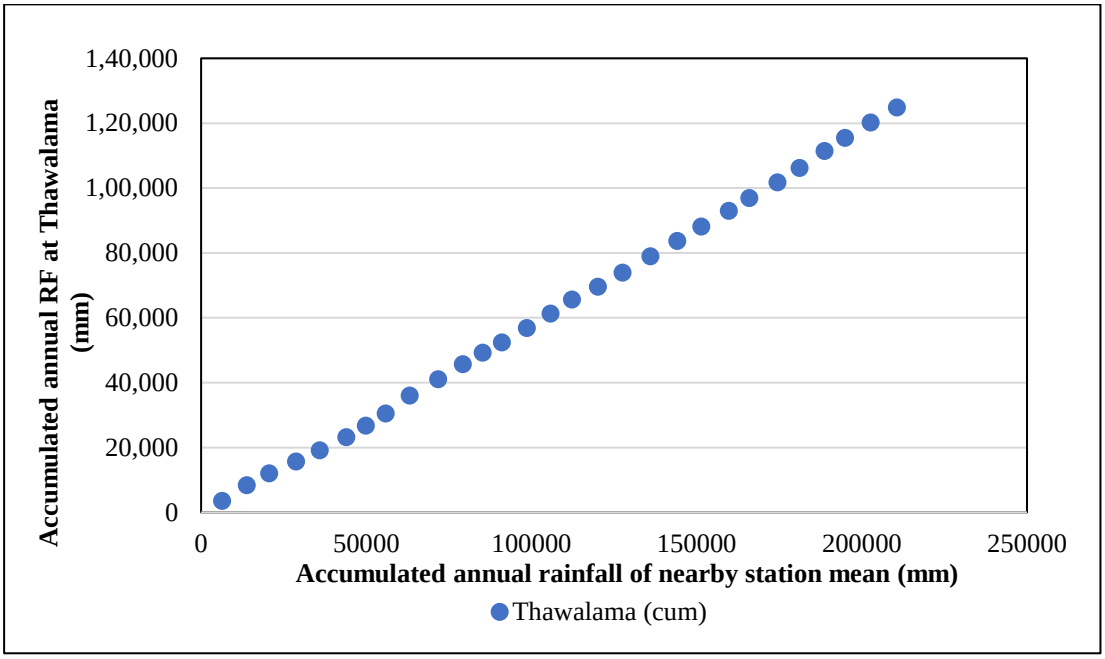

Figure A2- 6: Double Mass Curve of Thawalama rainfall station in the Thawalama Catchment

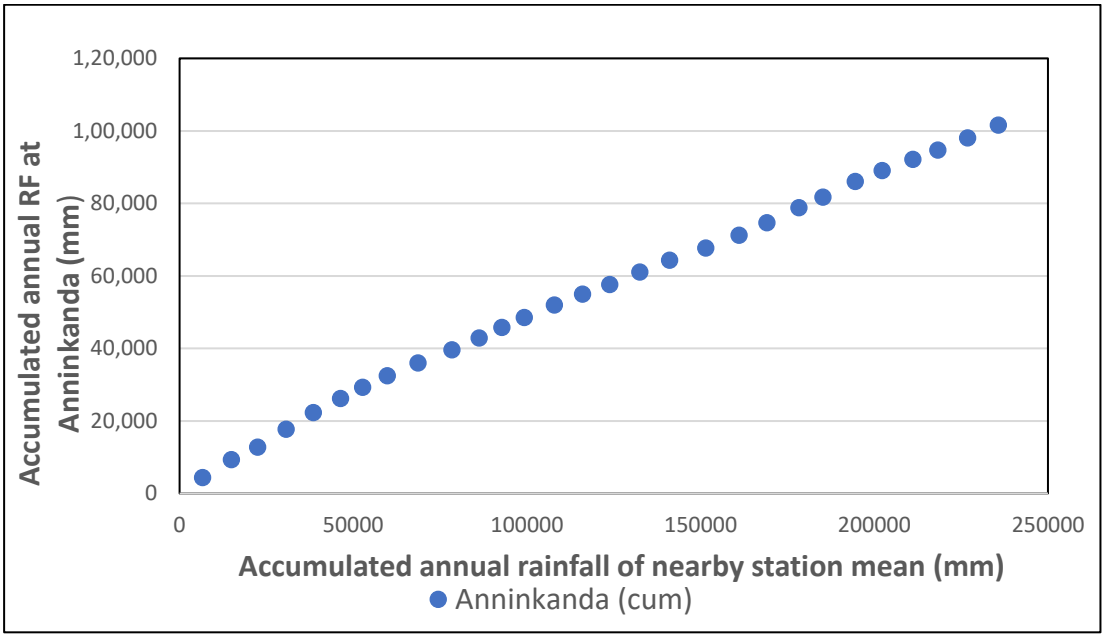

Figure A2- 7: Double Mass Curve of Anninkanda rainfall station in the Thawalama Catchment

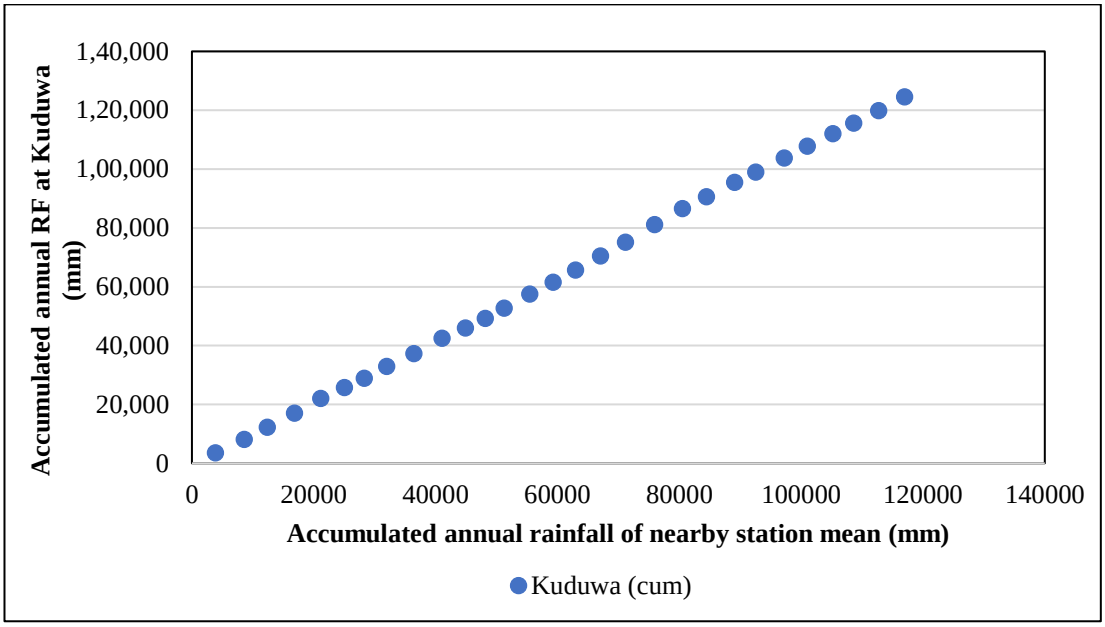

Figure A2- 8: Double Mass Curve of Kuduwa rainfall station in the Thawalama Catchment

The findings, interpretations and conclusions expressed in this thesis/dissertation are entirely based on the results of the individual research study and should not be attributed in any manner to or do neither necessarily reflect the views of UNESCO Madanjeet Singh Centre for South Asia Water Management (UMCSAWM), nor of the individual members of the MSc panel, nor of their respective organizations.